

Dissertation

Study on high efficiency electrohydraulic drive system using a servo motor driven variable speed, variable displacement hydraulic pump

サーボモータ駆動可変速・可変容量油圧ポンプを用いた高効率電動
油圧駆動システムに関する研究

**Graduate School of Engineering Science
Yokohama National University**

Ha Tham Phan
ハータムファン

June 2021

Abstract

In recent years, as a measure against environmental problems in the field of industrial machinery, there is a demand for power saving of hydraulic power transmission in hydraulic equipment. In the conventional hydraulic control system, the high-pressure oil generated by the hydraulic pump is supplied to the hydraulic actuator via the fluid throttle of the hydraulic control valve to control the movement, but the excess flow rate of high pressure and power loss in the control valves are large due to the throttle. On the other hand, the Electrohydraulic Drive System (EHDS), which drives a hydraulic pump with an electric motor and supplies the required pressure and flow rate of hydraulic power directly to the hydraulic actuator without going through control valves, is highly efficient. It is attracting attention as a hydraulic power transmission method. Most EHDS have FS-VP (Fixed Speed Motor-Variable Displacement Pump), which controls the discharge displacement of a variable-displacement hydraulic pump driven by an electric motor, and VS-FP (Variable Speed Motor-Fixed Displacement Pump) is roughly divided into those that control the flow rate by controlling the rotational speed of a servo motor that drives a fixed-displacement hydraulic pump, but both have the problem that the overall efficiency of the system decreases with changes in operating conditions. Therefore, in this research, in order to solve this problem, two-degree control (VS-VP: Variable Speed Motor-Variable Displacement Pump) of displacement control of variable displacement hydraulic pump and rotational speed control of servo motor is proposed and the efficiency characteristics of both motor and pump are considered together to operate hydraulic power transmission at high efficiency over the entire operating range. This dissertation consists of six chapters, and the outline of each chapter is given below.

Chapter 1 clarified the position of this research by stating the background and purpose of this research and clarifying the research subjects.

In Chapter 2, the equations expressing the theoretical efficiencies of the servomotors and variable displacement hydraulic pumps that make up the VS-VP at various operating points are derived, and the efficiency map of the servomotor and the efficiency map of the variable displacement pump are shown respectively. By integrating both efficiency maps, we constructed an algorithm that outputs the servomotor speed and the discharge displacement of the variable displacement hydraulic pump at the operating point where the total efficiency of the system is the highest for the target pressure and target flow rate. Furthermore, it was revealed

that VS-VP shows higher power transmission efficiency over the entire operating range compared to the conventional FS-VP and VS-FP.

In Chapter 3, the efficiency characteristics of the equipment to be actually used are expressed by applying the coefficients obtained from the measured efficiency results of the servomotor and pump to the coefficients included in the theoretical efficiency equation derived in Chapter 2. From these results, it was showed that efficiency maps can be generated. Using this efficiency maps, it was clarified that VS-VP shows higher power transmission efficiency over the entire operating range than FS-VP and VS-FP even in the actual machine.

In Chapter 4, by updating the efficiency maps applied to controller for changes in pressure target and flow rate target, the overall efficiency of the system can be maximized even for time-varying target inputs. It was shown that the rotational speed command and the swash plate angle command of the pump that determines the displacement of the variable displacement hydraulic pump can be generated, and the actual machines is controlled using these commands.

In Chapter 5, we proposed adding the functions of a servomotor to a conventional switched reluctance motor (SRM) that does not use a permanent magnet instead of the servomotor and a permanent magnet synchronous motor and showed the motor drive method. Furthermore, by integrating the efficiency characteristics of SRM and the efficiency characteristics of known pumps, this research showed the possibility of high-efficiency power transmission by controlling the two degrees of freedom of VS-VP even when using SRM to drive the pump.

Chapter 6 summarizes the results obtained in this research and describes future prospects.

Content

Abstract.....	3
Content.....	5
Nomenclature	8
List of Figures	10
List of Tables.....	16
Chapter 1 Introduction	17
1.1 Motivation	19
1.2 State of research	23
1.3 Dissertation outline.....	23
1.4 References	25
Chapter 2 Improvement of the theoretical overall efficiency for electro-hydraulic drive system.....	29
2.1 Power losses and efficiency of EHDS.....	31
2.1.1 Model of power losses and efficiency of servo system	31
2.1.2 Model of losses and efficiency in hydraulic pump.....	32
2.2 Energy efficiency map of EHDS.....	36
2.2.1 Efficiency map of electric motor	36
2.2.2 Efficiency map of hydraulic pump	37
2.3 Simulation improvement of the overall efficiency for EHDS	42
2.4 Summary of Chapter 2.....	52
2.5 References	53
Chapter 3 Experimental validation of improvement of the overall efficiency for electro-hydraulic drive system	55
3.1 Measuring instruments and data acquisition.....	57
3.2 Experiment.....	60
3.3 Establish the efficiency maps from experiment results.....	62

3.4	Quasi-Static improvement of overall efficiency of the proposed control strategy for EHDS.....	74
3.5	Summary of Chapter 3.....	75
3.6	References.....	76
Chapter 4 Improvement of the transient efficiency for electro-dydraulic drive system.....		77
4.1	Simulation of improvement of the transient efficiency for EHDS	79
4.1.1	Improvement of transient efficiency by using experimental efficiency maps	79
4.1.2	Improvement of transient efficiency by interpolation efficiency maps	84
4.1.3	Improvement of control command by using low pass filter	86
4.2	Controllers with efficiency maps for regulating displacement ratio and motor speed.....	93
4.3	Summary of Chapter 4.....	96
4.4	References.....	97
Chapter 5 Development of EHDS using SRM with servo function and improvement of overall efficiency by using overall efficiency maps.....		98
5.1	Operational principle of SRM.....	100
5.2	Control principle of SRM	102
5.3	Proposed SRM controller.....	103
5.4	PI gain design for improving drive system.....	106
5.5	Flow rate control experiment of hydraulic pump driven by SR servomotor in closed loop circuit	111
5.5.1	Evaluation of flow rate controllability.....	113
5.5.2	Evaluation of hydraulic motor speed response.....	114
5.6	Improvement overall efficiency of EHDS with switched reluctance motor and hydraulic pump by using overall efficiency maps.....	116

5.7	Summary of Chapter 5.....	119
5.8	References.....	120
	Chapter 6 Conclusion.....	121
6.1	Summary.....	123
6.2	Future work.....	124
	Appendix.....	126
	Related publications.....	132
	Acknowledgements.....	133

Nomenclature

(Unless otherwise mentioned, the followings are the meaning)

C_s	: leakage coefficient
C_{v1}	: viscous friction torque coefficient related to α
C_{v2}	: viscous friction torque coefficient irrelevant to α
C_f	: mechanical friction torque coefficient related to Δp
D	: displacement of pump
D_{max}	: maximum displacement of pump
I_M	: motor current
K_T	: torque coefficient
$K_{f1,2}$: iron losses coefficients
K_C	: current losses coefficient
n_m	: motor speed
n_p	: rotational speed of pump ($n_p = n_m$)
$n_{\eta_{max}}$: motor speed correlated to maximum η_t at the working point with $\Delta p_0, Q_0$
Q	: pump flow rate
R_M	: motor winding resistance
P_m	: motor power
T_m	: motor shaft torque
T_s	: torque losses independent of n_p and Δp
Δp	: pressure differential
ΔP_{Cu}	: copper losses in electric motor
ΔP_{Fe}	: iron losses in electric motor
ΔP_C	: current losses in amplifier
α	: displacement ratio of pump ($\alpha = D/D_{max}$)
$\alpha_{\eta_{max}}$: displacement ratio correlated to maximum η_t at the working point with $\Delta p_0, Q_0$
μ	: coefficient of viscosity
η_m	: motor efficiency
η_p	: pump efficiency
η_{pv}	: pump volumetric efficiency
η_{pm}	: pump mechanical efficiency

h_t : overall efficiency
 η_{max} : maximum overall efficiency at the working point with
 $\Delta p_0, Q_0$
 L flux linkage
 θ rotor angular position
 i electric current of winding

List of Figures

- 1.1 Valveless electro-hydraulic drive system
- 1.2 Exploded view of an SRM
- 2.1 Typical servo motor efficiency map
- 2.2 Efficiency map of hydraulic piston pump with $\alpha = 0.25$
- 2.3 Efficiency map of hydraulic piston pump with $\alpha = 0.5$
- 2.4 Efficiency map of hydraulic piston pump with $\alpha = 0.75$
- 2.5 Efficiency map of hydraulic piston pump with $\alpha = 1$
- 2.6 Combination of individual efficiency maps
- 2.7 Overall efficiency map of EHDS with $\alpha = 0.25$
- 2.8 Overall efficiency map of EHDS with $\alpha = 0.5$
- 2.9 Overall efficiency map of EHDS with $\alpha = 0.75$
- 2.10 Overall efficiency map of EHDS with $\alpha = 1$
- 2.11 Control strategy for improving overall efficiency
- 2.12 Overall efficiency η_t comparison at pressure differential $\Delta p = 24\text{MPa}$
- 2.13 Overall efficiency η_t comparison at pressure differential $\Delta p = 18\text{ MPa}$
- 2.14 Overall efficiency η_t comparison at pressure differential $\Delta p = 12.5\text{ MPa}$
- 2.15 Overall efficiency η_t comparison at pressure differential $\Delta p = 6.3\text{ MPa}$
- 2.16 Overall efficiency η_t comparison at pressure differential $\Delta p = 4\text{ MPa}$
- 2.17 Overall efficiency η_t comparison at output flow rate $Q = 24\text{ L/min}$
- 2.18 Overall efficiency η_t comparison at output flow rate $Q = 18\text{ L/min}$
- 2.19 Overall efficiency η_t comparison at output flow rate $Q = 12\text{ L/min}$
- 2.20 Overall efficiency η_t comparison at output flow rate $Q = 9\text{ L/min}$
- 2.21 Overall efficiency η_t comparison at output flow rate $Q = 5\text{ L/min}$
- 3.1 Schematic of hydraulic circuit for measuring the efficiency of system
- 3.2 Structure of variable displacement piston pump
- 3.3 Scatter chart of experiment of hydraulic piston pump
- 3.4 Scatter chart of experiment of servo motor
- 3.5 Efficiency map of servo system
- 3.6 Efficiency map of hydraulic piston pump with $\alpha=1.0$

- 3.7 Efficiency map of hydraulic piston pump with $\alpha=0.8$
- 3.8 Efficiency map of hydraulic piston pump with $\alpha=0.7$
- 3.9 Efficiency map of hydraulic piston pump with $\alpha=0.6$
- 3.10 Efficiency map of hydraulic piston pump with $\alpha=0.5$
- 3.11 Efficiency map of hydraulic piston pump with $\alpha=0.4$
- 3.12 Efficiency map of hydraulic piston pump with $\alpha=0.3$
- 3.13 Efficiency map of hydraulic piston pump with $\alpha=0.2$
- 3.14 Overall efficiency map of electro-hydraulic drive system with $\alpha=1.0$
- 3.15 Overall efficiency map of electro-hydraulic drive system with $\alpha=0.9$
- 3.16 Overall efficiency map of electro-hydraulic drive system with $\alpha=0.8$
- 3.17 Overall efficiency map of electro-hydraulic drive system with $\alpha=0.7$
- 3.18 Overall efficiency map of electro-hydraulic drive system with $\alpha=0.6$
- 3.19 Overall efficiency map of electro-hydraulic drive system with $\alpha=0.5$
- 3.20 Overall efficiency map of electro-hydraulic drive system with $\alpha=0.4$
- 3.21 Overall efficiency map of electro-hydraulic drive system with $\alpha=0.3$
- 3.22 Overall efficiency map of electro-hydraulic drive system with $\alpha=0.2$
- 3.23 Overall efficiency η_t comparison at output different pressure $\Delta p = 16$ MPa
- 3.24 Overall efficiency η_t comparison at output different pressure $\Delta p = 12.5$ MPa
- 3.25 Overall efficiency η_t comparison at output different pressure $\Delta p = 10$ MPa
- 3.26 Overall efficiency η_t comparison at output different pressure $\Delta p = 6.3$ MPa
- 3.27 Overall efficiency η_t comparison at output different pressure $\Delta p = 4$ MPa
- 3.28 Quasi-static analysis of experimental data
- 4.1 Command step flow rate Q (L/min) at constant pressure $\Delta p = 10$ MPa
- 4.2 Overall efficiency η_t comparison at output constant pressure $\Delta p = 10$ MPa for command step flow rate
- 4.3 Response flow rate and command flow rate comparison at output constant pressure $\Delta p = 10$ MPa for command step wave flow rate

- 4.4 Displacement ratio and motor speed command at output constant pressure $\Delta p = 10$ MPa for command step wave flow rate
- 4.5 Command sine wave flow rate Q (L/min) at constant pressure $\Delta p = 10$ MPa
- 4.6 Overall efficiency η_t comparison at output constant pressure $\Delta p = 10$ MPa for command sine wave flow rate
- 4.7 Response flow rate and command flow rate comparison at output constant pressure $\Delta p = 10$ MPa for command sine wave flow rate
- 4.8 Displacement ratio and motor speed command at output constant pressure $\Delta p = 10$ MPa for command sine wave flow rate
- 4.9 Overall efficiency η_t comparison at output constant pressure $\Delta p = 10$ MPa for command sine wave flow rate (improvement by using interpolation efficiency maps)
- 4.10 Response flow rate and command flow rate comparison at output constant pressure $\Delta p = 10$ MPa for command sine wave flow rate (improvement by using interpolation efficiency maps)
- 4.11 Displacement ratio at output constant pressure $\Delta p = 10$ MPa for command sine wave flow rate (improvement by using interpolation efficiency maps)
- 4.12 Motor speed command at output constant pressure $\Delta p = 10$ MPa for command sine wave flow rate (improvement by using interpolation efficiency maps)
- 4.13 Overall efficiency η_t comparison at output constant pressure $\Delta p = 10$ MPa for command sine wave flow rate (improvement by using interpolation efficiency maps and low pass filter with time constant $t=1$)
- 4.14 Response flow rate and command flow rate comparison at output constant pressure $\Delta p = 10$ MPa for command sine wave flow rate (improvement by using interpolation efficiency maps and low pass filter with time constant $t=1$)
- 4.15 Displacement ratio at output constant pressure $\Delta p = 10$ MPa for command sine wave flow rate (improvement by using interpolation efficiency maps and low pass filter with time constant $t=1$)
- 4.16 Motor speed command at output constant pressure $\Delta p = 10$ MPa for command sine wave flow rate (improvement by using interpolation efficiency maps and low pass filter with time constant $t=1$)

- 4.17 Overall efficiency η_t comparison at output constant pressure $\Delta p = 10$ MPa for command sine wave flow rate (improvement by using interpolation efficiency maps and low pass filter with time constant $t=0.5$)
- 4.18 Response flow rate and command flow rate comparison at output constant pressure $\Delta p = 10$ MPa for command sine wave flow rate (improvement by using interpolation efficiency maps and low pass filter with time constant $t=0.5$)
- 4.19 Displacement ratio at output constant pressure $\Delta p = 10$ MPa for command sine wave flow rate (improvement by using interpolation efficiency maps and low pass filter with time constant $t=0.5$)
- 4.20 Motor speed command at output constant pressure $\Delta p = 10$ MPa for command sine wave flow rate (improvement by using interpolation efficiency maps and low pass filter with time constant $t=0.5$)
- 4.21 Overall efficiency η_t comparison at output constant pressure $\Delta p = 10$ MPa for command sine wave flow rate (improvement by using interpolation efficiency maps and low pass filter with time constant $t=2$)
- 4.22 Response flow rate and command flow rate comparison at output constant pressure $\Delta p = 10$ MPa for command sine wave flow rate (improvement by using interpolation efficiency maps and low pass filter with time constant $t=2$)
- 4.23 Displacement ratio at output constant pressure $\Delta p = 10$ MPa for command sine wave flow rate (improvement by using interpolation efficiency maps and low pass filter with time constant $t=2$)
- 4.24 Motor speed command at output constant pressure $\Delta p = 10$ MPa for command sine wave flow rate (improvement by using interpolation efficiency maps and low pass filter with time constant $t=2$)
- 4.25 Diagram of experiment for improvement of the transient efficiency for EHDS
- 4.26 Connection of controller to servo amplifier
- 4.27 Mechanism for rotating the displacement adjusting screw of hydraulic pump
- 4.28 Step motor and driver
- 5.1 Typical structure of 8/6-type SRM
- 5.2 Inductance change in rotational direction of rotor

- 5.3 Four-quadrant operation of hydraulic pump driven by servomotor
- 5.4 Bidirection rotational speed control system of SRM
- 5.5 System flow of SRM drive system
- 5.6 SRM drive system
- 5.7 Illustration of square error area
- 5.8 Squared error area with square wave and sine wave
- 5.9 Experimental result for improving drive system response with $K_p = 1$
- 5.10 Experimental result for improving drive system response with $K_p = 3$
- 5.11 Experimental result for improving drive system response with $K_p = 5$
- 5.12 Experimental result for improving drive system response with $K_p = 7$
- 5.13 Experimental result for improving drive system response with $K_p = 9$
- 5.14 Experimental results for improving drive system response with frequency response 0.5 Hz
- 5.15 Experimental results for improving drive system response with frequency response 1.0 Hz
- 5.16 Experimental results for improving drive system response with frequency response 2.0 Hz
- 5.17 Hydraulic closed circuit with cylinder and motor application for bidirectional flow rate control using hydraulic servo pump driven by SR servomotor
- 5.18 Bidirectional rotational speed control system of SRM with variable orifice load
- 5.19 Sinusoidal bidirection flow rate control of hydraulic pump driven by SR servomotor (SRM speed -1000 to $+1000$ rpm, sine wave 0.5 Hz)
- 5.20 Bidirectional rotational speed control system of SRM with hydraulic motor
- 5.21 Sinusoidal bidirection speed control of hydraulic pump driven by SR servomotor (SRM speed -500 to $+500$ rpm, sine wave 0.5 Hz)
- 5.22 Efficiency map of SRM motor
- 5.23 Overall efficiency map of EHDS driven by SRM motor (displacement ratio $\alpha = 1.0$)
- 5.24 Overall efficiency map of EHDS driven by SRM motor (displacement ratio $\alpha = 0.75$)

- 5.25 Overall efficiency map of EHDS driven by SRM motor (displacement ratio $\alpha = 0.5$)
- 5.26 Overall efficiency map of EHDS driven by SRM motor (displacement ratio $\alpha = 0.25$)
- A.1 Simulink model of variable speed motor – variable hydraulic pump EHDS
- A.2 Simulink model of variable speed motor – fixed hydraulic pump EHDS
- A.3 Simulink model of fixed speed motor – variable hydraulic pump EHDS
- A.4 Control method of servo amplifier and stepping motor for regulating servo motor speed n_m and displacement ratio α
- A.5 Relation between VC (analog speed command) applied voltage and the servo motor speed
- A.6 Sink I/O interface of servo amplifier
- A.7 Source I/O interface of servo amplifier
- A.8 Connection of driver, power supply, controller and stepping motor
- A.9 Stepping motor movement and timing chart

List of Tables

- 1.1 Types of hydraulic power unit
- 2.1 Specifications of the simulation power unit
- 2.2 Overall efficiency of the EHDS for the given working point with $Q = 5$ L/min, $\Delta p = 10$ MPa
- 3.1 Main components' specifications of the test rig
- 3.2 Coefficients in motor efficiency equation
- 3.3 Coefficients in hydraulic pump efficiency equation
- 5.1 Experimental condition
- 5.2 Specifications of SRM and hydraulic pump/motor

Chapter 1

Introduction

Chapter 1. Introduction

1.1 Motivation

In recent decades, researchers and manufacturers have been striving to determine how energy can be saved during the operating process – in other words, how the overall efficiency of electro-hydraulic drive systems (EHDSs) can be increased. To develop high-efficient drive concepts, researchers and manufacturers have been concentrating on reducing throttling losses, avoiding inefficient component operating points and recovering potential energy.

To reduce throttling losses, one effective alternative drive system that has been proposed is the valveless electro-hydraulic drive system (Figure 1.1), which uses a variable speed motor and variable-displacement pump to supply hydraulic power to an actuator. The key advantage of this system is that it avoids both an excessive flow rate and power losses in the hydraulic control valves.

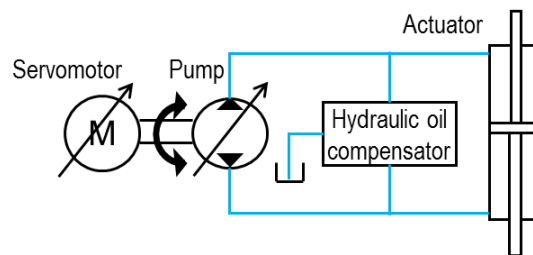
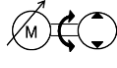
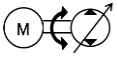
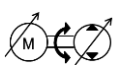


Fig. 1.1. Valveless electro-hydraulic drive system

In a valveless drive system, many ways to adjust the actuator flow exist: regulating the rotation speed of the motor, changing the displacement of the hydraulic pump, and simultaneously controlling the motor speed and pump displacement, as shown in Table 1.1. Moreover, most power losses in EHDSs occur in the stage during which electrical power is converted into hydraulic power (hydraulic pump). Therefore, the overall efficiency of EHDSs depends primarily on the efficiency of the hydraulic power unit. For these reasons, to improve the overall efficiency of the hydraulic power unit, many energy-saving methods have been proposed in recent decades ^{1.1)- 1.11)}.

Table 1.1: Types of hydraulic power unit

Type	Description	Symbol
VS-FP	Variable-speed motor and fixed-displacement pump	
FS-VP	Fixed-speed motor and variable-displacement pump	
VS-VP	Variable-speed motor and variable-displacement pump	

The first of these methods concerns the configuration of the hydraulic power unit. Helduser et al. ^{1.1)} and Tašner et al. ^{1.2)} presented three types of direct pump control for EHDSs: variable-speed fixed-displacement (VS-FP), fixed-speed variable-displacement (FS-VP), and variable-speed variable-displacement (VS-VP). Helduser found that the efficiency of VS-FP is higher than that of FS-VP and VS-VP, especially when the system operates with partial load and in idling mode. To the contrary, according to Tašner, VS-VP (two degrees of freedom) is more efficient than FS-VP and VS-FP (one degree of freedom each), although it exhibits a lower response. Haihong Huang et al. ^{1.3), 1.4)} established the theoretical model of hydraulic power units and experimentally validated that the overall efficiency of VS-VP could be improved by regulating the motor speed and the corresponding displacement under different load conditions; such efficiency improvement was not possible with VS-FP and FS-VP. Willkomm et al. ^{1.9)-1.11)} determined the potential of the VS-VP system and focused on improving its efficiency; this has been the focus of many essential researches ^{1.8)-1.14)}. Based on the above discussion, it is possible that, a VS-VP power unit with two degrees of freedom could be the most popular and efficient system in near future.

Second, to improve the overall efficiency of the VS-VP power unit, experimental tests and control methods have also been proposed. Quan et al. ^{1.8)} investigated a power-matching method combined with pump speed and displacement control to improve energy efficiency under different working conditions. Haihong Huang et al. ^{1.3, 1.4)} proposed separate controllers that estimate the optimal control parameters (speed, displacement) for separate working points of the hydraulic system (flow, pressure) to minimize total power losses. To determine a better motor speed for higher efficiency, artificial intelligence and big data were applied in the control method^{1.4)}. Willkomm et al. ^{1.9)-1.11)} transformed the dynamic loss model of the system into a mathematical problem and then proposed a novel predictive control concept to optimize the energy consumption

by utilizing the degree of freedom in the VS-VP system. Montgomery et al. ^{1.13)} presented a dynamic engine power demand estimator that minimizes engine power subject to a load demand.

In summary, the methods of prior studies normally determine the efficient rotating speed first, based on the specific displacement value, and then calculate the working displacement that corresponds to the rotating speed. However, the interaction between the electric motor and hydraulic pump was not considered in these control methods. Moreover, the characteristics of the electric motor and pump were only estimated by mathematical equations, meaning that the exact characteristics of the equipment have not been determined. As such, the claim exists that existing control methods exhibit disadvantages that could be further improved.

In electro-hydraulic drive system, there are some motor candidates included induction motors, permanent magnet synchronous motors, and reluctance motors (SRM, etc.). Induction motor is very often used as a motor for driving hydraulic pumps in factory equipment, but it is difficult to use it as a servo motor. Although the rotation speed of induction motor can be changed by controlling the drive frequency with an inverter. However, due to the operating principle, there is a slip in the actual rotation speed with respect to the rotation speed of the drive frequency, and the rotation speed changes according to the load. Moreover, slow rotation is difficult, and the speed control range is narrow. Therefore, it is not suitable for the drive motor of EHDS and is not dealt with in this study.

Recently, a high-performance servo motor is used in the current EHDS and shows the advantage of high response and high efficiency^{1.14)}. Therefore, this study deals with EHDS, which is a combination of a hydraulic piston pump and a permanent magnet synchronous motor (servo motor).

SRM has the potential to become a new EHDS drive motor if it is equipped with servomotor functions such as bidirectional rotation, speed control, and torque control. The SRM shown in Figure 1.2 is robust and requires no permanent magnet and rare-earth materials owing to its driving principle. Compared with permanent magnet and induction motors, SRMs have a simpler and more robust construction owing to its rotor structure without coils or permanent magnets, thereby affording a lower fabrication cost. Moreover, SRMs can provide similar or higher efficiencies in the medium and high-speed ranges.

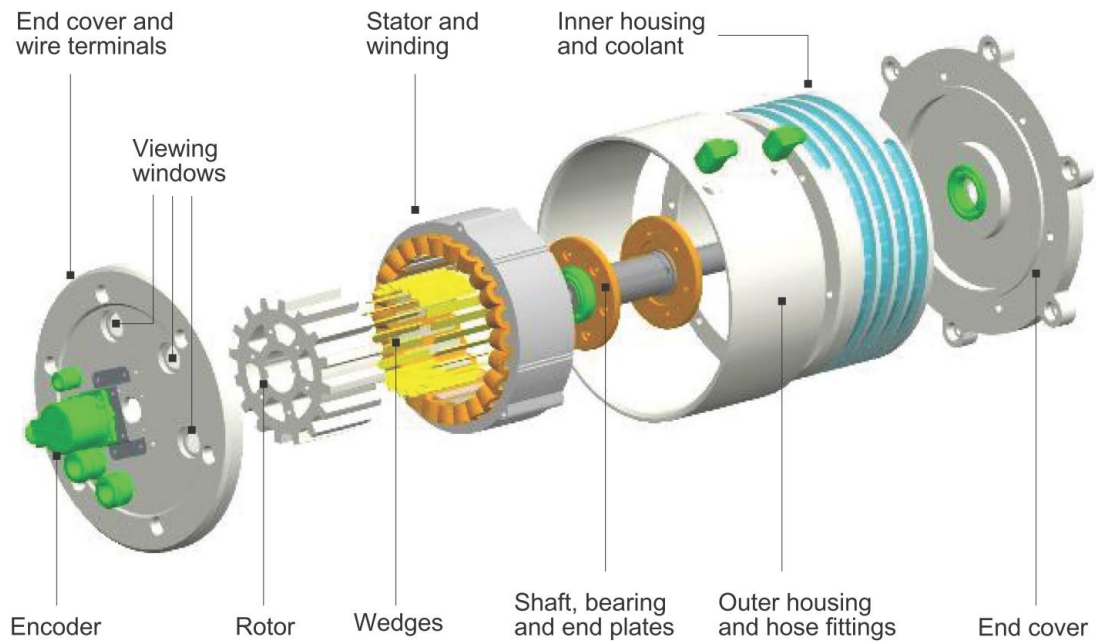


Fig. 1.2. Exploded view of an SRM. (From Jiang, W., *Three-phase 24/16 switched reluctance machine for hybrid electric powertrains: Design and optimization*, McMaster University Ph. D. Thesis, Hamilton, ON, 2015)^{1.34)}

In practical, an SRM is used in drive systems requiring high torque outputs in a wide speed range, one-directional rotation, and approximate speed control. To utilize SRMs for driving hydraulic pumps in closed hydraulic circuits, the controllability of the SRM must be improved, such as its bidirectional startup and a wide range of speed regulations. Yamai et al.^{1.15)} optimized the SRM motor drive parameters of a hydraulic pump unit using an open hydraulic circuit. They improved the motor efficiency by 6%, reduced the power consumption by 50%, and reduced the acoustic noise level by 5 dBA. Hamdy et al.^{1.16)} proposed a starting technique that exploits the natural magnetic asymmetry in the symmetrical machine geometry to provide bidirectional torque production at startup. However, this technique could not regulate the speed of the motor and was applied for only a 4/2 SRM with a low starting torque requirement. Gu et al.¹⁷⁾ focused on a phase shift design strategy to ensure both a large starting torque and bidirectional startup capability for a two-phase switched reluctance machine; however, the speed control function was not mentioned in the study. The studies mentioned above are related to bidirectional rotation SRM control. Other studies related to SRM control, such as^{1.18-1.23)}, did not mention such a topic. Meanwhile, several studies have reported hydraulic closed circuits that use power sources other than SRMs, such as permanent magnet synchronous servo motors and induction motors^{1.26-1.34)}.

However, the concept of driving a bidirectional rotation-type hydraulic pump using an SRM has not been reported. Herein, a driving method for SRMs is proposed in the form of a bidirectional rotation torque and a speed-controllable servomotor. Furthermore, the performance is evaluated based on the flow rate control of the hydraulic pump driven by the switched reluctance (SR) servomotor in a closed hydraulic circuit.

1.2 State of research

The aim of this dissertation is to show that it is possible to significantly improve the overall efficiency of electro-hydraulic drive system in general by using overall efficiency maps combined from component maps. By this way, the interaction between electric motor efficiency and hydraulic pump efficiency is considered properly to determine simultaneously the motor speed and pump displacement working to achieve high efficiency. This point is different from Quan et al.^{1.8)} research. Moreover, using overall efficiency maps, the control time could be reduced and there is no requirement of high-performance computer for controller as in Haihong Huang et al.^{1.3), 1.4)} theoretical models and Willkomm et al.^{1.9)-1.11)} research. In this research, the overall efficiency of drive system is improved at not only separated working points but also in working cycle entirely by controller for regulating motor speed and pump displacement simultaneously and continuously. This is the originality of this study compared with previous research.

To improve the efficiency of EHDS further, the development of electro-hydraulic drive system using conventional switched reluctance motor integrated a servo function is presented in this study. To be able to drive hydraulic pump in EHDS, the SRM motor has been equipped some servomotor functions such as bidirectional rotation, speed control, and torque control. These servo functions are not integrated into SRM motor together in previous research. To evaluate the flow rate controllability and hydraulic actuator speed response driven by this system, some experiments are conducted in unloading and loading conditions. Then, the proposed control strategy in EHDS with servo motor is applied for this system by combining the energy efficiency map of switched reluctance motor with efficiency map of hydraulic piston pump.

1.3 Dissertation outline

The content of this dissertation is divided into the following six chapters.

Chapter 1 shows the motivation and state of this research. The literature review of previous research is presented to show the difference and originality of this research.

Chapter 2 presents the improvement of the theoretical overall efficiency for electro-hydraulic drive system. Theoretical equations are used to create the efficiency maps and the overall efficiencies at typical working points of three types of electro-hydraulic system are determined and compared together to show advantage of the proposed control strategy.

Chapter 3 introduces the experiment of electro-hydraulic drive system to verify the simulation results in Chapter 2. Quasi-static analysis is conducted in this chapter for three types of electro-hydraulic system mentioned in Chapter 2.

Chapter 4 shows the research on the improvement of transient efficiency of the electro-hydraulic drive system. Simulation is conducted to generate motor speed and displacement ratio that are the control commands to operate VS-VP system at high-efficient areas in overall efficiency maps as shown in Chapter 3.

Chapter 5 presents the controller of SRM motor applied in electro-hydraulic drive system without control valves. The control strategy in Chapter 2 is proposed to improve the overall efficiency of this system as well.

Chapter 6 concludes the study presented in this thesis. Topics related to further development in the future are discussed.

1.4 References

1.1) Helduser, S.: Electric-hydrostatic drive—an innovative energy-saving power and motion control system, Proceedings of the Institution of Mechanical Engineers, Part I: Journal of Systems and Control Engineering, 213(5), p. 427-437 (1999)

1.2) Tašner, Tadej & Lovrec, Darko: Maximum efficiency control - a new strategy to control electrohydraulic systems, Paripex - Indian Journal of Research. Vol. 3, p. 107-109 (2012)

1.3) Huang, H., Jin, R., Li, L., and Liu: Improving the energy efficiency of a hydraulic press via variable-speed variable-displacement pump unit, ASME. J. Dyn. Sys., Meas., Control. November 2018; Vol.140, No. 111006, p. 1-10, (2018)

1.4) R. Jin, H. Huang, L. Li, L. Zhu, Z. Liu: Energy saving strategy of the variable-speed variable-displacement pump unit based on neural network, Procedia CIRP, 80, p. 84-88 (2019)

1.5) Seiya Itagaki, Ha Tham Phan and Yasukazu Sato: Study on high efficiency power transmission in servo motor-driven hydraulic system, The proceedings on Spring Conference of Japan Fluid Power System Society, p.45-47 (2019) (in Japanese)

1.6) Ha Tham Phan, Seiya Itagaki, and Yasukazu Sato: Development of hydraulic pump drive system using switched reluctance motor with servo function, Journal of Robotics and Mechatronics Vol. 32 No. 5, p. 984-993 (2020)

1.7) Japan Society of Hydraulic and Pneumatics: Oil and pneumatic handbook, ISBN 4-274-08602-X, Ohmsha, Ltd., p. 205-206 (1989) (in Japanese)

1.8) Ge L. Quan, L., Zhang, X. et al: Efficiency improvement and evaluation of electric hydraulic excavator with speed and displacement variable pump, Energy Conversion and Management, Vol. 150, p. 62-71 (2017)

1.9) Willkomm, J, Wahler, M, & Weber, J: Quadratic programming to optimize energy efficiency of speed- and displacement-variable pumps, Proceedings of the 8th FPNI Ph.D Symposium on Fluid Power, Lappeenranta, Finland, V001T05A002, p. 1-10 (2014)

1.10) Willkomm, Johannes, Wahler, Matthias, and Weber, Jürgen: Process-adapted control to maximize dynamics of speed- and displacement-variable

pumps, Proceedings of the ASME/BATH 2014 Symposium on Fluid Power and Motion Control. Bath, United Kingdom, V001T01A015, p. 1-10 (2014)

1.11) Willkomm, J.; Wahler, M.: Potentials of speed and displacement variable pumps in hydraulic applications, In Proceedings of the 10th International Fluid Power Conference, Dresden, Germany, p. 379-391 (2016)

1.12) Vacca, A., Franzoni, G., and Bonati, F.: An inclusive, system-oriented approach for the study and the design of hydrostatic transmissions: The case of an articulated boom lift, SAE Int. J. Commer. Veh. Vol. 1, No. 1, p. 437-445, (2009)

1.13) Montgomery, Alexander J., and Alleyne, Andrew G.: Optimizing the efficiency of electro-hydraulic powertrains, Proceedings of the ASME 2006 International Mechanical Engineering Congress and Exposition. Fluid Power Systems and Technology. Chicago, Illinois, USA. p. 211-219, (2006)

1.14) Kenichi Takaku, Hirokazu Hiraide, Koichi Oba, Application of the “ASR Series” AC servo motor driven hydraulic pump to injection molding machines, Proceedings of the 7th JFPS International Symposium on Fluid Power, Toyama, 2008.

1.15) H. Yamai, M. Kaneda, K. Ohyama, Y. Takeda, and N. Matsui, Optimal Switched Reluctance Motor Drive for Hydraulic Pump Unit, IEEE Conference on Industry Applications, Vol. 3, pp.1555-1562, 2000.

1.16) R. Hamdy, J. Fletcher, and B. W. Williams, Bidirectional Starting of a Symmetrical Two-Phase Switched Reluctance Machine, IEEE Transactions on Energy Conversion, Vol.15, No.2, June 2000.

1.17) L. Gu, W. Wang, B. Fahimi, A. Clark and J. Hearn, Magnetic Design of Two-Phase Switched Reluctance Motor with Bidirectional Startup Capability, in IEEE Transactions on Industry Applications, vol. 52, no. 3, pp. 2148-2155, May-June 2016.

1.18) S. Wei, S. Zhao and J. Zheng, Self-Tuning Fuzzy Control of Switched Reluctance Motor Directly-driven Hydraulic Press, WRI World Congress on Software Engineering, Xiamen, 2009, pp. 461-465.

1.19) J. Ahn and G. F. Lukman, Switched reluctance motor: Research trends and overview, in CES Transactions on Electrical Machines and Systems, vol. 2, no. 4, pp. 339-347, Dec. 2018.

1.20) Miller, TJE, Switched Reluctance Motors and Their Control, Clarendon Press, 1993.

1.22) B. Bilgin, J. W. Jiang, A. Emadi, Switched Reluctance Motor Drives – Fundamentals to Applications, Boca Raton, FL: CRC Press/Taylor & Francis Group, 2019.

1.23) T.Husain, W.Uddin, Y.Sozer, Performance Comparison of Short Pitched and Fully Pitched Switched Reluctance Machines Over Wide Speed Operations, IEEE Energy Conversion Congress and Exposition(ECCE), 2016.

1.23) K. Aiso, K. Akatsu, High Speed SRM using vector Control for Electric Vehicle, CES Transactions on Electrical Machines and Systems, Vol.4, Issue:1, 2020.

1.24) Y. Sato, K. Murakami, Y. Tsuboi, Sensorless Torque and Thrust Estimation of a Rotational/Linear Two Degrees-of-Freedom Switched Reluctance Motor, IEEE Trans. Mag., 52-7, Paper No. 8204504, 2016.

1.25) Y. Sato, Development of a 2-Degree-of-Freedom Rotational/Linear Switched Reluctance Motor, IEEE Trans. Mag, Vol. 43, No. 6, June 2007.

1.26) H. Tanaka, H. Kaminaga, Y. Nakamura, Pressure feedback control based on singular perturbation method of an electro-hydrostatic actuator for an exoskeletal power-assist system, JRM, Vol.24, No.2 2012.

1.27) H. Zhang, X. Liu, J. Wang, H. E. Karimi, Robust H^∞ Sliding Mode Control with Pole Placement for a Fluid Power Electrohydraulic Actuator (EHA) System, Int Adv Manuf Technol, 73:1095-1104, 2014.

1.28) S-H. Hyon, S. Tanimoto, Joint Torque Control of a Hydraulic Manipulator with Hybrid Servo Booster, The 10th JFPS International Symposium on Fluid Power 2017.

1.29) K. Rongjie, J. Zongxia, W. Shaoping and C. Lisha, Design and Simulation of Electro-hydrostatic Actuator with a Built-in Power Regulator, Chinese Journal of Aeronautics, Vol.22, Issue 6, 2009.

1.30) Y. Wang, S. Guo and H. Dong, Modeling and Control of a Novel Electro-Hydrostatic Actuator with Adaptive Pump Displacement, Chinese Journal of Aeronautics, Vol.33, Issue 1, 2020.

1.31) T. Sourander, T. Minav, M. Pietola, H. Hänninen, Sensorless Position Control of Direct Driven Hydraulic Actuators, the 10th JFPS International Symposium on Fluid Power, 2017.

1.32) A. Navatha, K. Bellad, S. S. Hiremath, S. Karunanidhi, Dynamic Analysis of Electro Hydrostatic Actuation System, Global Colloquium in Recent Advancement and Effectual Researches in Engineering, Science and Technology, 2016.

1.33) K. Tsuda, K. Umeda, I. Kota, S. Sakaino and O. Tsuji, Analysis on Rigidity of Hydraulic Hoses for Electro-Hydrostatic Actuators, 43rd Annual Conference of the IEEE Industrial Electronics Society, 2017.

1.34) A. Navatha, S. S. Hiremath, S. Makaram, K. Subramaniam and A. Talukdar, Review on Electro Hydrostatic Actuator for Flight Control, International Journal of Fluid Power, vol.17, 2016.

1.35) Jiang, J.W. et al., Design optimization of switched reluctance machine using genetic algorithm, in Proceedings of the IEEE International Electric Machines and Drives Conference (IEMDC), Coeur d'Alene, ID, May 2015, pp. 1671–1677

Chapter 2

**Improvement of the theoretical
overall efficiency for electro-hydraulic
drive system**

Chapter 2. Improvement of the theoretical overall efficiency for electro-hydraulic drive system

In this chapter, theoretical equations are used to create the energy efficiency maps for servo motor and hydraulic swash plate axial piston pump. Then the overall efficiency maps combined from maps mentioned above are utilized to regulate motor speed and displacement ratio to control the drive system works at high efficiency point.

The EHDS in this study includes a servo system and a variable swash plate piston pump. The overall efficiency of the system will depend on the individual efficiencies; in this section, these efficiencies will be evaluated based on power losses that occur during the working process.

2.1 Power losses and efficiency of EHDS

2.1.1 Model of power losses and efficiency of servo system

The servo system in the EHDS includes a servo amplifier and a servo motor. Three types of dominant losses are present in this system ^{2.1)-2.3)}:

- Copper losses in the electric motor:

$$\Delta P_{Cu} = 3R_M I_M^2 = 3R_M \left(\frac{T_m}{K_T} \right)^2 \quad (2.1)$$

- Iron losses in the electric motor:

$$\Delta P_{Fe} = K_{f1} n_m + K_{f2} n_m^2 \quad (2.2)$$

- Current losses in the amplifier:

$$\Delta P_C = K_C |I_M| = K_C \frac{T_m}{K_T} \quad (2.3)$$

The energy efficiency of servo system is determined by mechanical power at motor shaft and electrical power supplied to servo amplifier.

$$\eta_m = \frac{P_{out}}{P_{in}} = \frac{T_m n_m}{T_m n_m + \Delta P_{Cu} + \Delta P_{Fe} + \Delta P_C} \quad (2.4)$$

From Eqs. (2.1), (2.2), (2.3), it can be seen that the power losses in the servo system depend not only on working parameters (parameters measured during operation such as I_M , T_m and n_m) but also the experimental coefficients K_T , K_{f1} , K_{f2} , and K_C . These values will vary according to control strategy, operation mode, and

the working environment of the motor. Hence, accurately determining the performance of the servo system for a specified working point is difficult (combination of shaft torque T_m and speed n_m).

2.1.2 Model of losses and efficiency in hydraulic pump

The hydraulic pump efficiency includes volumetric and hydraulic-mechanical efficiency and can be determined using Eq. (2.5):

$$\eta_p = \eta_{pv} \eta_{pm} \quad (2.5)$$

a) The volumetric efficiency of hydraulic displacement pump

The volumetric efficiency of pumps will be defined and expressed in terms of the actual deliveries and ideal deliveries. This definition can be placed in mathematical form using the fact that the ideal delivery is $Q_i = (1/2\pi)D(2\pi/60)n_p$ and the leakage flow is Q_s and the loss in delivery due to inlet restriction is Q_R .

$$Q_p = Q_i - Q_s - Q_R \quad (2.6)$$

Q_s is simply the sum of all the elementary leakage flows.

In an axial piston pump: leakages at valve plate – barrel, slipper - swash plate, and piston – slipper bearing are estimated to be proportional to $\Delta p/\mu$, assuming the related geometry constant.

$$Q_{\text{valve plate - barrel}} = \beta_1 \frac{\Delta p}{\mu} \quad (2.7)$$

$$Q_{\text{slipper - swash plate}} = \beta_2 \frac{\Delta p}{\mu} \quad (2.8)$$

$$Q_{\text{piston - slipper bearing}} = \beta_3 \frac{\Delta p}{\mu} \quad (2.9)$$

Where, β_1 , β_2 , and β_3 are dimensional coefficients with the unit of volume. Assuming a coaxial clearance and laminar flow, leakage at one piston – barrel is expressed by the following formula:

$$Q_{\text{piston-barrel}} = \frac{\pi d h^3 \Delta p}{12 \mu l} = \left(\frac{\pi d h^3}{12 l} \right) \frac{\Delta p}{\mu} = \beta_4 \frac{\Delta p}{\mu} \quad (2.10)$$

Where, β_4 is dimensional coefficients with the unit of volume, l is the piston length remaining in the barrel, h is the clearance, and d is the diameter of piston. The mean leakage through the clearance due to reciprocal motion of the piston is ignored.

The displacement per revolution is expressed by:

$$D = \frac{\pi d^2}{4} N \cdot 2R \tan \gamma = \frac{\pi d^2}{4} N \cdot l_{stroke} \quad (2.11)$$

Where N is the piston number, R is the pitch center radius of the pistons, γ is tilting angle of the swash plate, and l_{stroke} is the stroke of the piston.

The mean piston length remaining in the barrel is:

$$l = l_0 + \frac{1}{2} l_{stroke} \quad (2.12)$$

l_0 is the minimum length remaining in the barrel.

Q_s is simply the sum of all the elementary leakage flows expressed as:

$$Q_s = (\beta_1 + \beta_2 + \beta_3 + \beta_4) \frac{\Delta p}{\mu} = \beta \frac{\Delta p}{\mu} \quad (2.13)$$

where β is dimensional coefficients with the unit of volume.

In the reference^{2,4)}, Q_s is defined as the sum of all the elementary leakage flows of a conceptual positive displacement pump and expressed as in the following form:

$$Q_s = C_s \frac{D \Delta p}{2\pi \mu} \quad (2.14)$$

This expression is assumed as the leakage of the pump since C_s is non-dimensional coefficient and β_4 includes components of the displacement.

The definition of volumetric efficiency η_{pv} given above lead to the following equations:

$$\begin{aligned} \eta_{pv} &= \frac{Q_p}{Q_i} = \frac{(1/2\pi) D \cdot (2\pi/60) n_p - C_s \frac{(1/2\pi) D \Delta p}{\mu} - Q_R}{(1/2\pi) D \cdot (2\pi/60) n_p} \\ &= 1 - \frac{C_s \Delta p}{(2\pi/60) \mu n_p} - \frac{Q_R}{(1/2\pi) D \cdot (2\pi/60) n_p} \end{aligned} \quad (2.15)$$

where C_s represents a geometrical constant of the pump, D is the displacement per revolution of the pump, n_p is the rotational speed of the pump with the unit of rpm, Δp is the pressure differential across the pump, μ is the coefficient of viscosity.

If Q_R is neglected, the volumetric efficiency is expressed simply as below:

$$\eta_{pv} = 1 - \frac{C_s \Delta p}{(2\pi/60)n_p \mu} \quad (2.16)$$

The equation (2.16) is the volumetric efficiency for fixed displacement pumps.

According to references^{2.5), 2.6)}, for variable displacement pumps, the effect of displacement ratio $\alpha = D/D_{\max}$ should be considered in the volumetric efficiency equation:

$$\eta_{pv} = 1 - \frac{C_s \Delta p}{\mu (2\pi/60)n_p \alpha} \quad (2.17)$$

Although Equation of volumetric efficiency is presented in series of different forms^{2.7)-2.10)}, but the target of this study is not to compare the volumetric efficiency equations together, so the equation (2.17) was used to create the simulation data for this research.

b) The mechanical efficiency (torque efficiency) of positive displacement pump.

In a positive displacement pump, there distinct types of torques must be considered.

- Viscous torque T_v results from viscous shear.
- Friction torque T_f is due to friction originating at the contact of surfaces moving relative to each other
- Constant torque T_c results from the forces that arise on surfaces in close contact and is independent of the unbalanced pressure forces.

Viscous torque T_v may be expressed in the following equation:

$$T_v = \left(C_v \frac{D}{2\pi} \right) \mu (2\pi/60)n_p \quad (2.18)$$

where C_v is a coefficient of viscous drag dependent upon the pump geometry, and, μ and n_m have been defined previously. C_v is a non-dimensional coefficient and $C_v D/2\pi$ is a dimensional with the unit of volume. D is the displacement but is used as a representative typical geometry of the pump.

Friction torque T_f is the function of the resultant hydraulic forces and the geometry of the pump.

$$T_f = \left(C_f \frac{D}{2\pi} \right) \Delta p \quad (2.19)$$

where C_f is a coefficient of friction dependent upon the pump geometry, and Δp has been defined previously. C_f a non-dimensional coefficient and $C_f D/2\pi$ is a

dimensional with the unit of volume. D is the displacement but is used as a representative typical geometry of the pump.

The total torque T_p required to drive a pump can be expressed in terms of the ideal torque $T_i = \Delta p D / 2\pi$ and the torques listed above as:

$$T_p = \frac{\Delta p D}{2\pi} + C_v \mu (2\pi/60) n_p + C_f \Delta p + T_c \quad (2.20)$$

The definitions of mechanical efficiency η_{pm} can be expressed as the following equations:

$$\begin{aligned} \eta_{pm} &= \frac{T_i}{T_p} = \frac{\frac{\Delta p D}{2\pi}}{\frac{\Delta p D}{2\pi} + C_v \left(\frac{D}{2\pi}\right) \mu \left(\frac{2\pi}{60}\right) n_p + C_f \left(\frac{D}{2\pi}\right) \Delta p + T_c} \\ &= \frac{1}{1 + \left\{ C_v \left(\frac{D}{2\pi}\right) \mu \left(\frac{2\pi}{60}\right) n_p + C_f \left(\frac{D}{2\pi}\right) \Delta p + T_c \right\} \frac{2\pi}{\Delta p D}} \\ \eta_{pm} &= \frac{1}{1 + \left\{ C_v \left(\frac{2\pi}{60}\right) \frac{\mu n_p}{\Delta p} + C_f + \frac{2\pi T_c}{\Delta p D} \right\}} \end{aligned} \quad (2.21)$$

According to references^{2.5),2.6)}, for variable displacement pumps, the effect of displacement ratio $\alpha = D/D_{\max}$ should be considered in the torque efficiency equation:

$$\eta_{pm} = \frac{1}{1 + \left\{ \frac{C_v}{\alpha} \left(\frac{2\pi}{60}\right) \frac{\mu n_p}{\Delta p} + \frac{C_f}{\alpha} + \frac{2\pi T_c}{\Delta p D_{\max} \alpha} \right\}} \quad (2.22)$$

According to reference^{2.6)}, for variable displacement axial piston pumps, the coefficient C_v can be expressed as following:

$$C_v = C_{v1} \alpha^2 + C_{v2}$$

Therefore, the equation (2.22) can be written as following:

$$\eta_{pm} = \frac{1}{1 + \left\{ (C_{v1} \alpha^2 + C_{v2}) \left(\frac{2\pi}{60}\right) \frac{\mu n_p}{\Delta p} + C_f + \frac{2\pi T_c}{\Delta p D_{\max}} \right\} \frac{1}{\alpha}} \quad (2.23)$$

Although Equation of mechanical-hydraulic efficiency is presented in series of different forms^{2.7)-2.10)}, but the target of this study is not to compare these

efficiency equations together, so the equation (2.23) was used to create the simulation data for this research.

It is apparent from Eqs. (2.17) and (2.23) that, similar to servo systems, the efficiency of hydraulic pumps is the function of not only the working parameters Δp , μ , n_p , and α but also the experimental parameters C_s , C_{v1} , C_{v2} , C_f , and T_c . To determine the value of those experimental parameters, conducting many experiments and analyzing the experimental data using approximate methods is necessary. Moreover, when Eqs. (2.17) and (2.23) are used, considering the effect of flow loss due to the inlet restriction on the operating process of the hydraulic pump is not possible. As a result, using these equations to set up the control system to optimize the overall performance of the system for a given operating point is difficult. Furthermore, the required speed of the hydraulic pump exhibits a significant effect on the performance of the servo motor. Therefore, considering the interaction between all component efficiencies in the drive system is necessary, namely the interaction between the servo motor and hydraulic pump.

2.2 Energy efficiency map of EHDS

The proper controllers of any servo system and piston pump in an EHDS must be implemented to maximize overall efficiency. These controllers will often operate the servo motor and piston pump at the most efficient point for a given power requirement. To do so, the servo system and piston pump characteristics must be understood, and this is best done by creating an efficiency map. An efficiency map is a chart that shows how the efficiency changes based on output power. It involves operating the equipment at all possible torque and speed points. In existing control methods for improving transmission efficiency, an efficiency map has been effectively used to save energy^{2.11)-2.14)}.

2.2.1 Efficiency map of electric motor

To make an efficiency map of a servo motor and hydraulic pump, a series of experiments must be conducted, especially for typical working points of equipment. However, the aim of this chapter is only to validate the effectiveness of the proposed control strategy; as such, simulation efficiency maps were created using the efficiency equations in Sections 2.1.1 and 2.1.2 and the assumed power unit specifications in Table 2.1.

The experimental parameters in the efficiency equations were chosen by referring to the performance characteristic curves of the servo motor and hydraulic

piston pump^{2.6),2.7),2.15),2.16)}. The efficiency map of servo system is shown in Figure 2.1.

Table 2.1. Specifications of the simulation power unit

Component	Specification
Servo motor	Rated output: 12.5 kW Rated torque: 60 Nm Rated speed: 1500 rpm Maximum speed: 3000 rpm
Hydraulic pump	Swash plate axial piston pump Displacement: 16.3 cm ³ /rev Rated operating pressure: 28 MPa Shaft speed: 600~3600 rpm

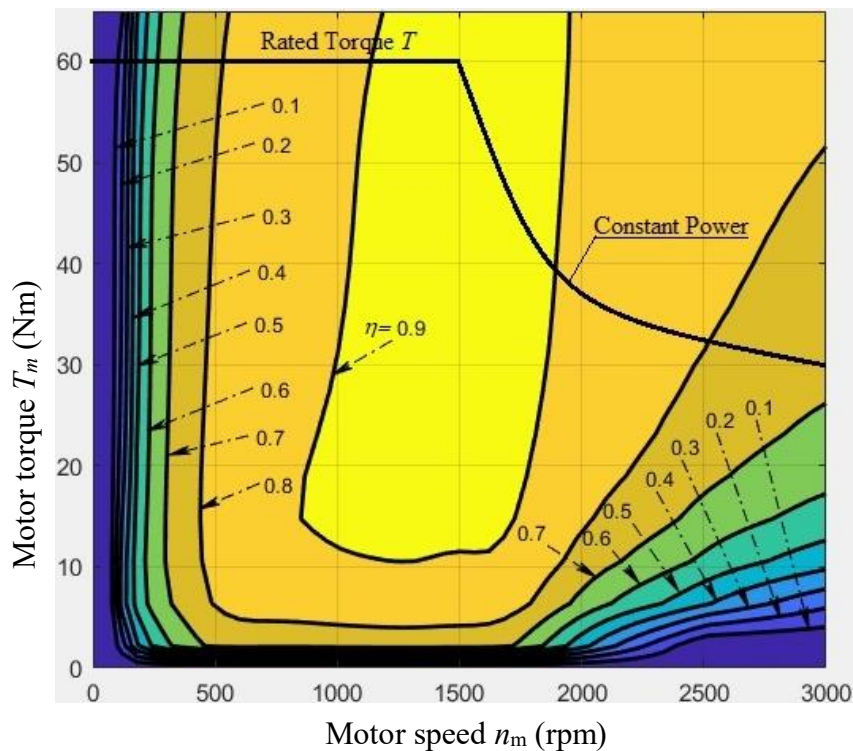


Fig. 2.1 Typical servo motor efficiency map

2.2.2 Efficiency map of hydraulic pump

To create the efficiency data, the working ranges of the servo motor and piston pump were constrained. Based on the specifications in Table 2.1 and the

controllability of motor speed, the limits of the working parameters in that drive system were as follows:

$$\text{Servo motor: } \begin{cases} P_m \leq 25 \text{ kW} \\ T_m \leq 64 \text{ Nm} \\ 0 < n_m \leq 3000 \text{ rpm} \end{cases} \quad (2.24)$$

$$\text{Hydraulic piston pump: } \begin{cases} \Delta p \leq 28 \text{ MPa} \\ 0.2 \leq \alpha \leq 1 \\ 0 < n_p \leq 3000 \text{ rpm} \end{cases} \quad (2.25)$$

To reduce the complexity of creating a pump efficiency map, the displacement ratio α was set as a discrete parameter. In other words, the series of value α is 0.2; 0.25; 0.3; 0.35; 0.4; 0.45; 0.5; 0.55; 0.6; 0.65; 0.7; 0.75; 0.8; 0.85; 0.9; 0.95 and 1. Hence, the number of pump efficiency maps is 17, whereas a single motor efficiency map exists. Due to the difference of displacement ratio α , the pressure and flow rate limits in the pump efficiency maps differ from one another.

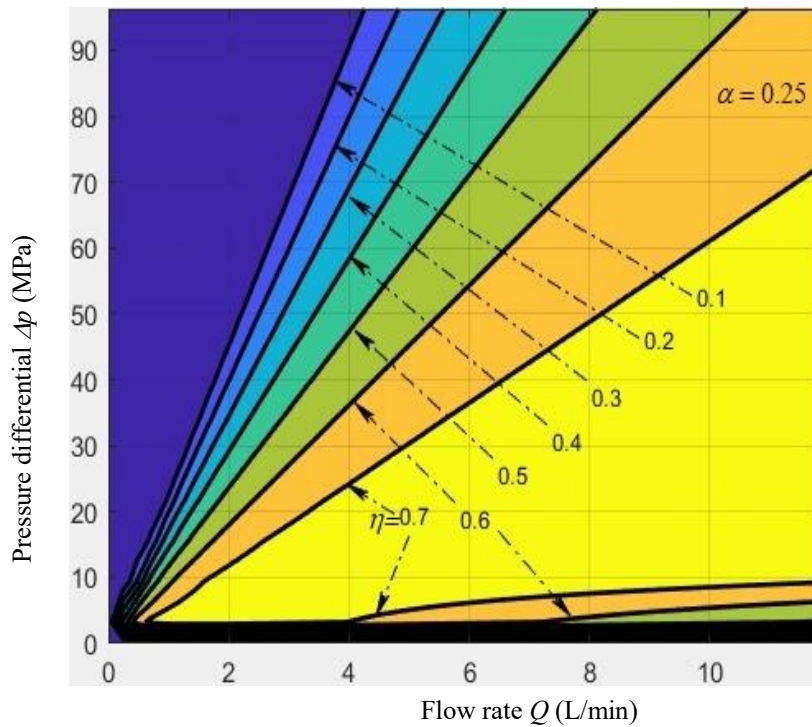


Fig.2.2. Efficiency map of hydraulic piston pump with $\alpha = 0.25$

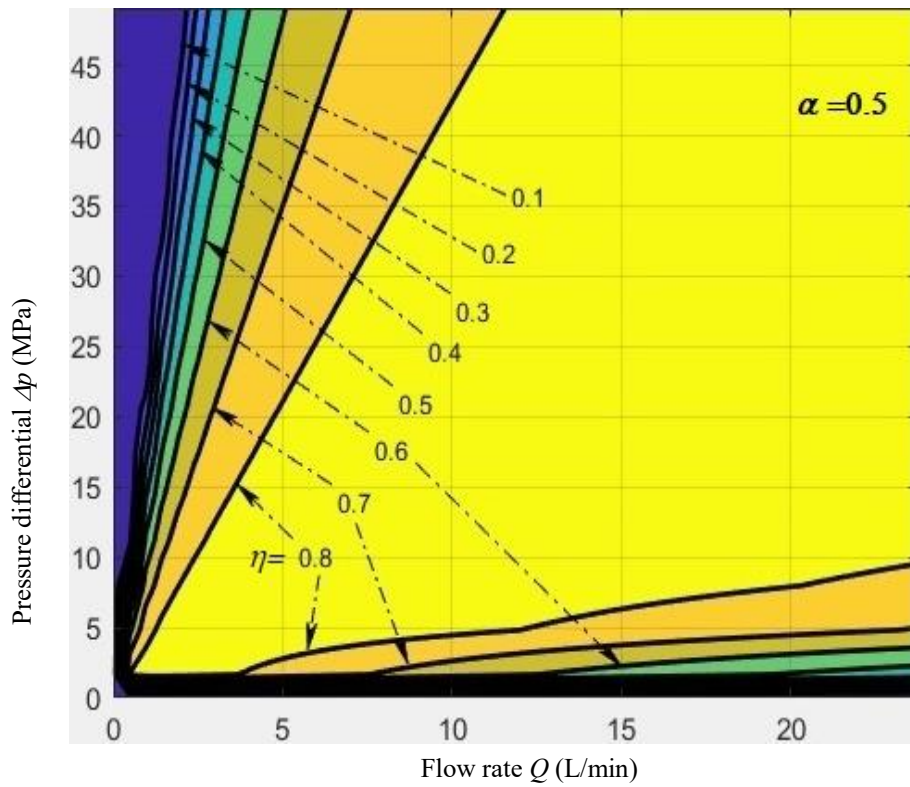


Fig.2.3. Efficiency map of hydraulic piston pump with $\alpha = 0.5$

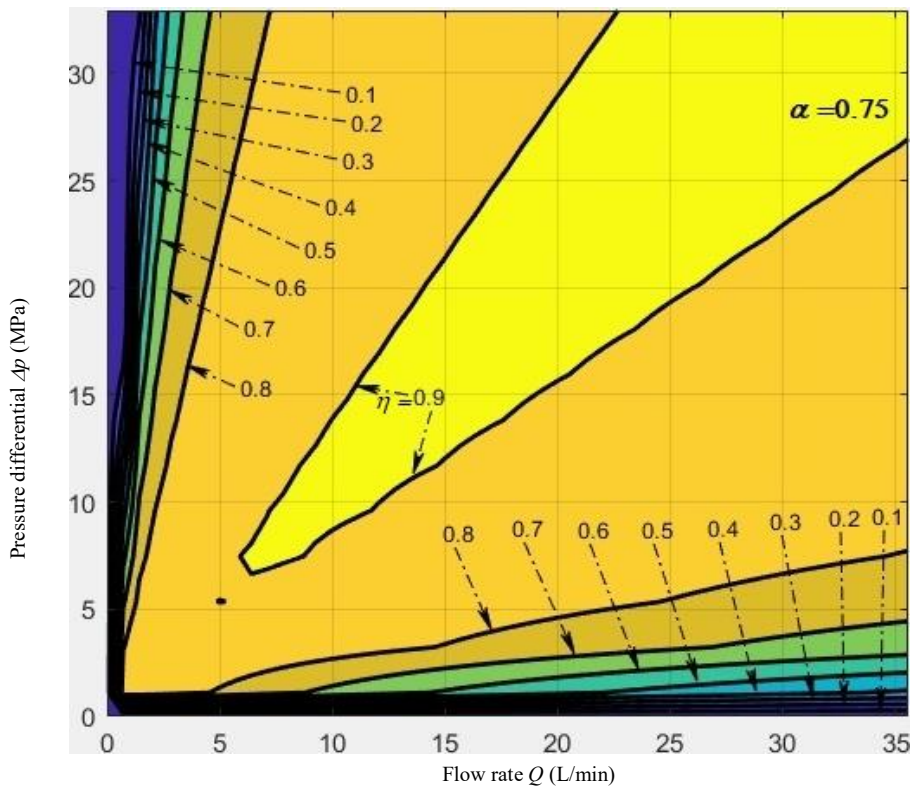


Fig.2.4. Efficiency map of hydraulic piston pump with $\alpha = 0.75$

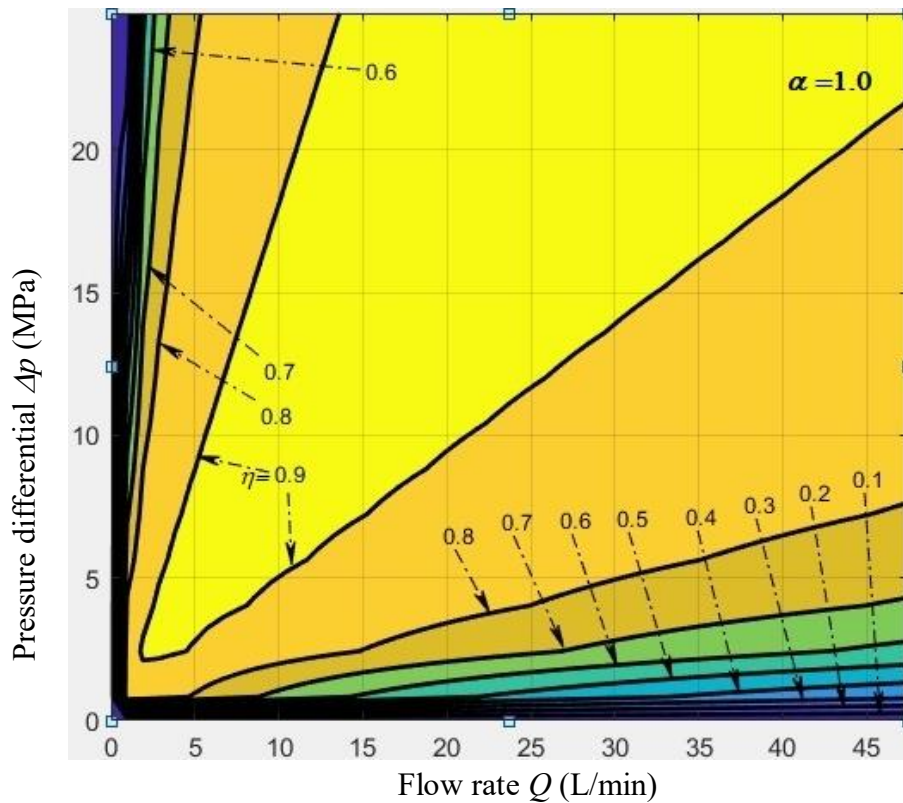


Fig.2.5. Efficiency map of hydraulic piston pump with $\alpha = 1$

The efficiency maps of hydraulic piston pump (at typical values of displacement ratio) are shown in Figures 2.2. As shown in Figure 2.1, the motor efficiency reaches the highest values when the speed is near the rated value 1500 rpm and the output torque is higher than 10 Nm. Moreover, the motor efficiency decreases quickly at a low-speed range and small torque range. However, it can be seen from the efficiency maps in Figures 2.2 to 2.5 that the efficiency of the hydraulic pump at the maximum displacement ratio ($\alpha = 1$) is higher than that of smaller displacement ratios. In other words, for increased efficiency, the hydraulic pump should be operated at maximum displacement.

Regarding the efficiency maps in Figures 2.2 to 2.5, there are some contour lines with low smoothness as efficiency $\eta_p = 0.9$ lines in Figure 2.4 and 2.5. Moreover, there is an irregular area in Figure 2.4 which may lead to some inaccurate values of efficiency. To improve these issues, the number of simulation points in these maps is increased from 16 points to 300 points and the comparison of two maps as shown in Figure 2.6. Although the number of simulation points is increased, the shape of contour lines and efficiency values are almost not changed.

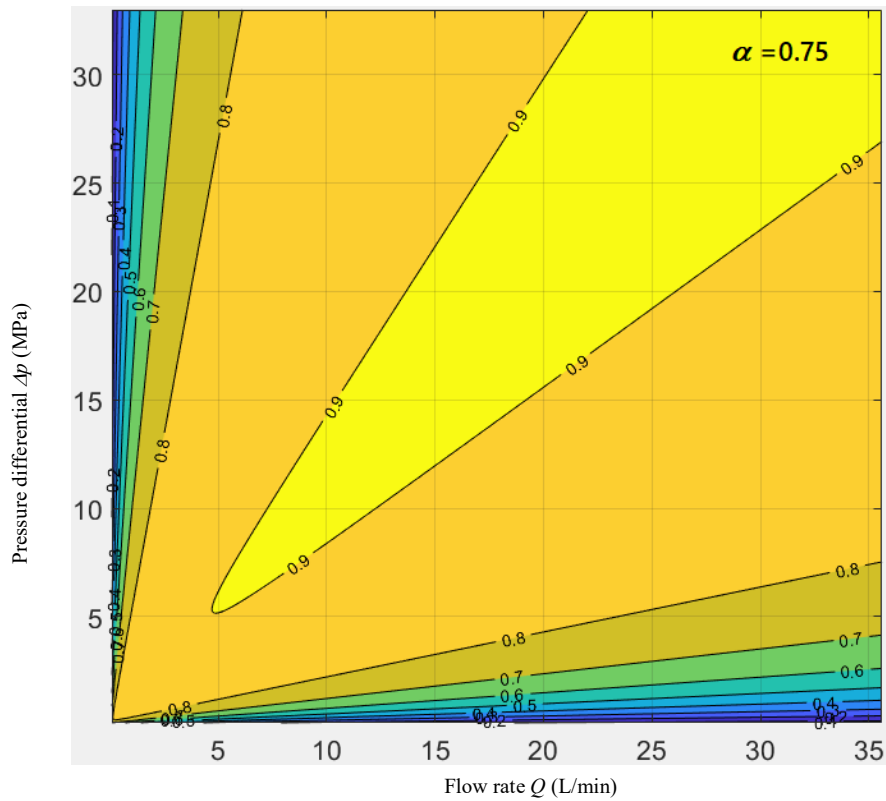


Fig.2.6. Efficiency map of hydraulic piston pump with $\alpha = 0.75$

From the Figures 2.2 to 2.5, for a given flow rate Q , there are series of combinations of motor speed n_m and pump displacement ratio α . If the hydraulic pump is operated at $\alpha = 1$ to achieve the highest efficiency value, the motor speed n_m must be reduced to achieve the required flow rate Q . This results in decreased motor efficiency and overall efficiency. This issue also occurs when the opposite solution is implemented, in which the motor speed remains at the rated value, and the displacement ratio is controlled to produce a sufficient flow rate. This could result in an efficient motor but a less efficient hydraulic pump. From the above discussion, it can be seen that, when studying the overall efficiency of an EHDS, the interaction between the servo motor speed n_m and displacement ratio of the hydraulic pump α should be considered entirely in working range of these parameters. This issue will be solved by utilizing the overall efficiency maps, which were created by combining the individual efficiency maps (servo motor and hydraulic pump) and will be presented in Section 2.3.

In this study, the efficiency maps were made by using theoretical equations, so the effect of transient characteristics on servo motor and flow loss due to the inlet restriction on hydraulic pump are not considered. Experimental efficiency

maps, which are established by experimental data, could consider properly these effects.

2.3 Simulation improvement of the overall efficiency for EHDS

The overall efficiency of the EHDS in this research is determined by servo system efficiency and hydraulic piston pump efficiency.

$$\eta_t = \eta_m \eta_p \quad (2.26)$$

Using Eq. (2.26), the overall efficiency map was established by combining the axes from efficiency maps of the servo system (amplifier and motor) and hydraulic piston pump, as shown in Figure 2.7. The coordinate axes of the servo system efficiency map (torque T_m and speed n_m) were converted to pressure differential Δp and flow rate Q using Eqs. (2.27) and (2.28), respectively, for a given displacement ratio value. In this stage, η_{pm} and η_{pv} were assumed as not affected by the values of Q and Δp , respectively. In the next stage, these efficiencies were determined by experimental data corresponding to a given working point (Δp , Q). The overall efficiency maps for typical displacement values are shown in Figure 2.8 to 2.11.

$$\Delta p = \frac{2\pi T_m \eta_{pm}}{D_{\max} \alpha} \quad (2.27)$$

$$Q = n_m D_{\max} \alpha \eta_{pv} \quad (2.28)$$

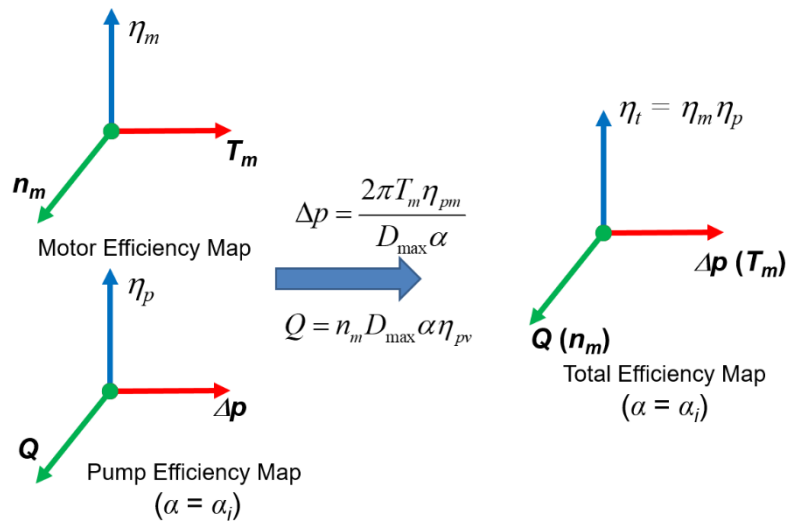


Fig. 2.7. Combination of individual efficiency maps

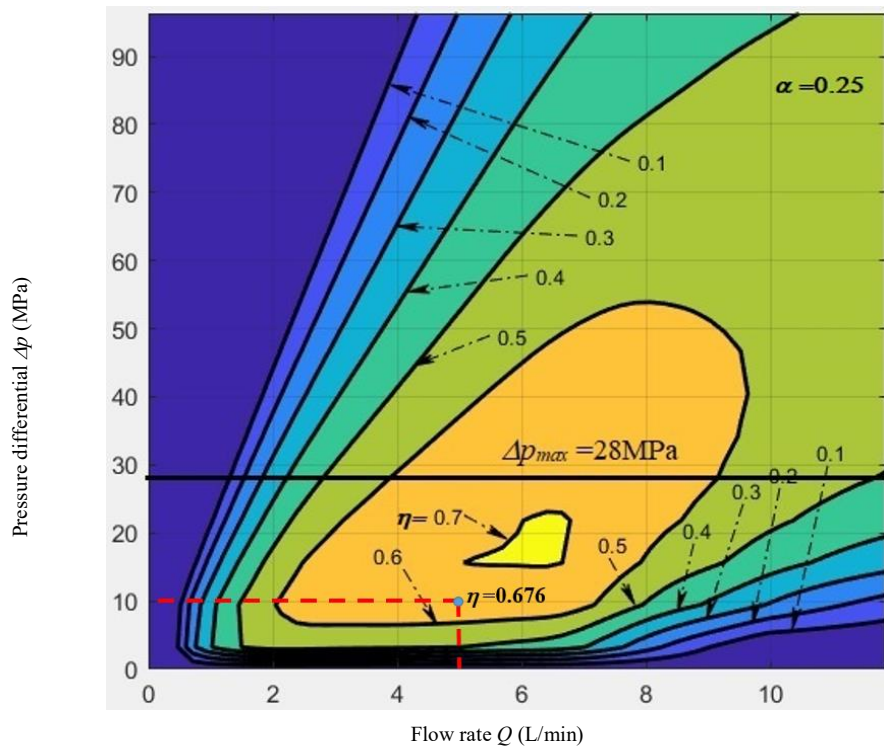


Fig. 2.8. Overall efficiency map of EHDS with $\alpha = 0.25$

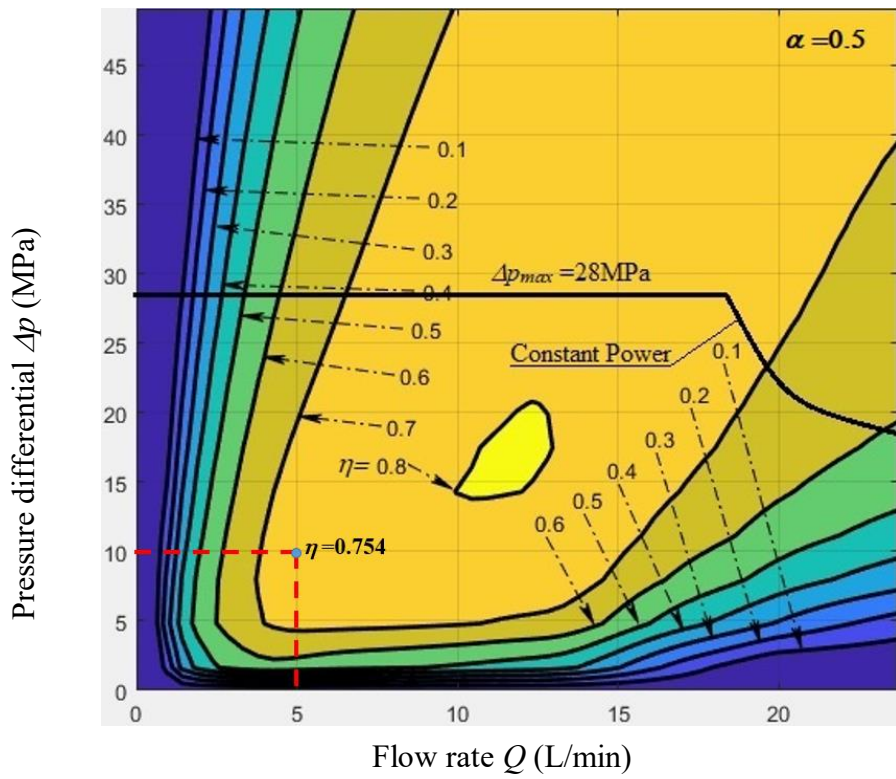


Fig. 2.9. Overall efficiency map of EHDS with $\alpha = 0.5$

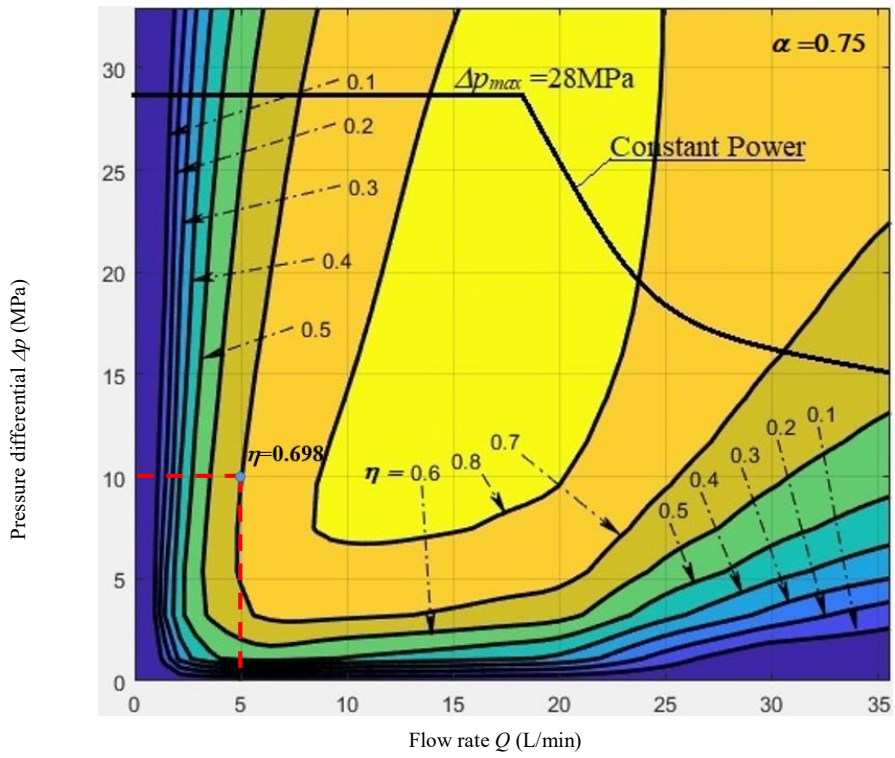


Fig. 2.10. Overall efficiency map of EHDS with $\alpha = 0.75$

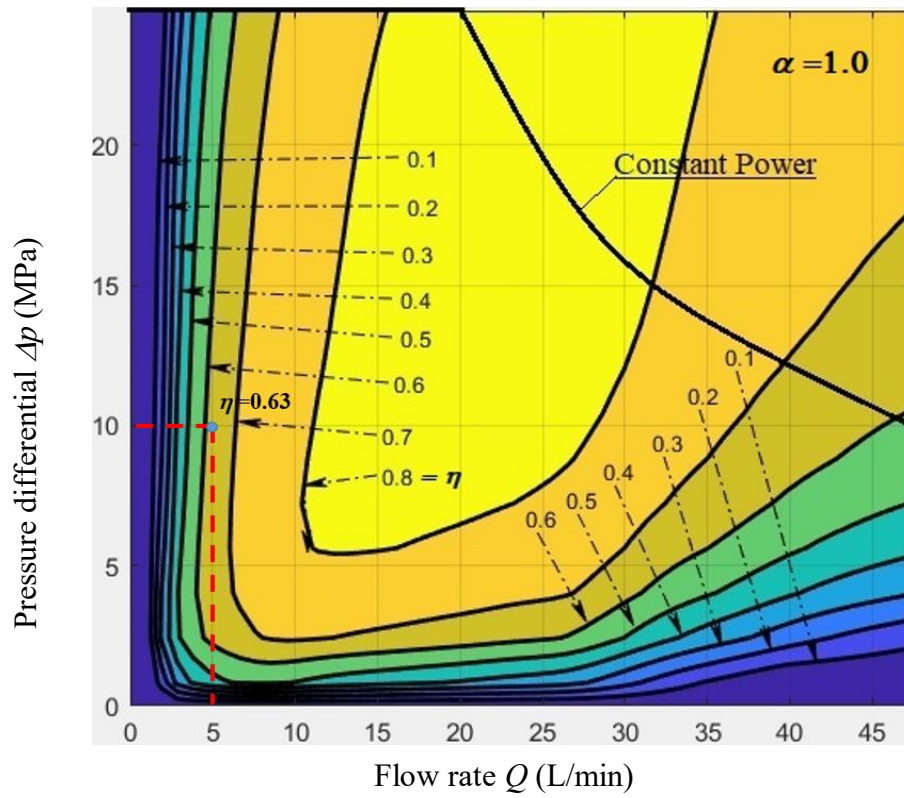


Fig. 2.11. Overall efficiency map of EHDS with $\alpha = 1$

To analyze the overall efficiency maps in Figure 2.8 to 2.11, the working point with $Q = 5 \text{ L/min}$, $\Delta p = 10 \text{ MPa}$ was taken as an example. The overall efficiency of EHDSs with different ratios α is shown in Table 2.2.

Table 2.2. Overall efficiency of the EHDS for the given working point with $Q = 5 \text{ L/min}$, $\Delta p = 10 \text{ MPa}$

Displacement ratio α	0.25	0.5	0.75	1
Overall efficiency η_t	0.676	0.754	0.698	0.63
Motor speed n_m rpm	1265	632.5	421.6	316.2
Motor torque T_m Nm	6.745	13.23	19.72	26.2

It can be seen that the overall efficiency achieves the highest value at $\alpha = 0.5$, although, in this case, the efficiencies of neither the servo motor nor the hydraulic pump are maximum values. The efficiency of pump with $\alpha = 1$ was higher than that with $\alpha = 0.5$; however, motor speed n_m and motor efficiency decreased. In this study, if the efficiency of the servo motor and hydraulic pump are taken into account separately, the system will not reach the highest efficiency.

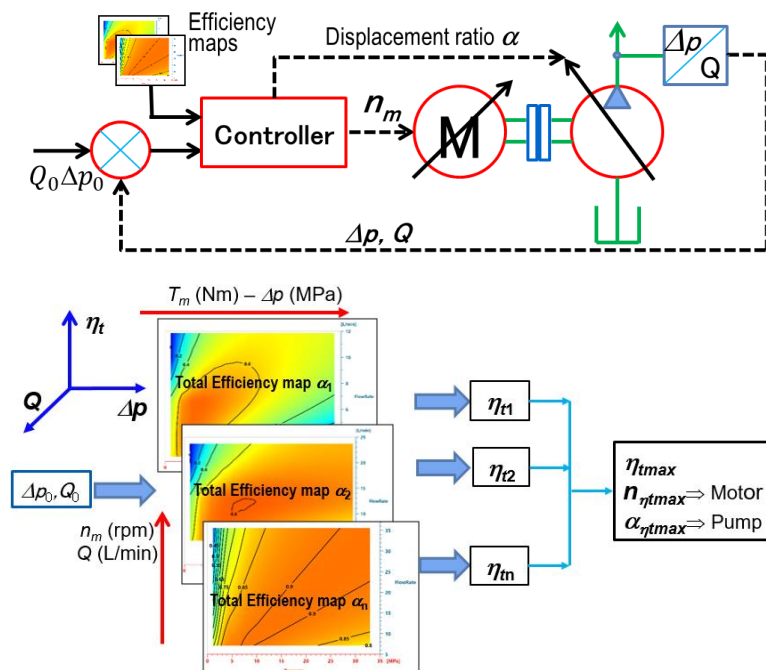


Fig. 2.12. Control strategy for improving overall efficiency

To improve the overall efficiency of the hydraulic power unit compared with the conventional one, the control system in Figure 2.12 was proposed to control the motor speed n_m and displacement ratio α simultaneously. The target of this system is to optimize overall efficiency by regulating n_m and α for specified given working conditions (Δp , Q) based on the data of the overall efficiency maps. In other words, for a given value of Δp , Q the controller will determine the value of efficiency in every single overall efficiency map ($\alpha = \alpha_i$) and then compare these values while still considering the given constraints in Section 2.2.2. The working parameters (n_m , α) were determined when the map was at its highest efficiency for the corresponding working point. Using overall efficiency maps, the EHDS could be controlled at this operating point. Moreover, the flexibility of n_m and α could help the system operate within its permitted working range (motor speed and torque, hydraulic pump speed and pressure) and thus avoid overloading in the servo motor and hydraulic pump.

To evaluate the advantages of the proposed control strategy, numerical simulation was implemented for a series of working points using the simulation power unit detailed in below. The efficiency of the working points for three cases were determined and compared:

Case 1: (VS-FP) ($\alpha = \alpha_{\max}$)

Case 2: (FS-VP) ($n_m = n_{\text{rated}}$)

Case 3: (VS-VP)

Normally, in an EHDS, an induction motor is used as the constant rotation speed motor. The efficiency of the induction motor is inferior to that of the servo motor with a permanent magnet over the entire operating range. However, this study does not compare efficiencies due to differences in motor types, so a servo motor operating at its rated speed serves as the constant rotation speed motor (Case 2). The simulation results regarding flow control mode and pressure control mode are shown in Figures 2.13 and 2.22, respectively.

In the flow control model (Figure 2.12 to 2.16), the VS-VP unit achieved better overall efficiency than others at almost all given working points because of the flexibility of both n_m and α . The advantage of the VS-VP unit can be seen clearly at a low flow rate range ($Q = 5\sim 12$ L/min). Considering the work point of $Q = 5$ L/min; $\Delta p = 24$ MPa, the efficiency of the VS-VP unit is 7% and 4% higher than that of the VS-FP unit and FS-VP unit, respectively. These differences were

up to 6% and 25%, respectively, in the case of working point with $Q = 5$ L/min; $\Delta p = 4$ MPa. When comparing the efficiency of VS-VP unit with VS-FP unit in the high pressure and low flow operation with $Q < 9$ L/min; $\Delta p > 12.5$ Mpa, the variance in overall efficiency of the VS-VP and VS-FP units is up to 7%. This could be explained by the decrease of motor efficiency at low speed, although the hydraulic pump of the VS-FP unit operates at maximum displacement (i.e., maximum pump efficiency).

In case of FS-VP unit, even though servo motor operates at a rated speed (i.e., high motor efficiency), its overall efficiency is significantly lower than that of the VS-VP unit due to the change of ratio α , which exhibits a noticeable effect on the efficiency of the hydraulic pump. The overall efficiencies of all units are nearly identical at a large flow rate range since the hydraulic pump and servo motor must operate at maximum ratio $\alpha = 1$ and rated speed, respectively, to achieve the necessary flow rate Q .

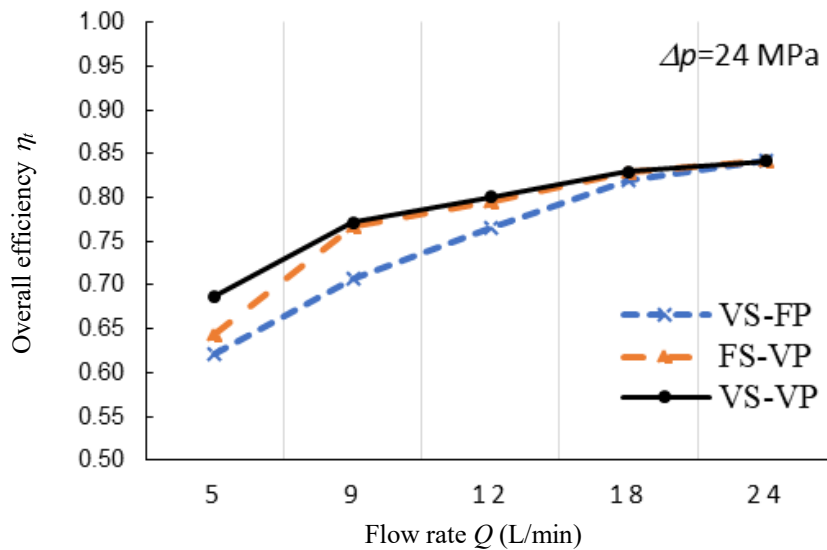


Fig. 2.13. Overall efficiency η_i comparison at pressure differential $\Delta p = 24$ MPa

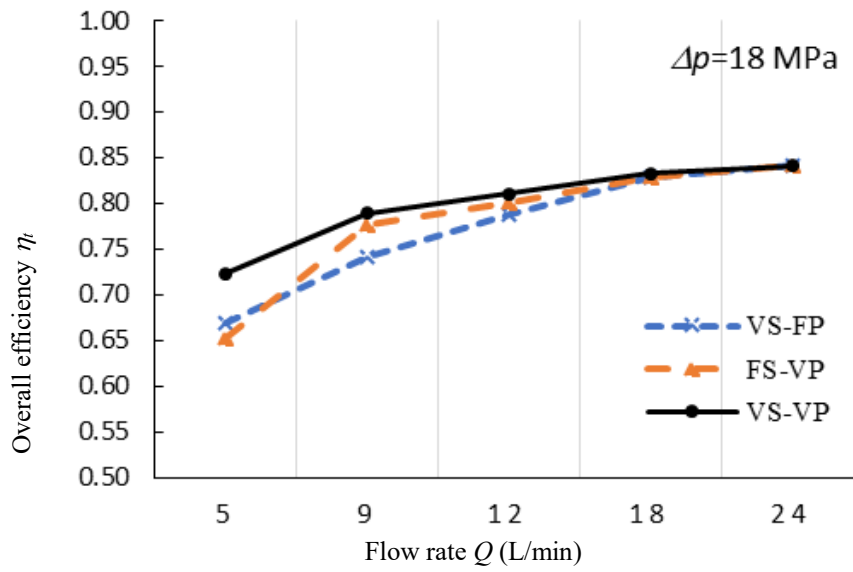


Fig. 2.14. Overall efficiency η_i comparison at pressure differential $\Delta p = 18$ MPa

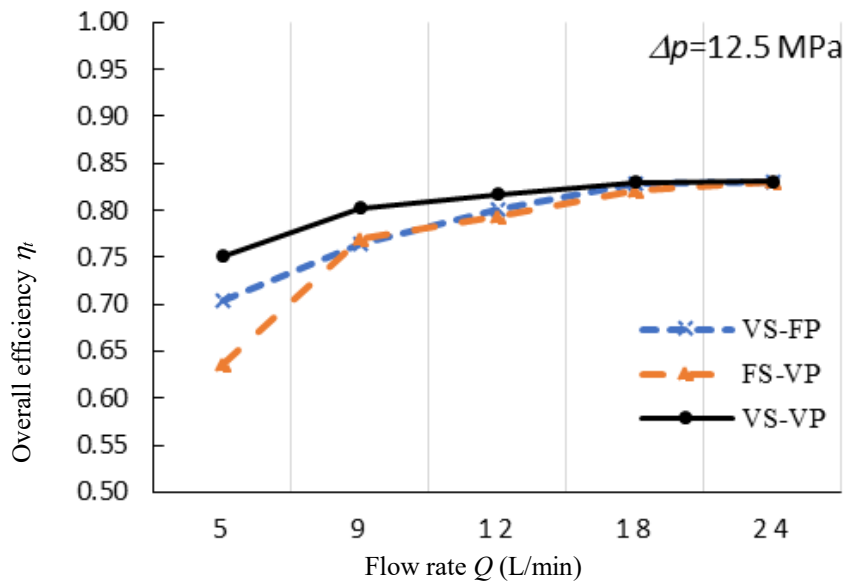


Fig. 2.15. Overall efficiency η_i comparison at pressure differential $\Delta p = 12.5$ MPa

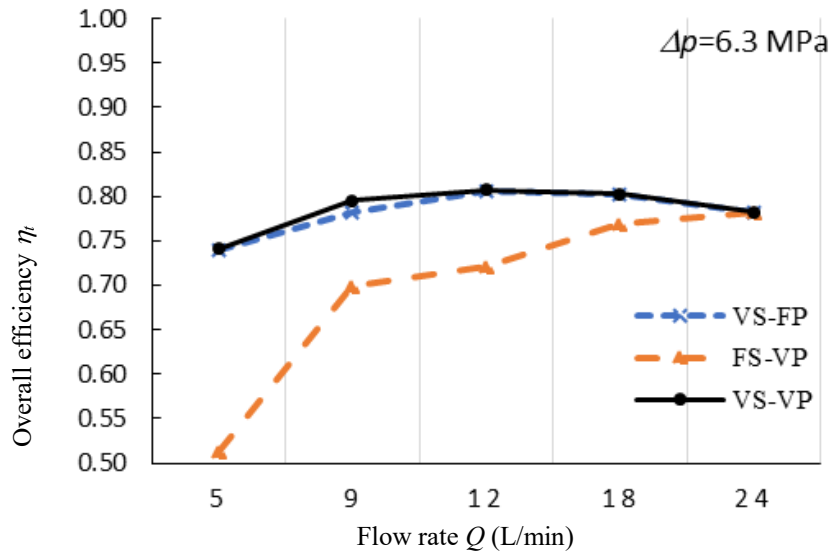


Fig. 2.16. Overall efficiency η_i comparison at pressure differential $\Delta p = 6.3$ MPa

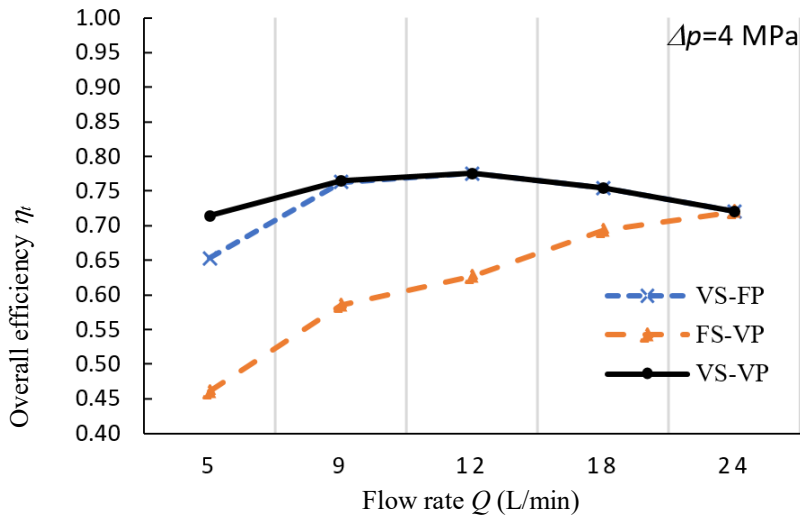


Fig. 2.17. Overall efficiency η_i comparison at pressure differential $\Delta p = 4$ MPa

In the pressure control model (Figure 2.18 to 2.22), the VS-Vp unit is still the most efficient system at almost all required power points because of the flexibility of both n_m and α . At a low flow rate operation, VS-Vp offers better η_i for both the low and high pressure mode because both n_m and α are changed. The range of efficiency in the VS-Vp unit remains 0.7~0.8 and, unlike in the FS-VP unit, does not decline when the pressure differential decreases. As shown in Figure 2.7, the FS-VP unit is the least efficient unit since the pump often works at low

displacement. However, at a low flow rate range ($Q = 5\sim 9$ L/min), the overall efficiency of all units decreased significantly when the pressure differential Δp increases. This could be explained by the increase of hydraulic oil leakage in the hydraulic pump at the high pressure.

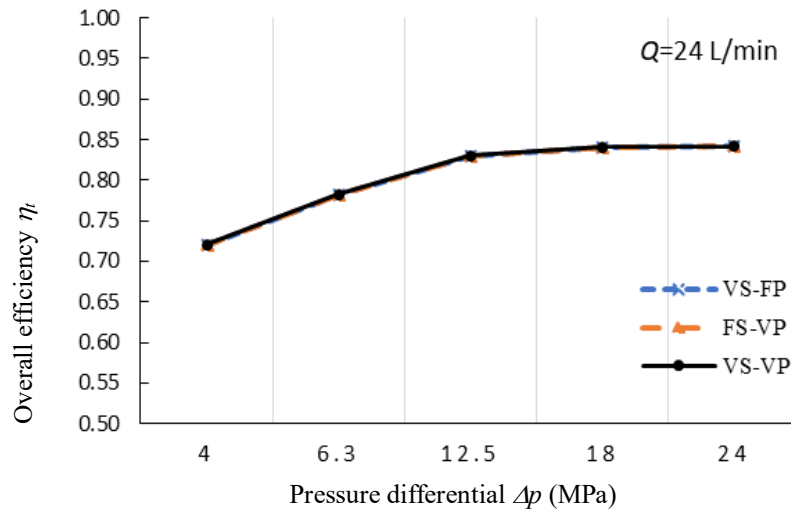


Fig. 2.18. Overall efficiency η_t comparison at output flow rate $Q = 24$ L/min

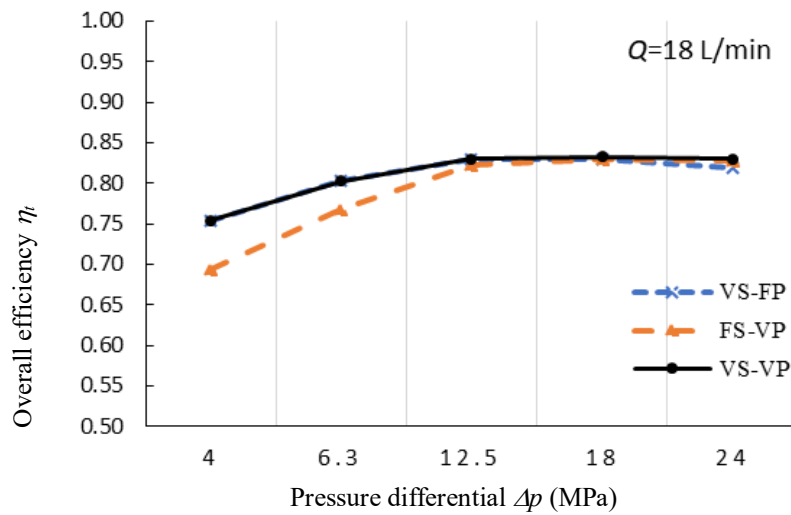


Fig. 2.19. Overall efficiency η_t comparison at output flow rate $Q = 18$ L/min

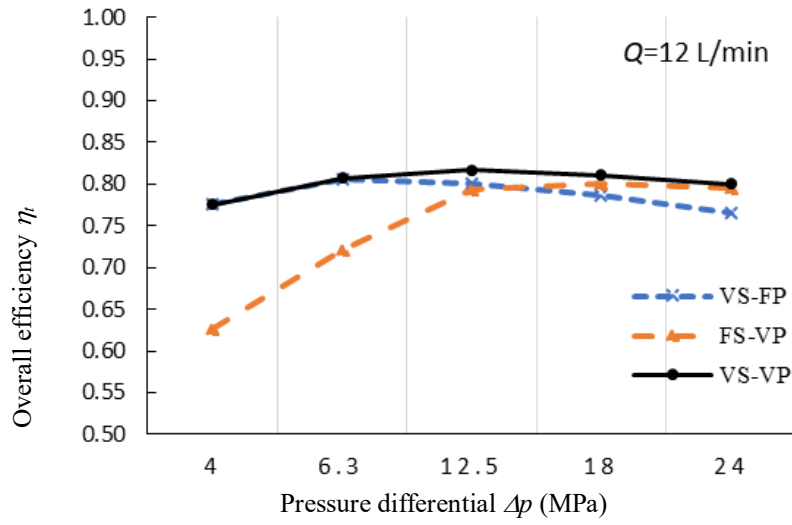


Fig. 2.20. Overall efficiency η_i comparison at output flow rate $Q = 12$ L/min

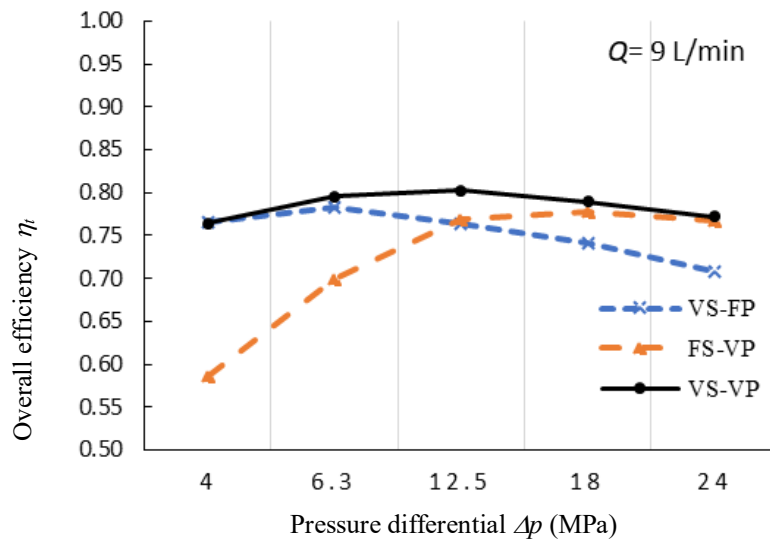


Fig. 2.21. Overall efficiency η_i comparison at output flow rate $Q = 9$ L/min

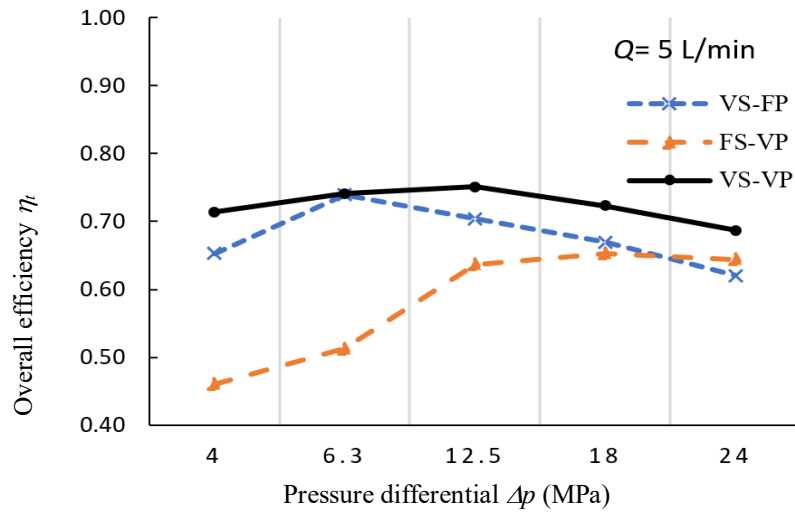


Fig. 2.22. Overall efficiency η_i comparison at output flow rate $Q = 5 \text{ L/min}$

2.4 Summary of Chapter 2

- A novel control strategy was proposed to improve the overall efficiency of an EHDS by overall efficiency maps. By these maps, interaction between motor and pump could be considered properly.
- Based on the overall efficiency maps, the optimized values of the working parameters (motor speed and pump displacement ratio) can be determined to achieve the highest efficiency for a given working point. This method is simpler than method using mathematical function in previous research.
- The simulation results show that the efficiency of the proposed control strategy was improved significantly compared with conventional single-variable power units.
- To verify these results, the experiment will be conducted in Chapter 3.

2.5 References

2.1) Willkomm, J, Wahler, M, & Weber, J: Quadratic programming to optimize energy efficiency of speed- and displacement-variable pumps, Proceedings of the 8th FPNI Ph.D Symposium on Fluid Power, Lappeenranta, Finland, V001T05A002, p. 1-10 (2014)

2.2) Willkomm, Johannes, Wahler, Matthias, and Weber, Jürgen: Process-adapted control to maximize dynamics of speed- and displacement-variable pumps, Proceedings of the ASME/BATH 2014 Symposium on Fluid Power and Motion Control. Bath, United Kingdom, V001T01A015, p. 1-10 (2014)

2.3) Willkomm, J.; Wahler, M.: Potentials of speed and displacement variable pumps in hydraulic applications, In Proceedings of the 10th International Fluid Power Conference, Dresden, Germany, p. 379-391 (2016)

2.4) Wilson, W.E., Positive Displacement Pumps and Fluid Motors, (1950), Pitmann, New York.

2.5) D McCandlish and R E Dorey, The Mathematical Modelling of Hydrostatic Pumps and Motors, Proceedings of the Institution of Mechanical Engineers, Part B: Journal of Engineering Manufacture, 1984.

2.6) Japan Society of Hydraulic and Pneumatics: Oil and pneumatic handbook, ISBN 4-274-08602-X, Ohmsha, Ltd., p. 205-206 (1989) (in Japanese)

2.7) Ivantysyn, J. and Ivantysynova, M.: Hydrostatic pumps and motors, principles, designs, performance, modelling, analysis, control and testing, New Delhi. Academia Books International, ISBN -81-85522-16-2, p. 78-90 (2001)

2.8) Hall, Samuel Jason, Statistical analysis of multiple hydrostatic pump flow loss models, (2014). Graduate Theses and Dissertations. 13753.

2.9) Dorey, R., 1988, Modelling of losses in pumps and motors, 1st Bath International Fluid Workshop, University of Bath.

2.10) Manring, Noah D., Fluid Power Pumps and Motors: Analysis, Design and Control, US: McGraw-Hill Professional, 2013.

2.11) Gang, L., & Zhi, Y.: Energy saving control based on motor efficiency map for electric vehicles with four-wheel independently driven in-wheel motors, Advances in Mechanical Engineering Vol. 10, No. 8 p. 1-18 (2018)

2.12) Qiu, L., Qian, L., Abdollahi, Z. et al.: Engine-map-based predictive fuel-efficient control strategies for a group of connected vehicles, *Automot. Innov.* 1, p. 311-319 (2018)

2.13) Feroldi, D., Serra, M., & Riera, J.: Energy management strategies based on efficiency map for fuel cell hybrid vehicles, *Journal of Power Sources*, 190, p. 387-401 (2009)

2.14) Mahmoudi, Amin & Soong, Wen & Pellegrino, Gianmario & Armando, Eric.: Efficiency maps of electrical machines, *IEEE Energy Conversion Congress and Exposition (ECCE)*, p. 2791-2799 (2015)

2.15) <https://www.mitsubishielectric.co.jp> (accessed on 1 August, 2020)

2.16) <https://www.yuken.co.jp> (accessed on 1 August, 2020)

Chapter 3

**Experimental validation of
improvement of the overall efficiency
for electro-hydraulic drive system**

Chapter 3. Experimental validation of improvement of the overall efficiency for electro-hydraulic drive system

In the previous chapter, a detailed research of improvement of the theoretical overall efficiency for electro-hydraulic drive system by using efficiency maps was presented. The simulation results indicated that proposed control strategy has the potential to significantly improve the overall efficiency of EHDS, particularly at low pressure and low flow rate.

In this chapter, the experiment is conducted to measure the efficiencies of servo system and hydraulic piston pump. Based on measured data and proposed control strategy, the quasi-static analysis is implemented to demonstrate the advantage of proposed control strategy.

3.1 Measuring instruments and data acquisition

The testing circuit used for measuring the efficiency of system is shown in Fig. 3.1. In this circuit, the servo motor (2) drives the hydraulic swash plate axial piston pump (5). Speed of servo motor is controlled by servo amplifier (1) and displacement screw of hydraulic pump is used to regulate the displacement of hydraulic pump as shown in Fig. 3.2. The relief valve (9) serves for the setting of different pressure at the pump outlet.

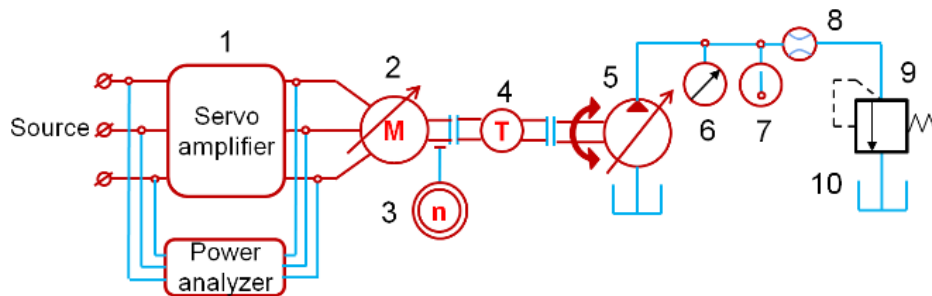


Figure 3.1 Schematic of hydraulic circuit for measuring the efficiency of system

1. Servo Amplifier ;
- 2.AC Servomotor ;
3. Rotation Speed Sensor ;
- 4.Torque sensor ;
- 5.Variable Displacement Pump ;
- 6.Pressure Gauge ;
- 7.Pressure Sensor ;
8. Flow meter ;
9. Relief Valve ;
10. Oil Tank.

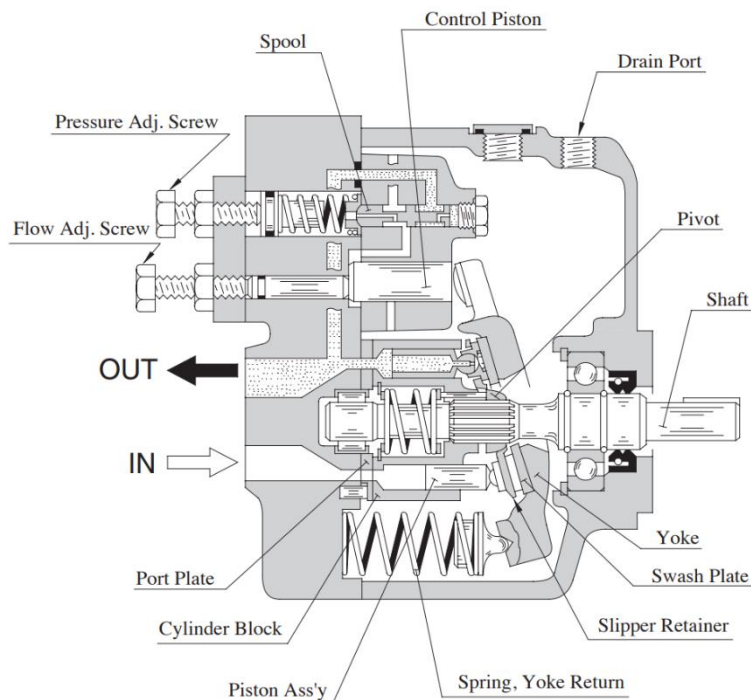


Figure 3.2. Structure of variable displacement piston pump
 (Referenced from A "Series Variable Displacement Piston Pumps technical documents by Yuken Company) ^{3.2)}

The specifications of components in experimental equipment are shown in Table 3.1 below.

Table 3.1. Main components' specifications of the test rig

Components	Specifications
Servo amplifier	Input: 3-phase 200V, 50Hz Rated current: 28.0 A
Servo motor	Rated output: 5.0 kW Rated torque: 23.9 Nm Rated speed: 2000 rpm
Swash plate axial piston pump	Displacement: 2-10 cm ³ /rev Rated operating pressure: 16 MPa Shaft speed: 600-1800 r/min
Relief valve	Pressure adjustment: 3.5-21 MPa Max Flow: 80 l/min
Power analyzer	Input: 4 channels Data update rate: 50 ms

The physical quantities to be measured are the input/output power [W] (current [A] and voltage [V]) of the servo amplifier, the shaft rotation rate [rpm] and output torque [Nm] of the AC servo motor, and the push-out volume of the variable displacement hydraulic piston pump [cm³/rev] (obtained from the amount of protrusion of the flow rate adjusting screw), discharge pressure [MPa], discharge flow rate [L/min], and hydraulic oil temperature [°C].

The measuring device and measuring method for each physical quantity are described below.

Power measurement

The "3390 Power Analyzer" manufactured by Hioki Electric Co., Ltd. was used to measure the input/output power to the servo amplifier. The "3390 Power Analyzer" is a wideband, high-precision power measuring instrument that covers from DC to inverter frequencies. Equipped with 4-channel input as standard, it can support single-phase to three-phase inverter motor systems. The efficiency of the servo amplifier was measured by measuring the current and voltage using the "3390 power analyzer" and the attached "L9438-50 voltage cord" and "9709 AC / DC current sensor".

Rotation speed measurement

To measure the shaft rotation speed of the servo motor, a gear is attached to the shaft, and the shaft rotation speed is detected by detecting the rotation speed of the gear using the "direction discrimination magnetic gear speed sensor RFP16A-85" manufactured by Coco Research Co., Ltd. When assembling to the experimental device, it is necessary to install this sensor vertically on the gear, so use the bolt through hole of the servo motor mounting bracket to assemble the L-shaped block and install the sensor there.

To read the detected signal (pulse wave) as the rotation speed, "Universal speedometer TDP-4931" manufactured by Coco Research Co., Ltd. was used.

Torque measurement

A "torque converter TP-5KMCB" manufactured by Kyowa Electric Co., Ltd. was used to measure the torque generated by the AC servomotor. It was placed between the AC servo motor and the variable displacement hydraulic piston pump, and the shaft was connected by a jaw type coupling. In order to read the detected signal as a voltage proportional to the generated torque, "Dynamic strain measuring instrument DPM-911B" manufactured by Kyowa Electric Co., Ltd. was used.

Pressure measurement

Two pressure sensors (pressure sensors) were attached to the flow path to measure the discharge pressure of the variable displacement hydraulic piston pump.

The first is "Glycerin Pressure Gauge OPG-AT-R 1 / 4-60 x 25MPa" manufactured by ASK Co., Ltd. This machine was used to grasp the set pressure value when adjusting the pressure with the relief valve ("Relief valve R-T03-3-12" manufactured by Nachi-Fujikoshi Co., Ltd.).

Second, to grasp the pressure value more accurately, "Pressure Transducer TP-AR300K" manufactured by TEAC Electronics Measurement Co., Ltd. was used. To read the detected signal as a voltage proportional to the pressure, the "dynamic strain measuring instrument DPM-911B" manufactured by Kyowa Electronics Co., Ltd. was used.

Flow rate measurement

To measure the discharge flow rate of the variable displacement hydraulic piston pump, "Flow meter DC051-6113-5105-000" manufactured by Flowdata was attached to the flow path.

The "flow meter DC051-6113-5105-000" supplies current and outputs a pulse wave with a frequency corresponding to the flow rate of the flowing oil. Therefore, as a current supply source, "DC stabilized power supply" manufactured by AND Co., Ltd. A 12 [V] direct current (DC) was supplied using the AD-8723D.

The output pulse wave was observed using the "Digital Oscilloscope ViewGo DS5334" manufactured by Iwatsu Electric Co., Ltd. Using the frequency calculation function of this machine, the frequency of the output pulse wave was calculated, and the flow rate was measured.

Temperature measurement

"Digital Fine Thermo DG2N-100" manufactured by Hakkou Denki Co., Ltd. was used to measure the temperature of hydraulic oil.

3.2 Experiment

Various quantities were measured under each experimental condition. The parameters that can be set are AC servo motor speed $n_m = 200 - 1800$ rpm as the recommended speed from hydraulic pump manufacturer. The displacement of the variable displacement hydraulic piston pump is $D = 2.0-10.0$ (cm³/rev) and the discharge pressure $\Delta p = 1.2-16$ MPa. In the experiment, $D = 2, 3, 4, 5, 6, 7, 8, 9$,

10 (cm³/rev) was set and motor speed n was changed from 200 rpm to 1800 rpm while changing $\Delta p = 1.2, 4.0, 6.3, 10.0, 12.5, 16$ MPa. The data was acquired by increasing the speed up to 1800 rpm by 200 rpm. The working points for experiment of servo system and hydraulic piston pump shown in Figure 3.3 and 3.4, respectively. The electric power supply for servo amplifier and servo motor was measured by power analyzer. The torque and speed in servo motor shaft were measured by speed counter 3 and torque sensor 4. Output parameters of system are pressure and flow rate determined by pressure gauge 6 and flow gauge 8.

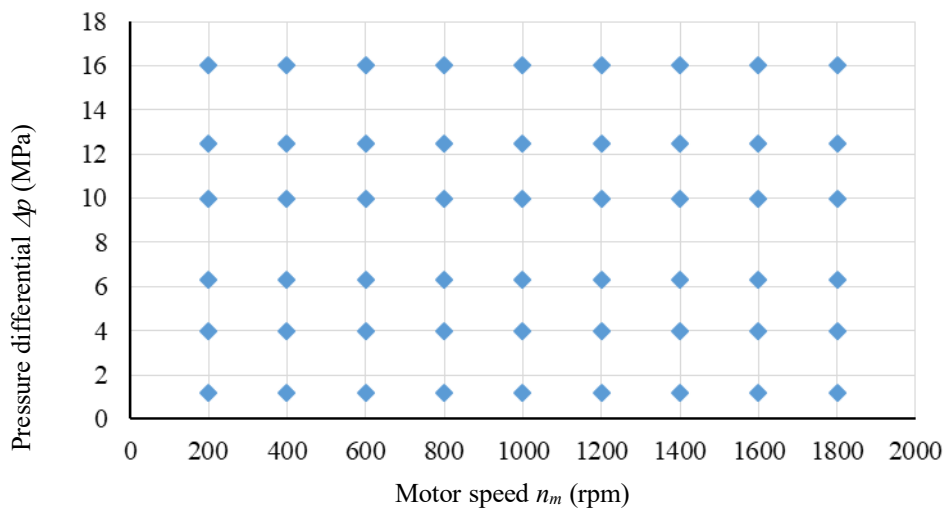


Fig. 3.3. Scatter chart of experiment of hydraulic piston pump

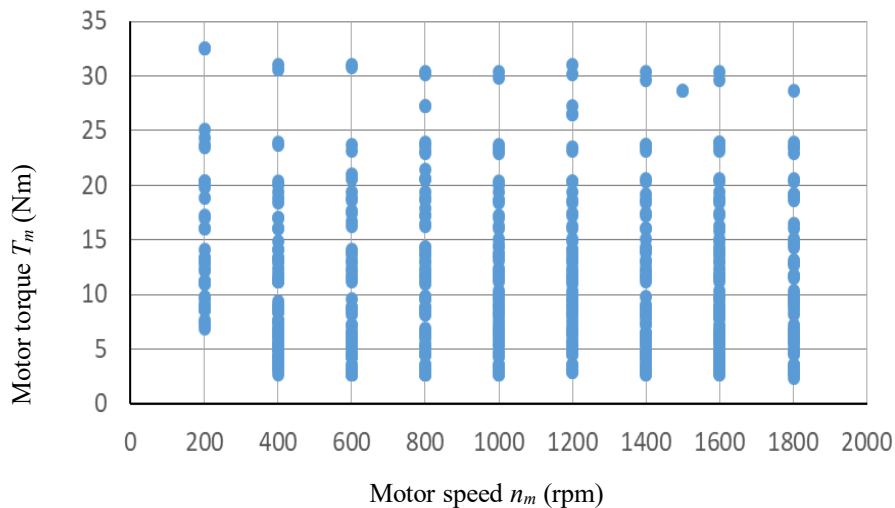


Fig. 3.4. Scatter chart of experiment of servo motor

3.3 Establish the efficiency maps from experiment results

From experimental data, coefficients in efficiency functions (2.1) to (2.3) for servo system and (2.17) to (2.23) for hydraulic pump and are determined by the least squares method using Matlab^{3.3)}. The results are listed in Table 3.2 and 3.3. These coefficient values should be used for modeling the efficiency of servo motor and hydraulic piston pump in this research.

Table 3.2. Coefficients in motor efficiency equation

No.	Symbol	Value
1	K_T	1.5
2	R_m	1.3905
3	K_C	1.7245
4	K_{f1}	0.0013
5	K_{f2}	0.0002

Table 3.3. Coefficients in hydraulic pump efficiency equation:

No.	C_{sv}	C_{v1}	C_{v2}	C_f	T_c
$\alpha=0.2$	7.37739E-09	3.93E+10	-1.6E+09	-0.01342	1.560038
$\alpha=0.3$	5.54204E-09	1.52E+11	-1.4E+10	-0.04272	1.680122
$\alpha=0.4$	4.34704E-09	-7.38E+09	1.18E+09	-0.00723	1.483469
$\alpha=0.5$	4.14206E-09	-2.45E+09	6.12E+08	-0.00163	1.705157
$\alpha=0.6$	4.12863E-09	-1.44E+09	5.18E+08	-0.00134	1.70583
$\alpha=0.7$	3.799E-09	7.44E+09	-3.6E+09	0.034942	1.375551
$\alpha=0.8$	2.32489E-09	2.24E+09	-1.4E+09	0.049786	1.335034
$\alpha=0.9$	2.29981E-09	4.79E+10	-3.9E+10	0.14449	4.15653
$\alpha=1.0$	2.90674E-09	-1.76E+10	1.76E+10	0.114516	1.724293

The efficiency maps of servo motor and hydraulic pump at different displacement ratios are shown in Figure 3.5 and Figure 3.6 to 3.13, respectively.

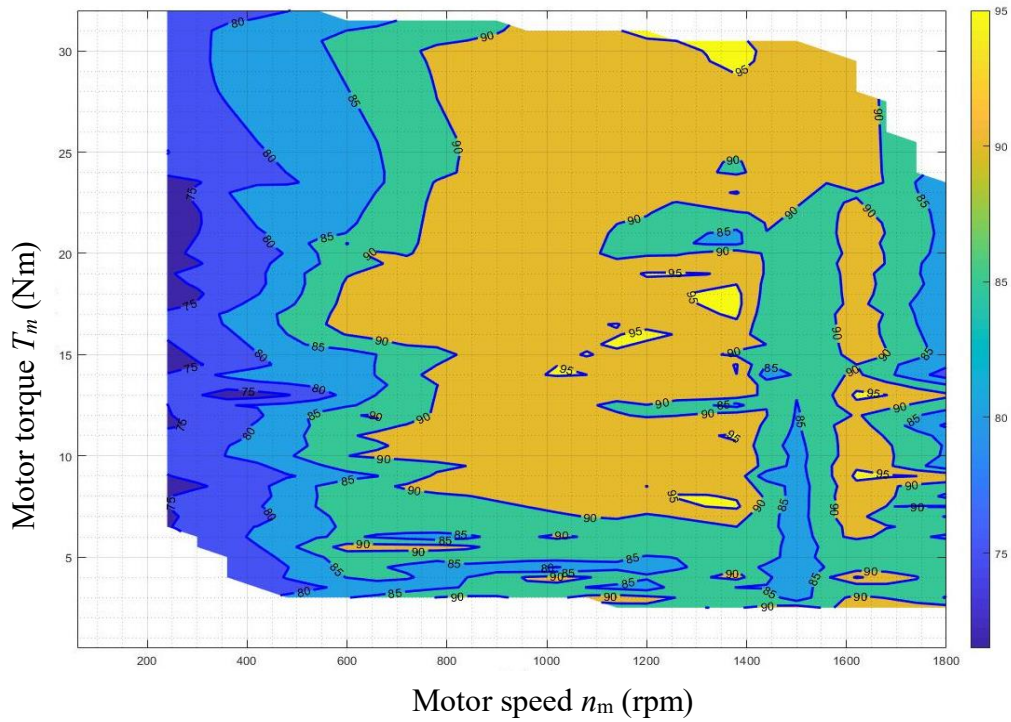


Fig. 3.5. Efficiency map of servo system

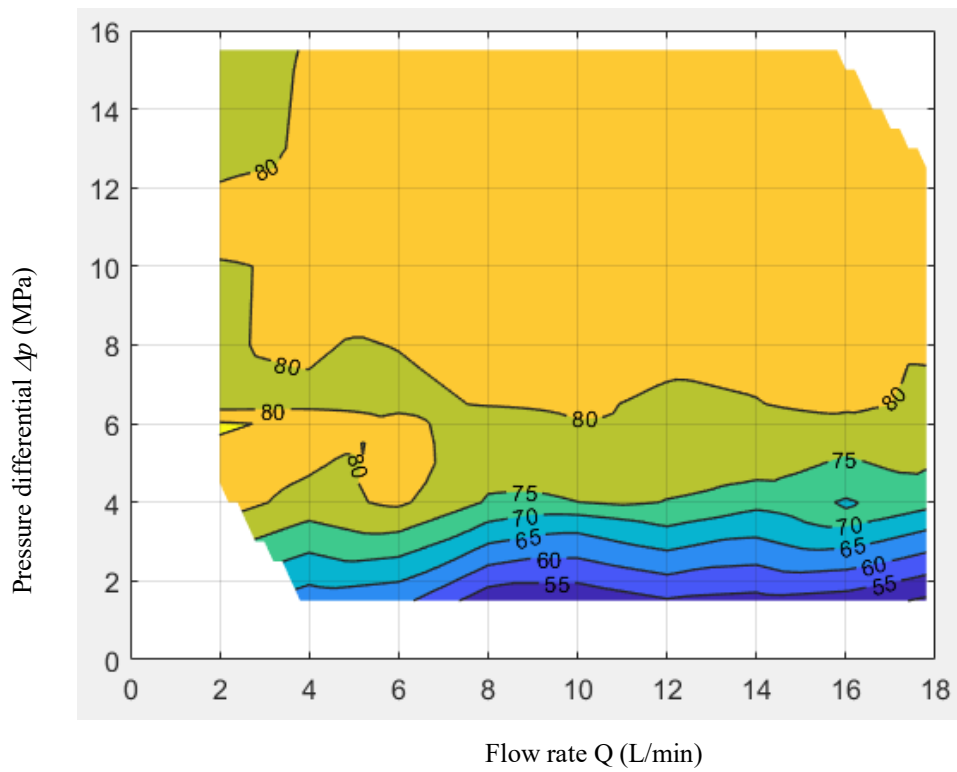


Fig. 3.6. Efficiency map of hydraulic piston pump with $\alpha=1.0$

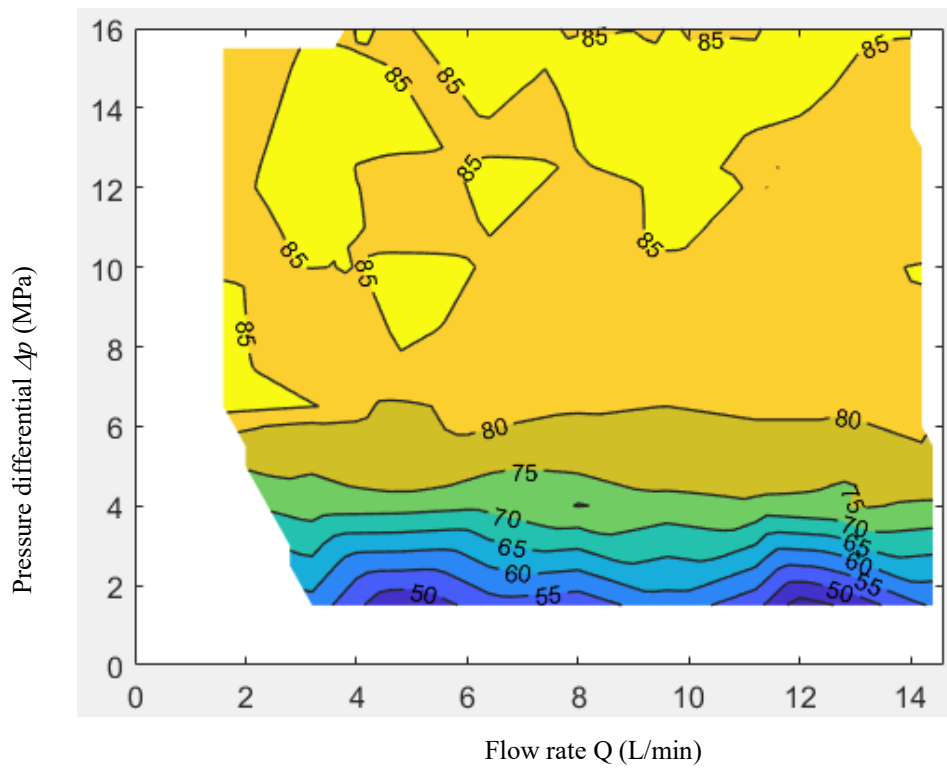


Fig. 3.7. Efficiency map of hydraulic piston pump with $\alpha=0.8$

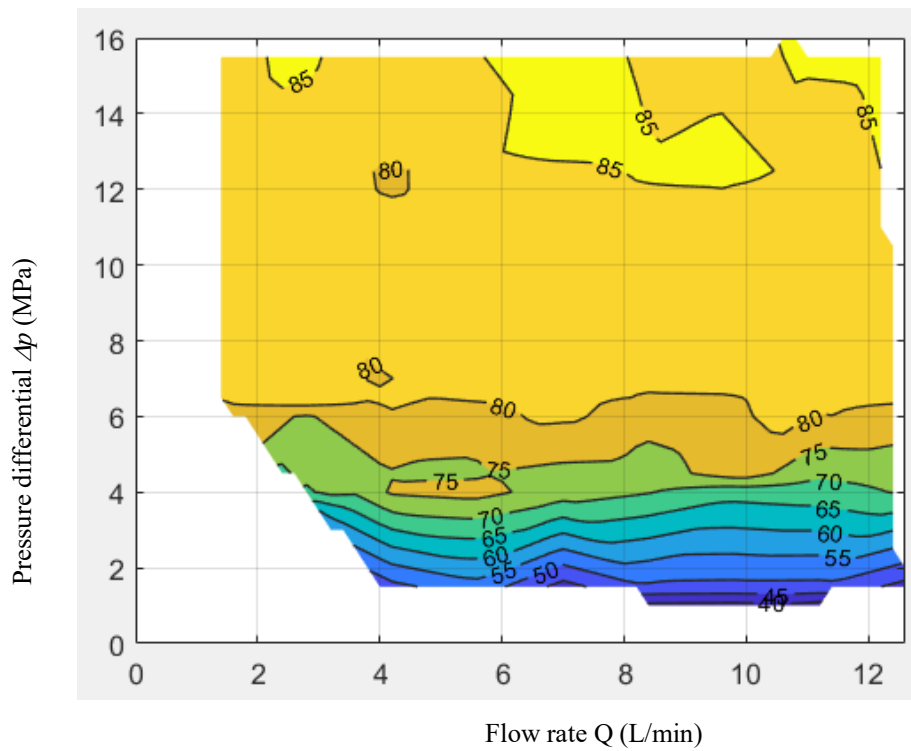


Fig. 3.8. Efficiency map of hydraulic piston pump with $\alpha=0.7$

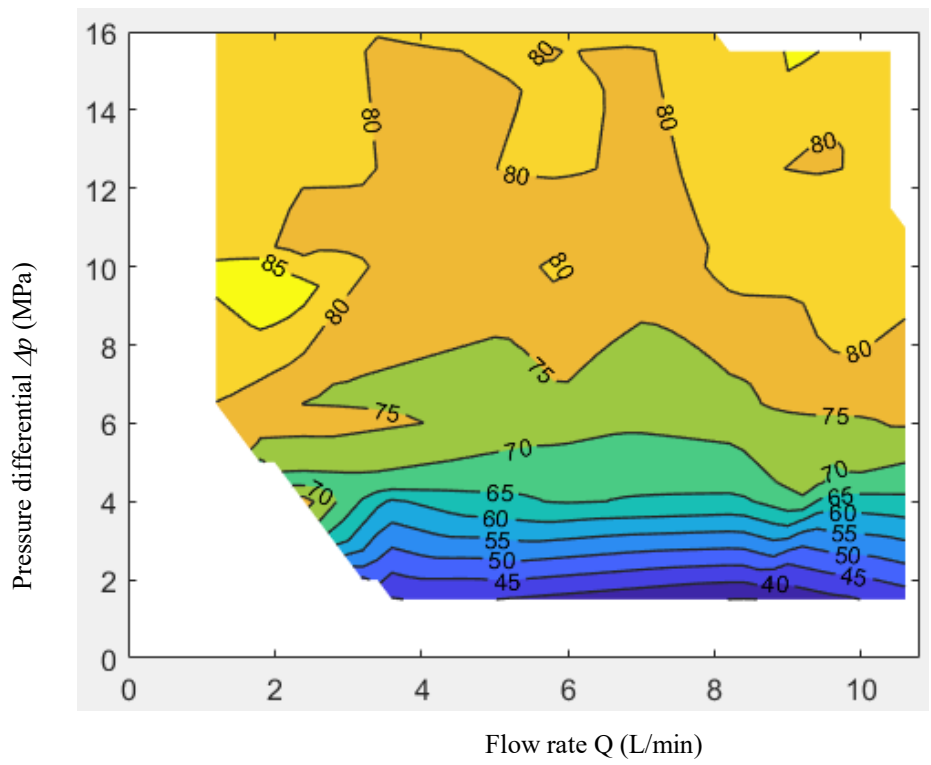


Fig. 3.9. Efficiency map of hydraulic piston pump with $\alpha=0.6$

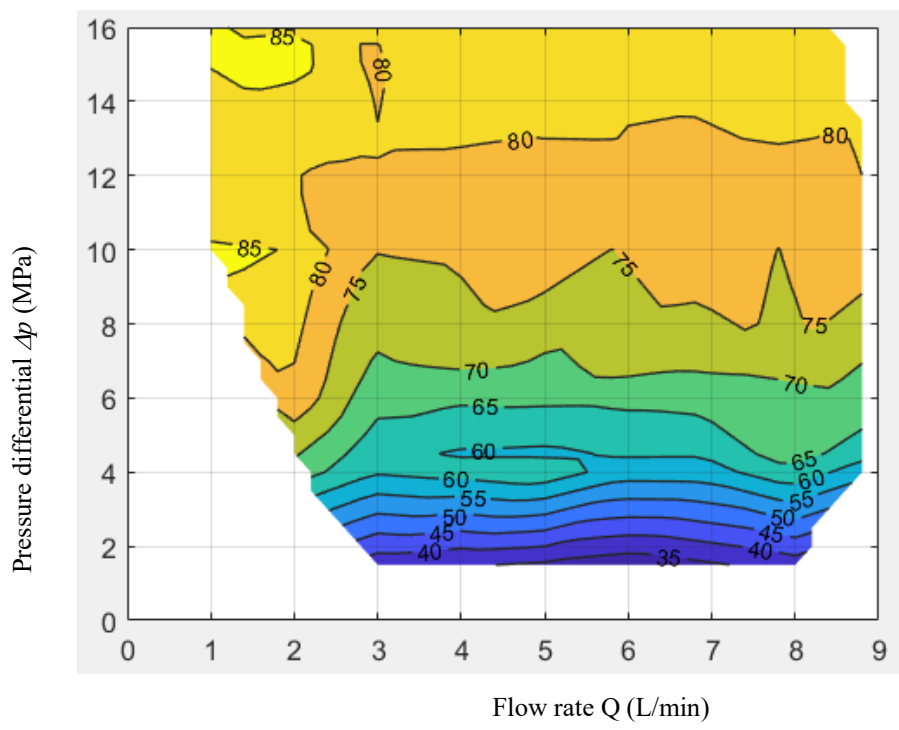


Fig. 3.10. Efficiency map of hydraulic piston pump with $\alpha=0.5$

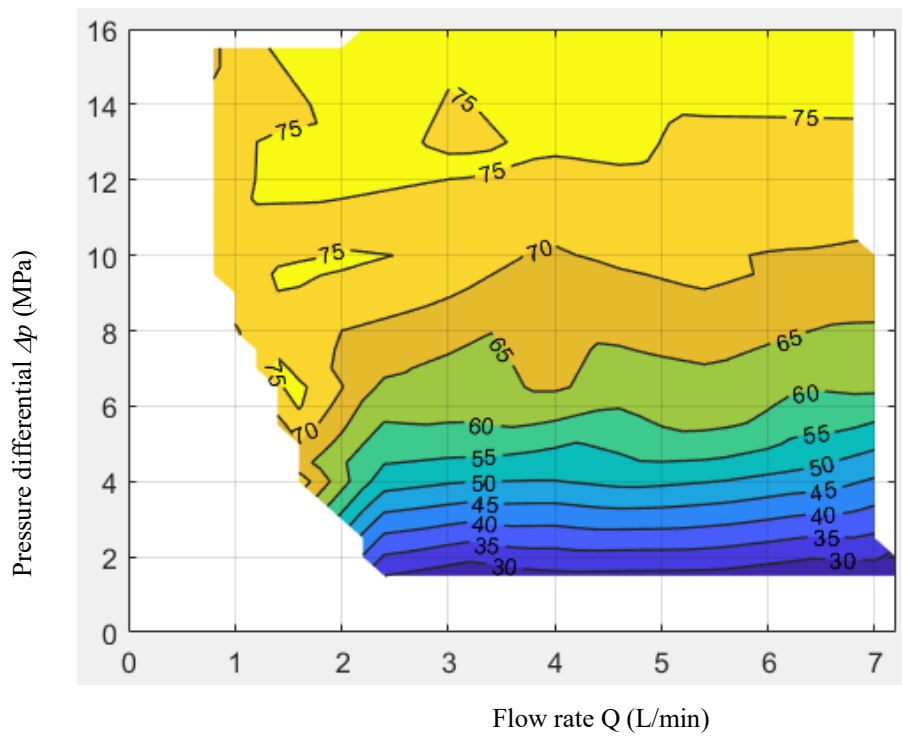


Fig. 3.11. Efficiency map of hydraulic piston pump with $\alpha=0.4$

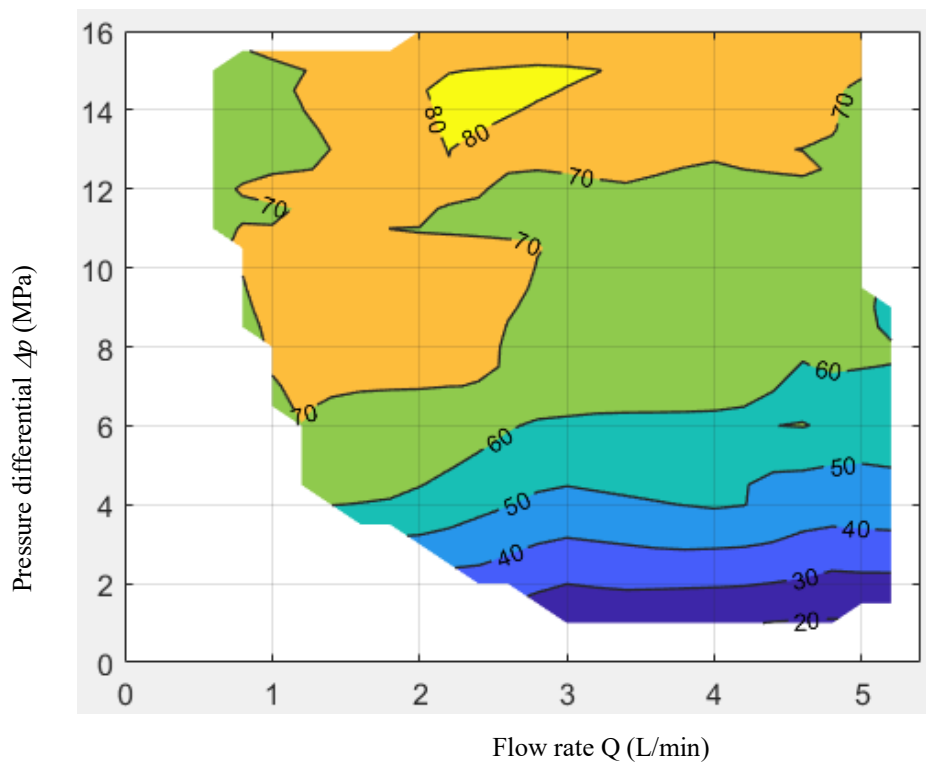


Fig. 3.12. Efficiency map of hydraulic piston pump with $\alpha=0.3$

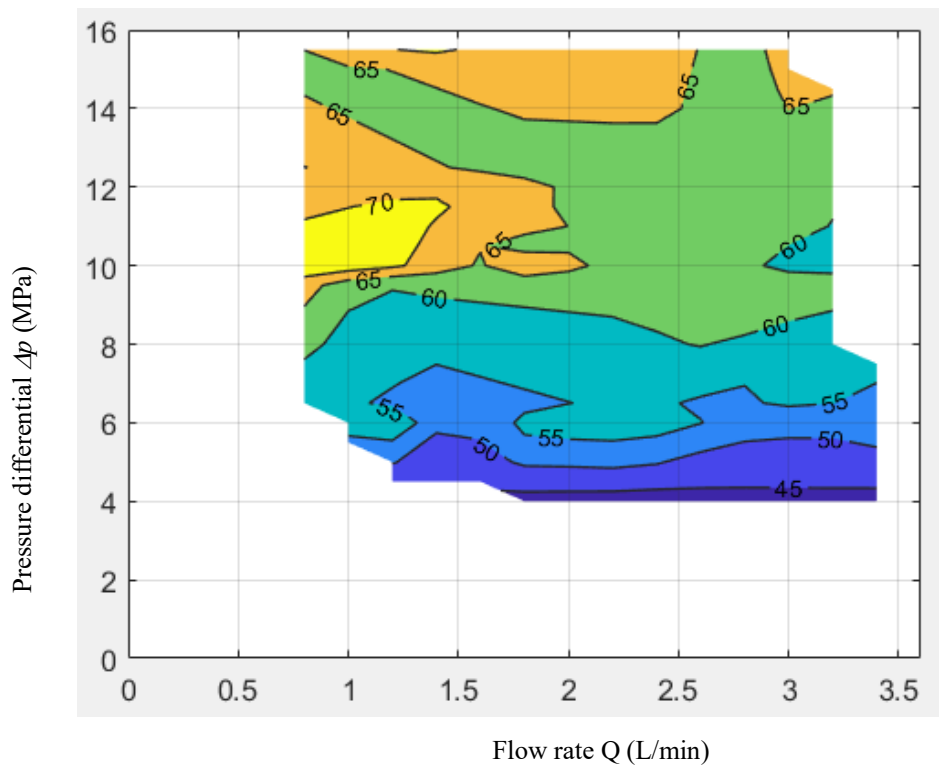


Fig. 3.13. Efficiency map of hydraulic piston pump with $\alpha=0.2$

From efficiency maps of servo motor and hydraulic piston pump, the overall efficiency maps are created as shown in Figure 3.14 to 3.22.

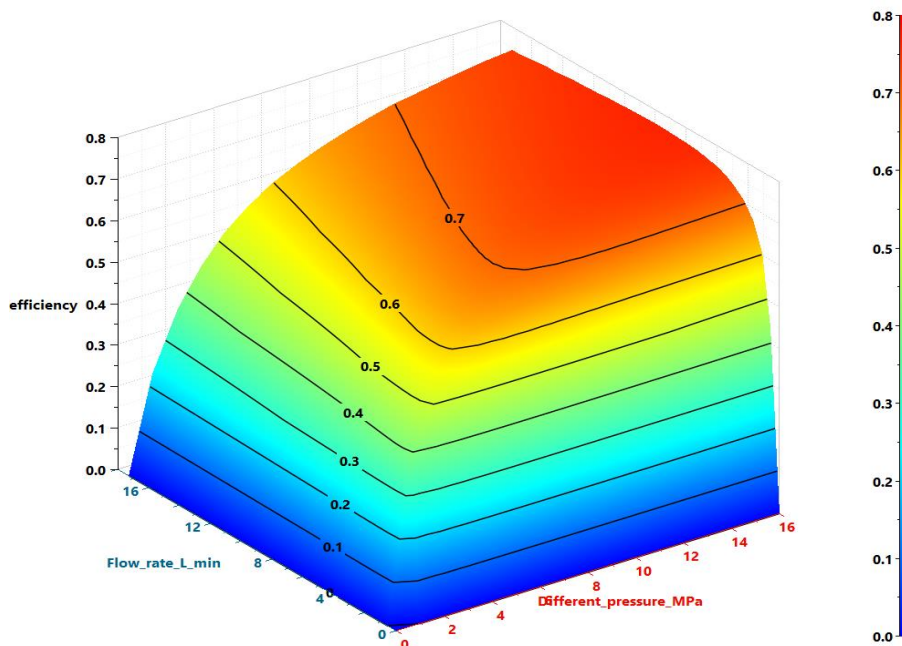


Fig. 3.14. Overall efficiency map of electro-hydraulic drive system with $\alpha=1.0$

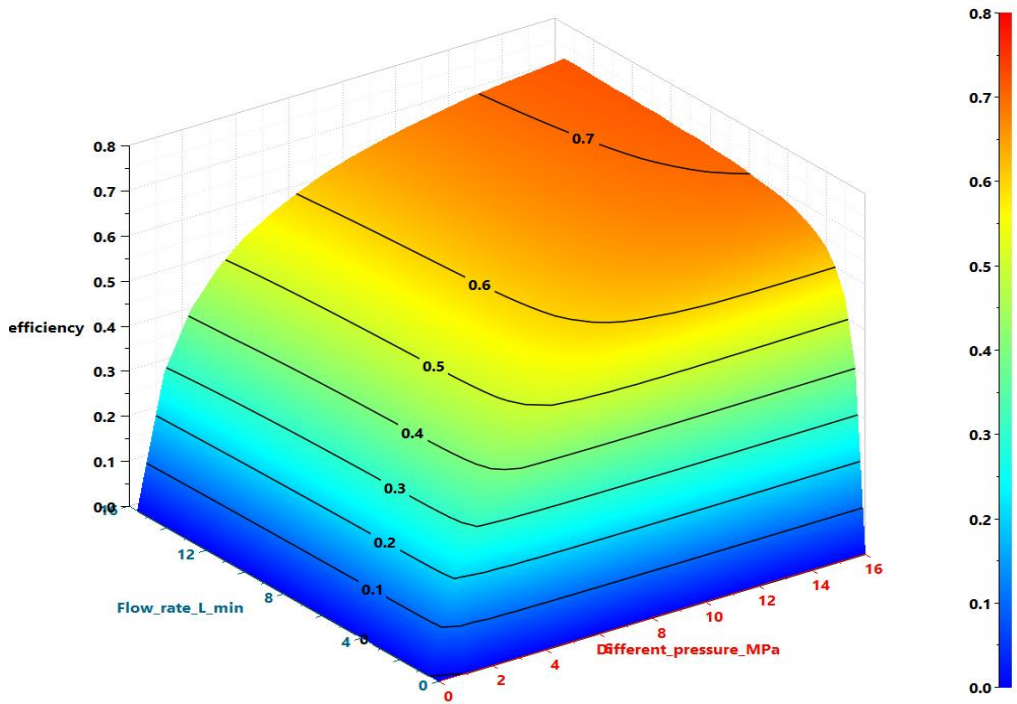


Fig. 3.15. Overall efficiency map of electro-hydraulic drive system with $\alpha=0.9$

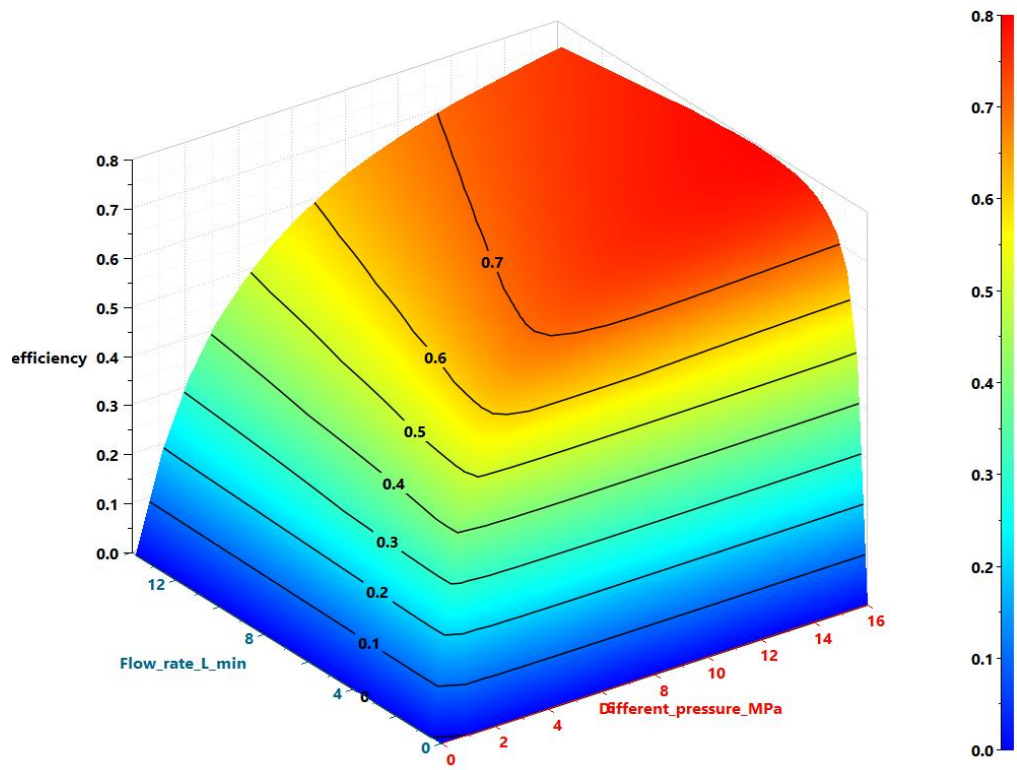


Fig. 3.16. Overall efficiency map of electro-hydraulic drive system with $\alpha=0.8$

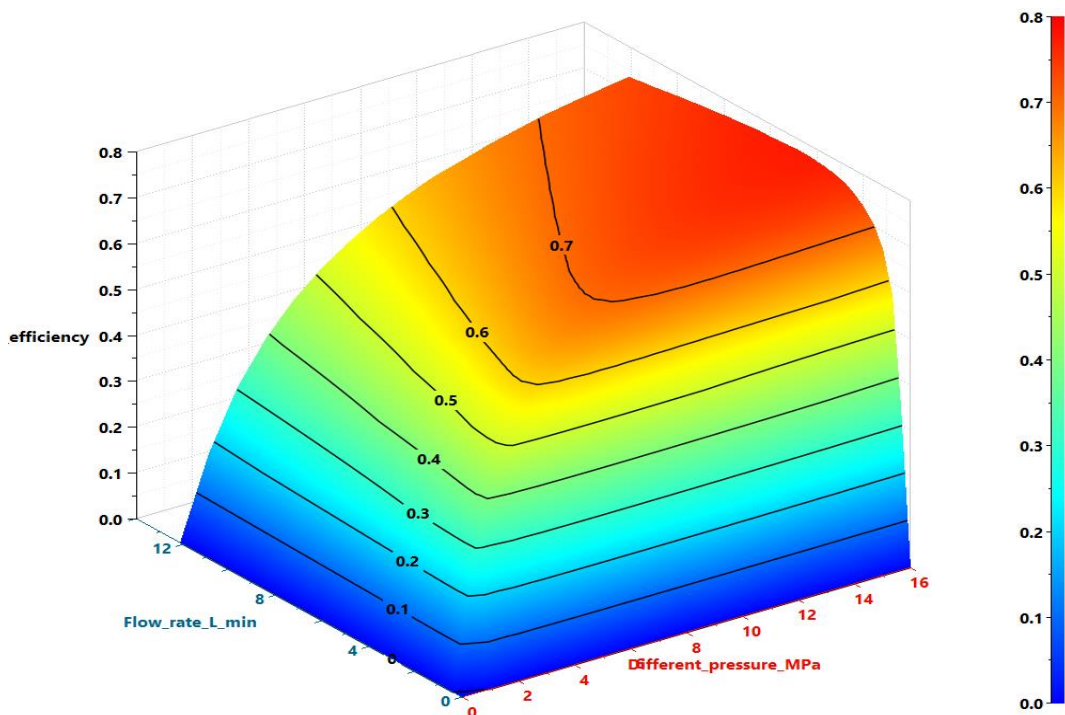


Fig. 3.17. Overall efficiency map of electro-hydraulic drive system with $\alpha=0.7$

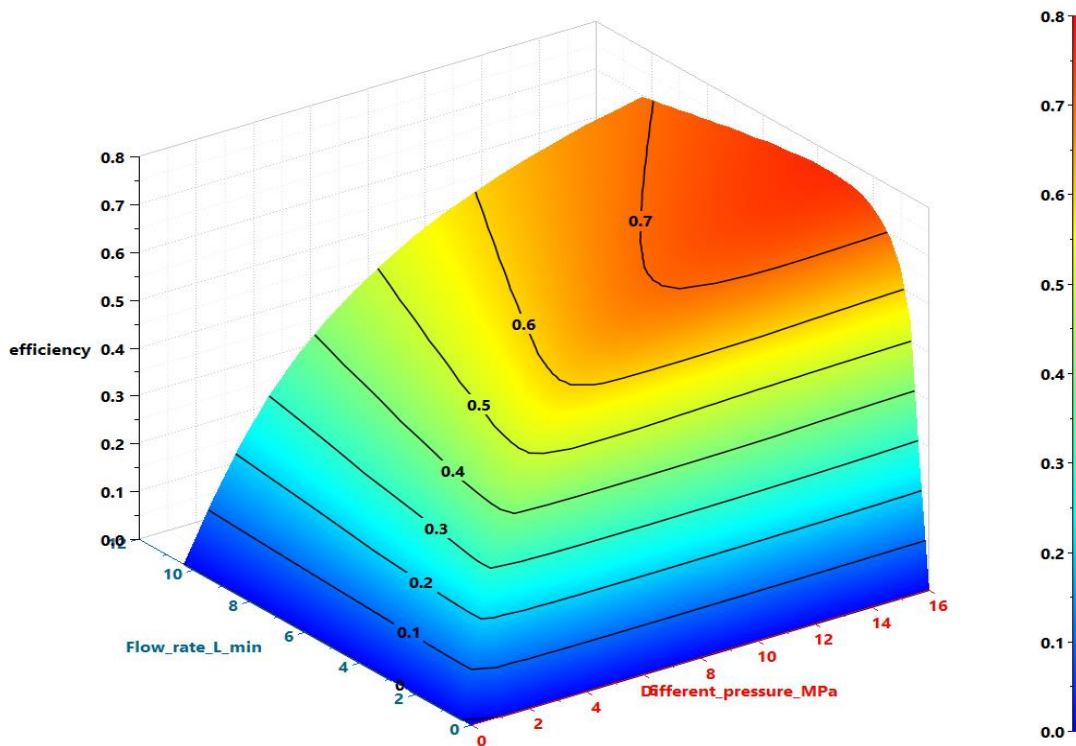


Fig. 3.18. Overall efficiency map of electro-hydraulic drive system with $\alpha=0.6$

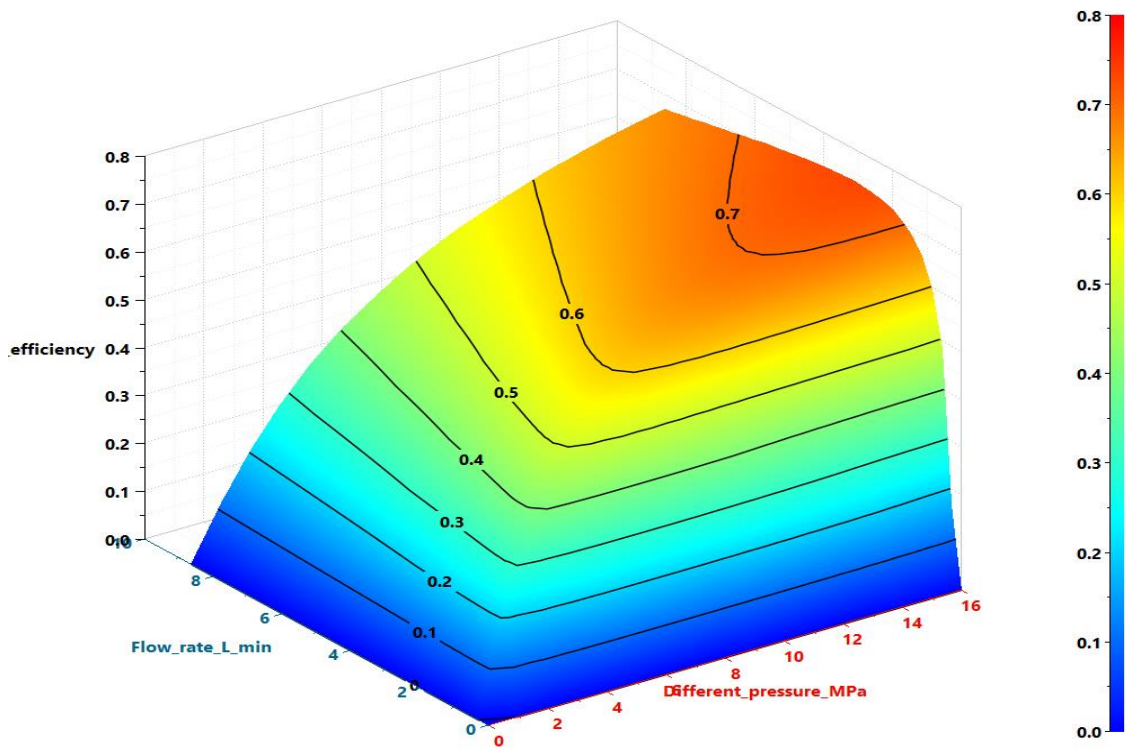


Fig. 3.19. Overall efficiency map of electro-hydraulic drive system with $\alpha=0.5$

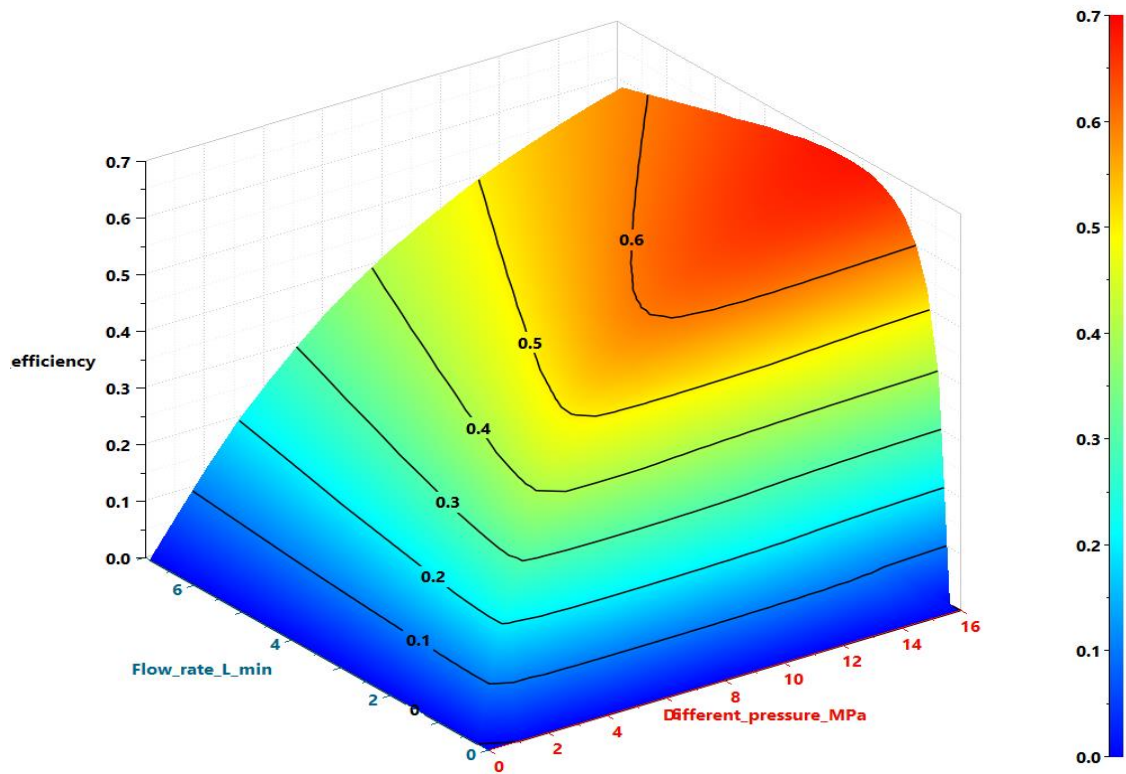


Fig. 3.20. Overall efficiency map of electro-hydraulic drive system with $\alpha=0.4$

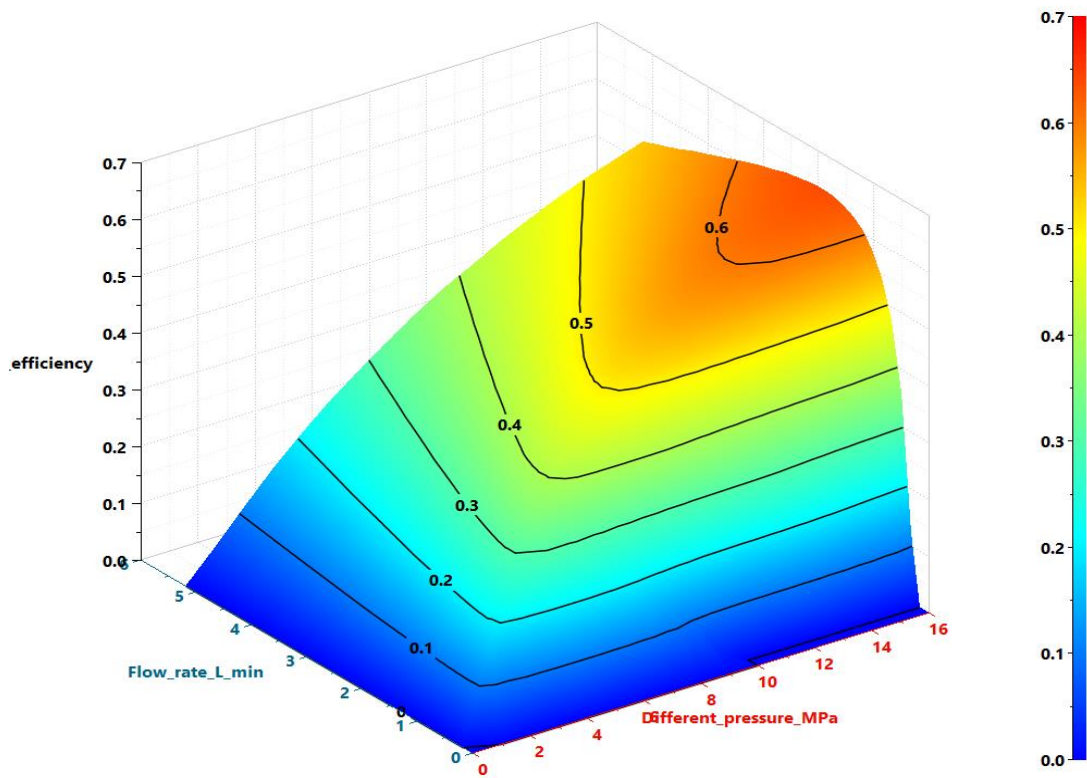


Fig. 3.21. Overall efficiency map of electro-hydraulic drive system with $\alpha=0.3$

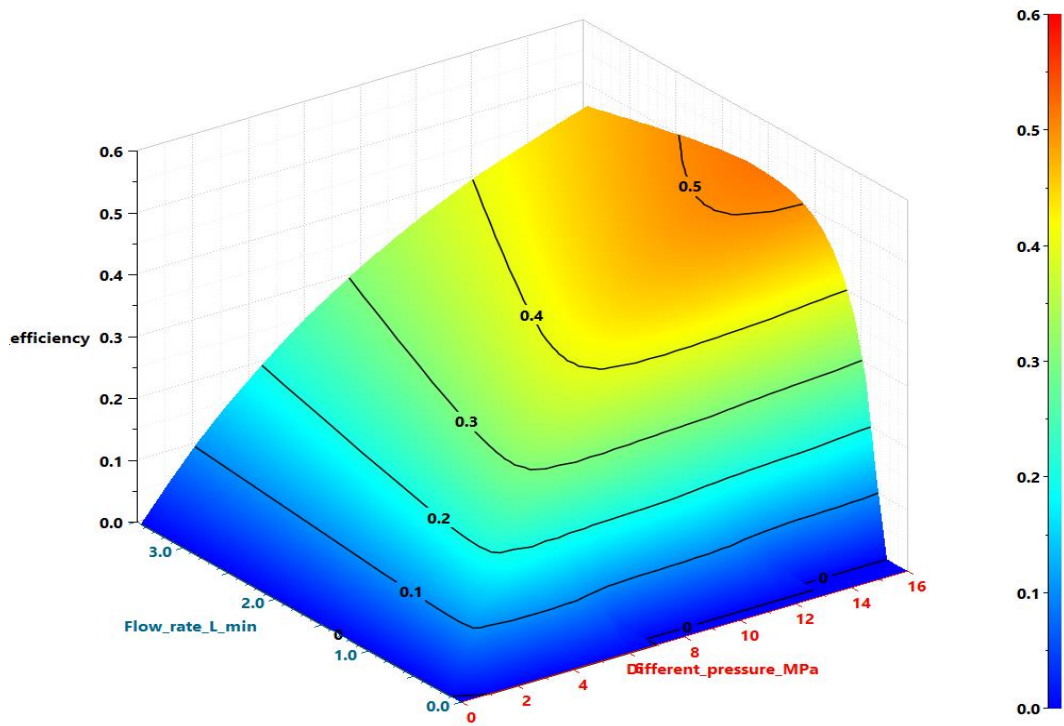


Fig. 3.22. Overall efficiency map of electro-hydraulic drive system with $\alpha=0.2$

Based on overall efficiency maps in Figure 3.4 to 3.22, the overall efficiency of 3 drive concepts presented in Chapter 2 are compared to verify the advantage of proposed control strategy. The comparison is shown in Figure 3.23 to 3.27.

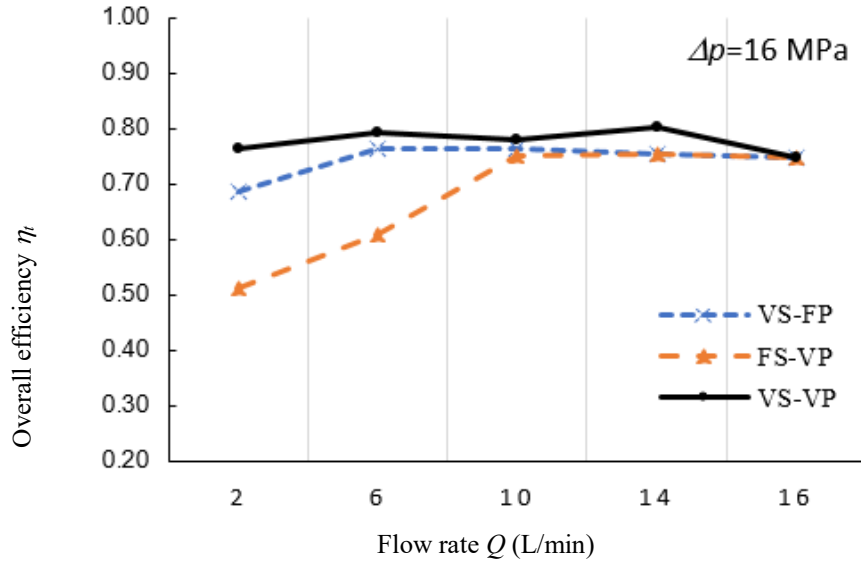


Fig. 3.23. Overall efficiency η_i comparison at output different pressure $\Delta p = 16$ MPa

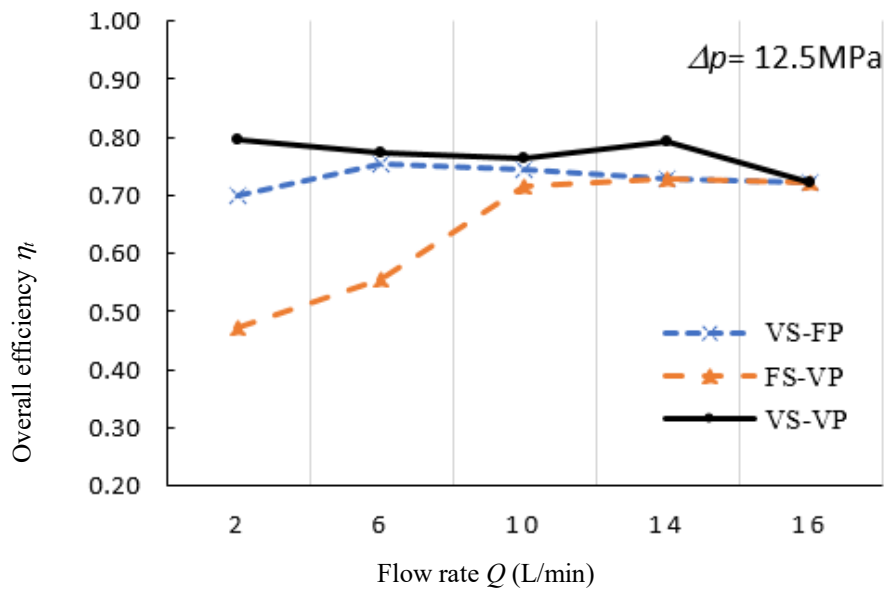


Fig. 3.24. Overall efficiency η_i comparison at output different pressure $\Delta p = 12.5$ MPa

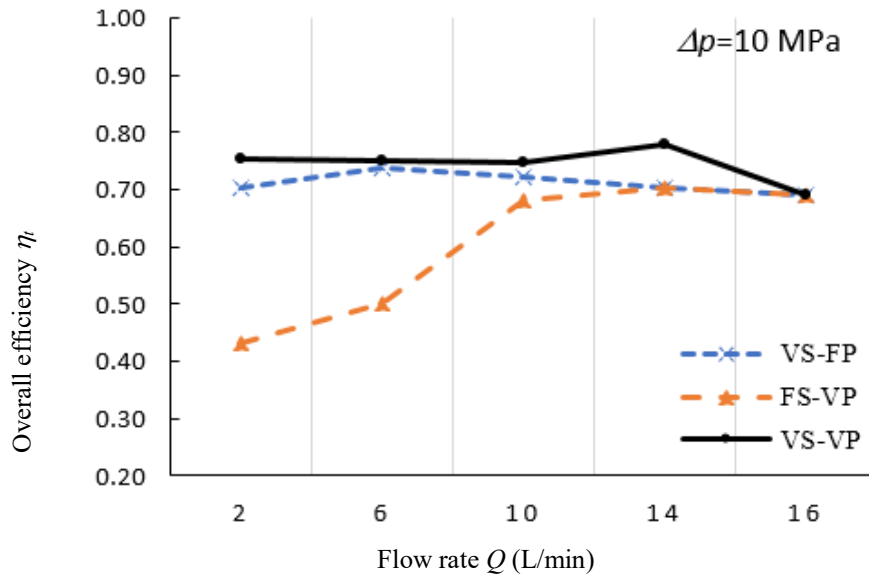


Fig. 3.25. Overall efficiency η_i comparison at output different pressure $\Delta p = 10$ MPa

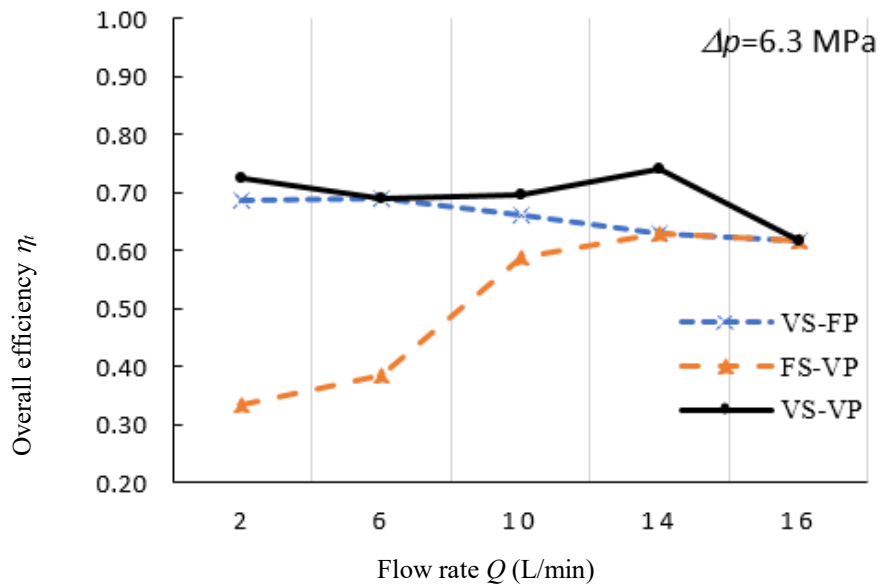


Fig. 3.26. Overall efficiency η_i comparison at output different pressure $\Delta p = 6.3$ MPa

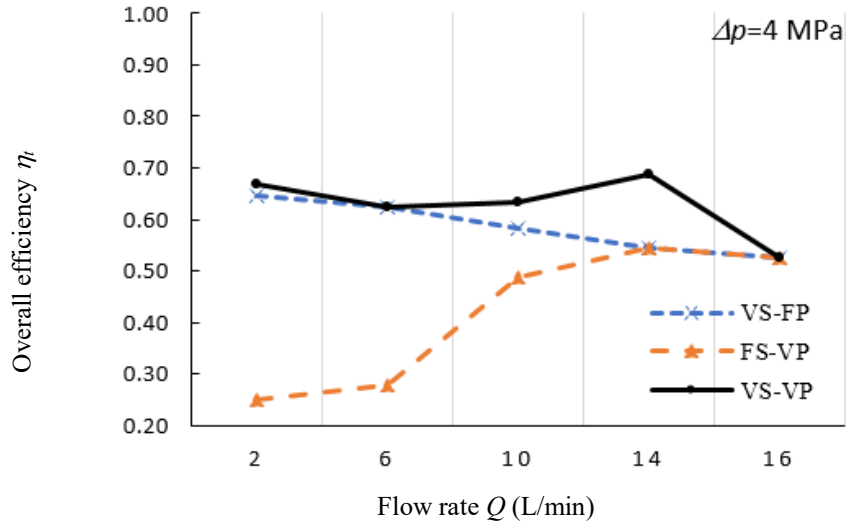


Fig. 3.27. Overall efficiency η_i comparison at output different pressure $\Delta p = 4$ MPa

In Figure 3.23 to 3.27, VS-VP unit achieved better overall efficiency than others at almost all given working points because of the flexibility of both n_m and α . The advantage of the VS-VP unit can be seen clearly at a low flow rate range ($Q = 2 \sim 14$ L/min). Considering the work point of $Q = 2$ L/min; $\Delta p = 16$ MPa, the efficiency of the VS-VP unit is 30% and 10% higher than that of the VS-FP unit and FS-VP unit, respectively. These results in Figure 3.23 to 3.27 matches with the simulation results as shown in Chapter 2.

3.4 Quasi-Static improvement of overall efficiency of the proposed control strategy for EHDS

To verify the experimental maps established in this chapter, quasi-static analysis is performed as shown in Figure 3.28. The separated experiment is performed for different working points and compared to results from experimental overall efficiency maps. The solid lines are efficiency values from experimental maps, the dash lines are the lines connect experimental points.

From Figure 3.28, there are differences of efficiency values between two types of efficiency, from experimental maps and from quasi-static performance. This may be explained by the errors during experiment and determination of experimental coefficients.

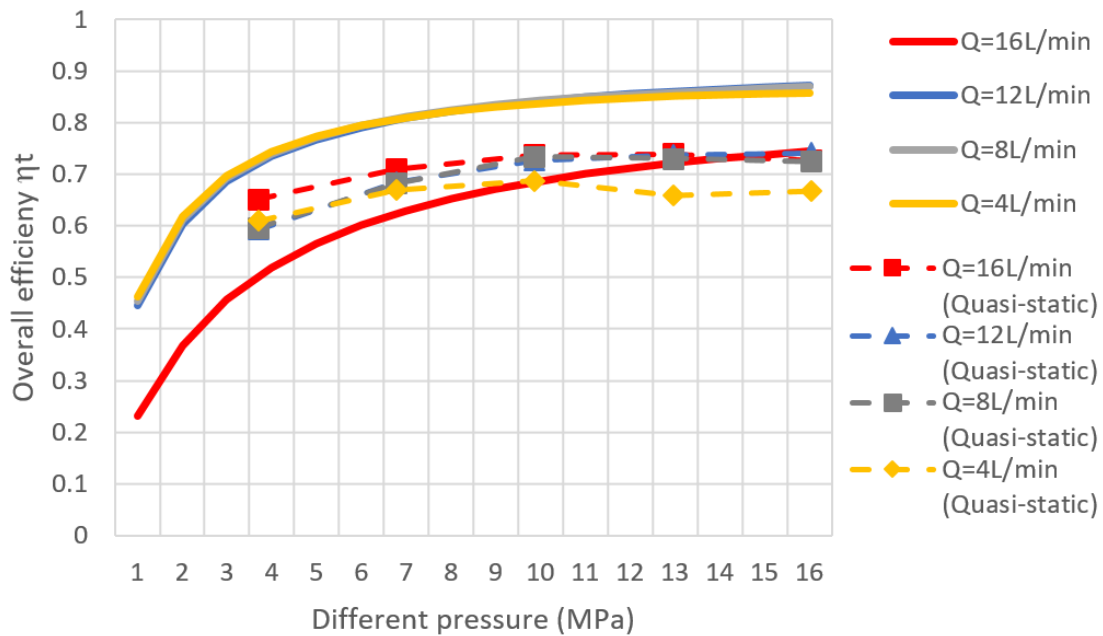


Fig. 3.28. Quasi-static analysis of experimental data

3.5 Summary of Chapter 3

- Experiment is conducted to determine coefficients in efficiency formulas of servo motor and hydraulic piston pump.
- From experimental efficiency formulas, 9 overall efficiency maps of EHDS were built with different displacement ratios.
- The investigation in these maps show the superiority of control strategy proposed in Chapter 2 compared one-degree-of-freedom system.
- To verify the overall efficiency maps, quasi-static process is done.

3.6 References

- 3.1) <https://www.mitsubishielectric.co.jp> (accessed on 1 August, 2020)
- 3.2) <https://www.yuken.co.jp> (accessed on 1 August, 2020)
- 3.3) Manring, Noah D., Fluid Power Pumps and Motors: Analysis, Design and Control, US: McGraw-Hill Professional, 2013.

Chapter 4

**Improvement of the transient
efficiency for electro-hydraulic drive
system**

Chapter 4. Improvement of the transient efficiency for electro-hydraulic drive system

The results shown in Chapter 2 and 3 demonstrate the advantage of proposed control strategy in separated working points of EHDS. For applying in electro-hydraulic drive system, the controller should improve the overall transient efficiency of the system. In this Chapter, the transient efficiency of EHDS is studied.

4.1 Simulation of improvement of the transient efficiency for EHDS

4.1.1 Improvement of transient efficiency by using experimental efficiency maps

The transient efficiency of EHDS in Chapter 3 is simulated in for two types of command signal of flow rate, step signal and sine signal in Figure 4.1 and 4.5, respectively. The output parameters in this simulation (response flow rate, displacement ratio and motor speed command) are determined through interpolations based on 09 experimental efficiency maps in Chapter 3.

For step signal of flow rate, the flow rate is changed from 2 L/min to 14 L/min, different pressure Δp is constant at 10 MPa. The simulation results are shown in Figure 4.2 to 4.4 for step signal. From the simulation results, VSVP unit operates at higher efficiency mode compared FSVP and VSFP unit.

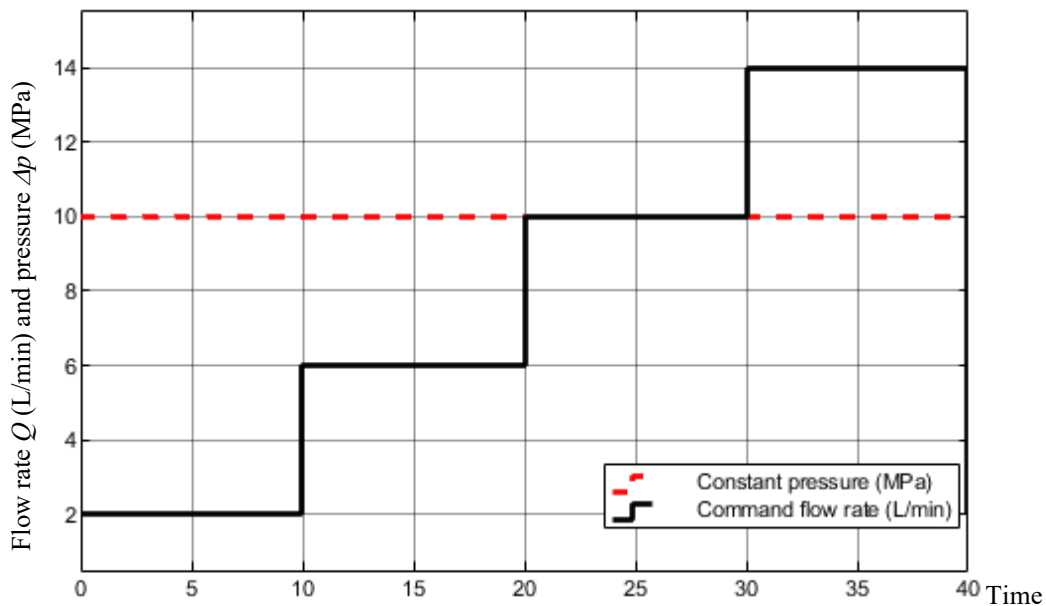


Fig. 4.1 Command step flow rate Q (L/min) at constant pressure $\Delta p = 10$ MPa

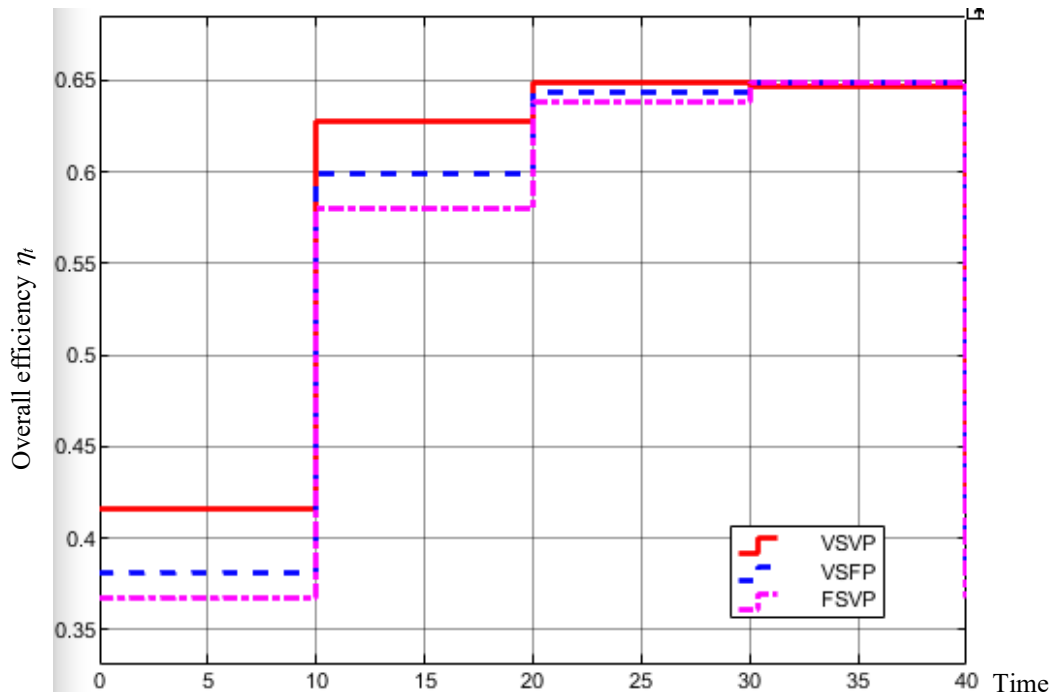


Fig. 4.2. Overall efficiency η_t comparison at output constant pressure $\Delta p = 10$ MPa for command step flow rate

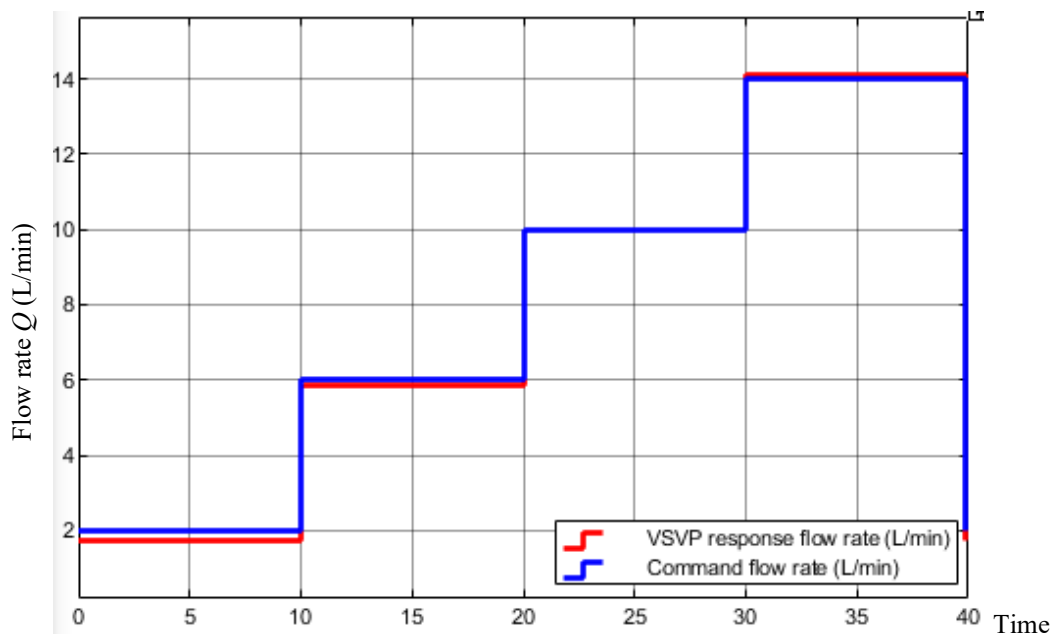


Fig. 4.3. Response flow rate and command flow rate comparison at output constant pressure $\Delta p = 10$ MPa for command step wave flow rate

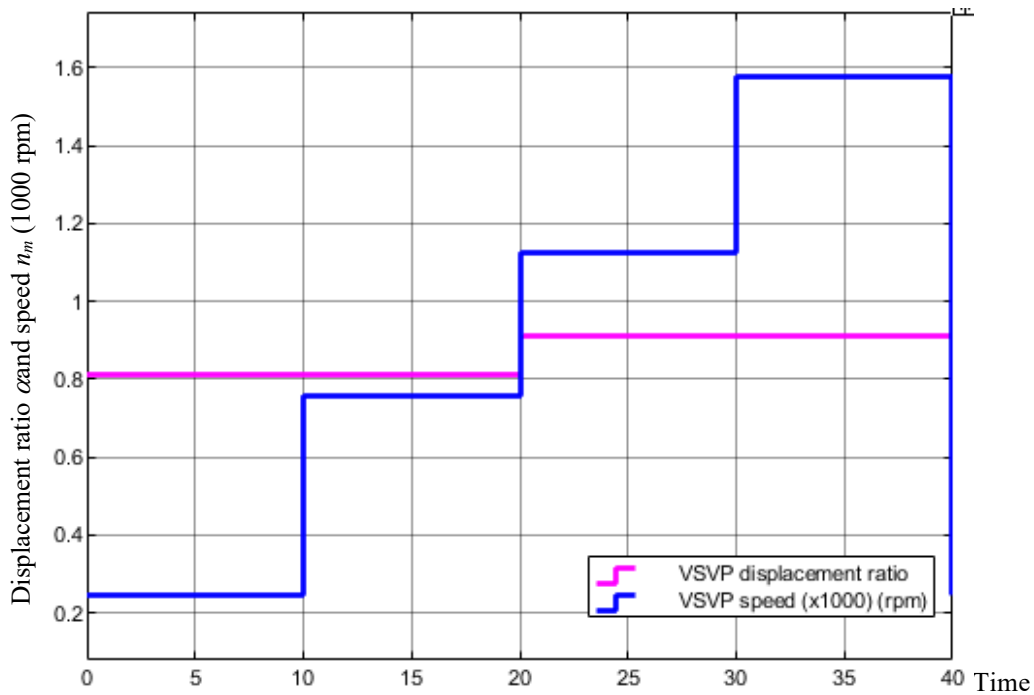


Fig. 4.4. Displacement ratio and motor speed command at output constant pressure $\Delta p = 10$ MPa for command step wave flow rate

For sine wave signal of flow rate, the flow rate Q is changed from 2 L/min to 10 L/min, different pressure is constant at 10 MPa. The simulation results are shown in Figure 4.6 to 4.8 for sine wave signal. From the simulation results, VSVP unit operates at higher efficiency mode compared FSVP and VSFP unit as shown in Figure 4.6.

Figure 4.7 is the comparison of response flow rate versus command flow rate. To achieve that response flow rate, the hydraulic pump and motor will be controlled as follow the commands as shown in Figure 4.8.

As shown in Figure 4.7, the output flow rate was consistent with the sinusoidal command flow rate, however, there is a slight deviation at low flow rate point. Moreover, in Figure 4.8, there are two irregular values of displacement ratio and motor speed command which suddenly changed. This may be explained by the number of efficiency maps are not sufficient for creating a continuous control command of displacement ratio and motor speed. As a result, it is not able to control the actual hydraulic pump and electric motor follow these discontinuous commands.

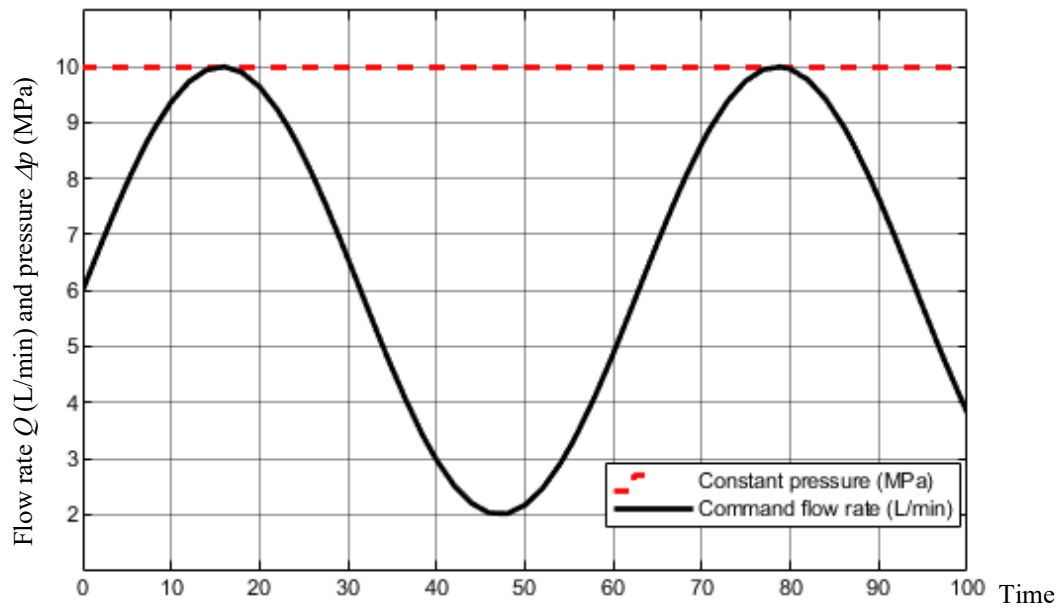


Fig. 4.5. Command sine wave flow rate Q (L/min) at constant pressure $\Delta p = 10$ MPa

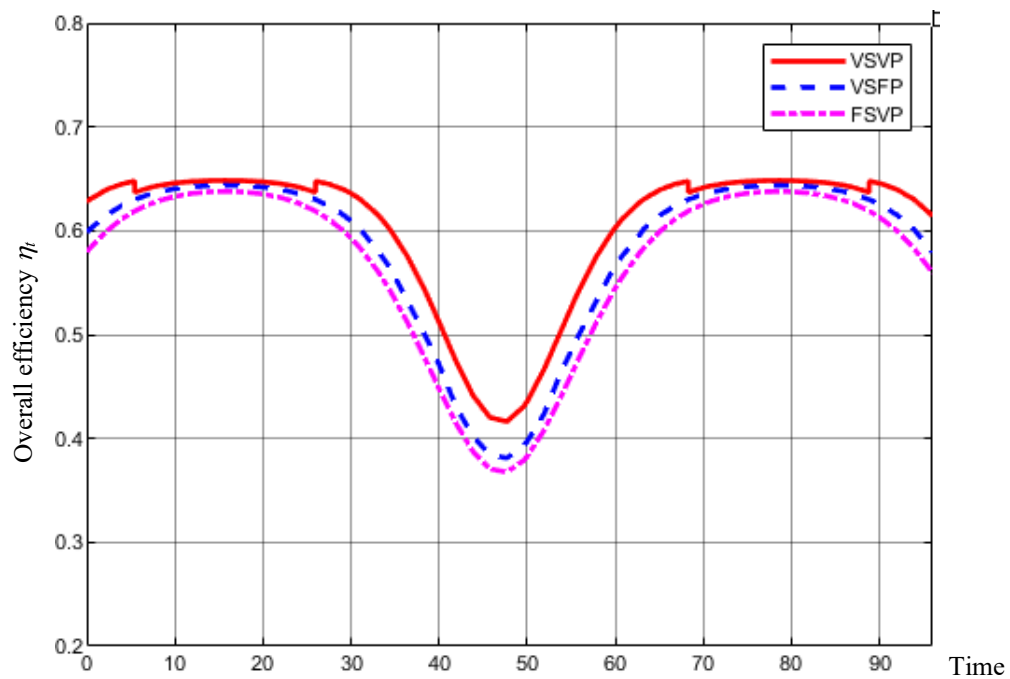


Fig. 4.6. Overall efficiency η_i comparison at output constant pressure $\Delta p = 10$ MPa for command sine wave flow rate

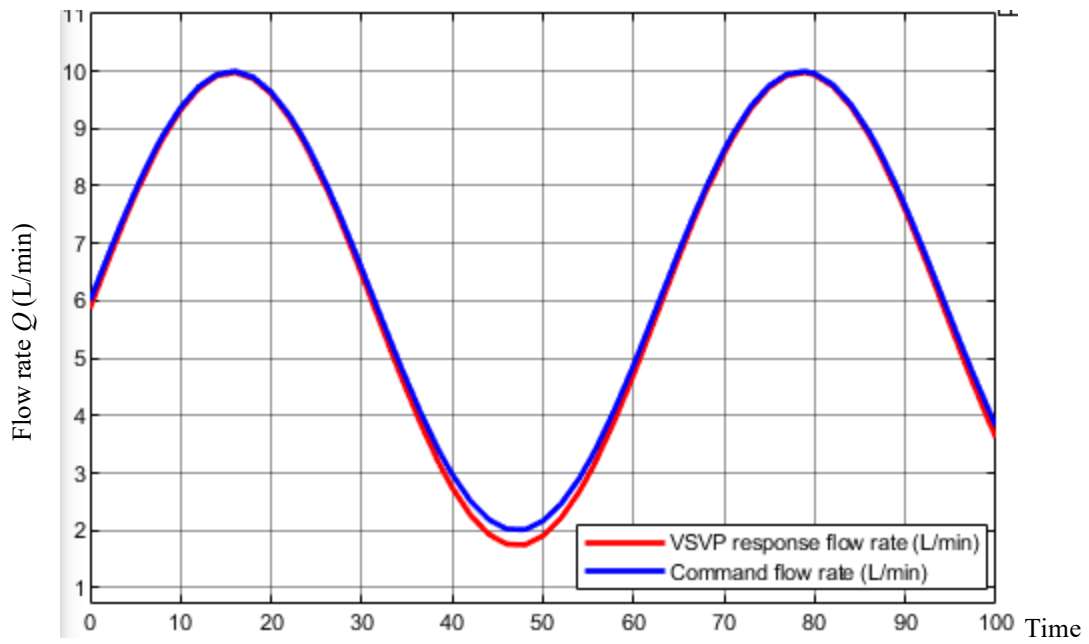


Fig. 4.7. Response flow rate and command flow rate comparison at output constant pressure $\Delta p = 10$ MPa for command sine wave flow rate

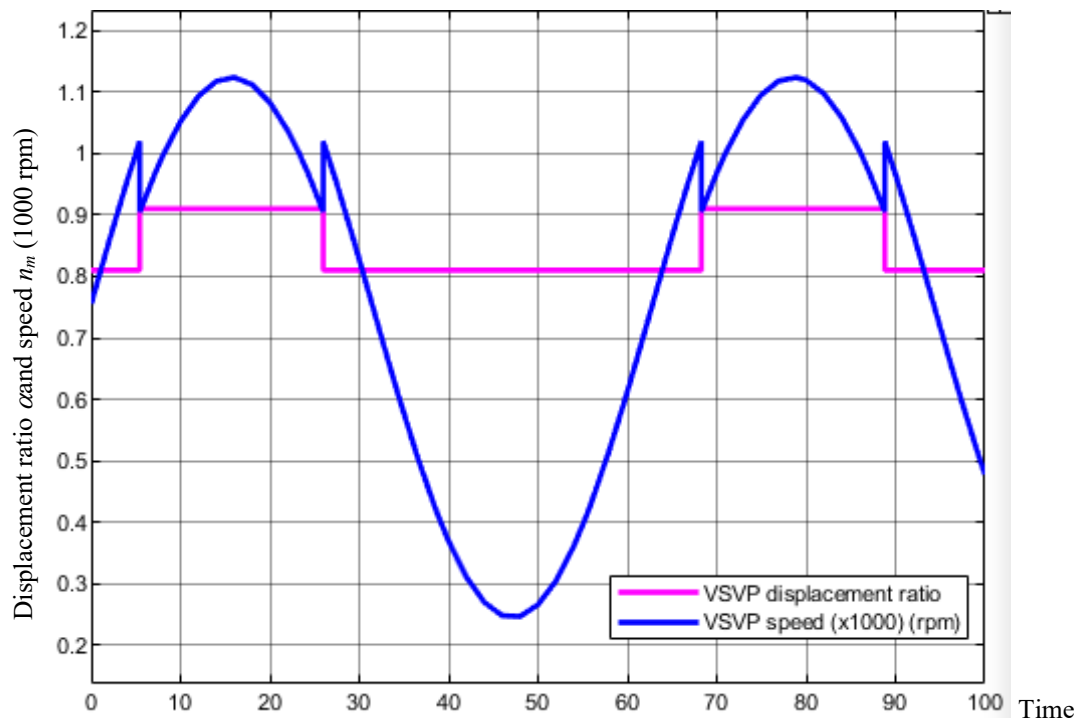


Fig. 4.8. Displacement ratio and motor speed command at output constant pressure $\Delta p = 10$ MPa for command sine wave flow rate

4.1.2 Improvement of transient efficiency by interpolation efficiency maps

4.1.2.1 *bvbnb*

To improve the smoothness of control command in Figure 4.8, the number of efficiency maps in this part is increased from 09 to 33 by using interpolation to determine the efficiency coefficients based on values in Table 3.3. The displacement ratio is now changed from 0.2 to 1.0 by a spacing 0.025. The sine wave flow rate in Figure 4.5 will be used again to determine output parameters. The graphs of result are shown in Figure 4.9 to 4.12.

4.1.2.2 *jhjhj*

In Figure 4.9, the efficiency of VSVP is still higher than VSFP and FSVP. Compared to Figure 4.6, the efficiency of VSVP is noticeably improved at low flow rate area because of the increase of number of α and n_m combination. Among of these increased combinations, controller could find potential one which can achieve higher efficiency.

Regarding the comparison of response flow rate and command flow rate in Figure 4.10, it can see that the response result is matched with command one for entire cycle. Moreover, the increase of map number has a clear effect on the smoothness of displacement ratio command and speed command as shown in Figure 4.11 and 4.12, respectively. However, these commands should be improved further to be apply in practical machines.

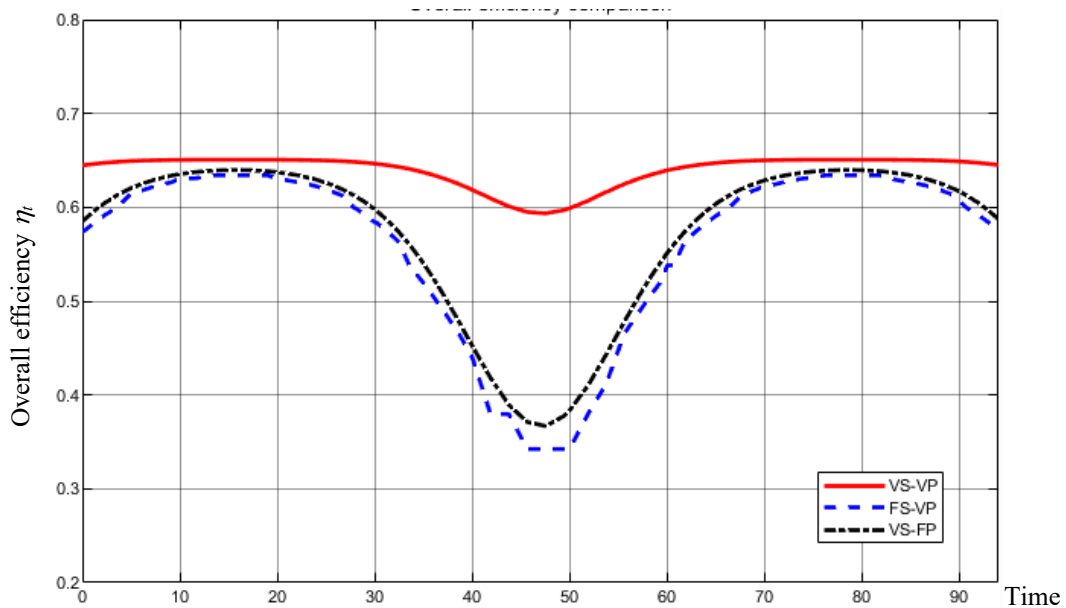


Fig. 4.9. Overall efficiency η_i comparison at output constant pressure $\Delta p = 10$ MPa for command sine wave flow rate (improvement by using interpolation efficiency maps)

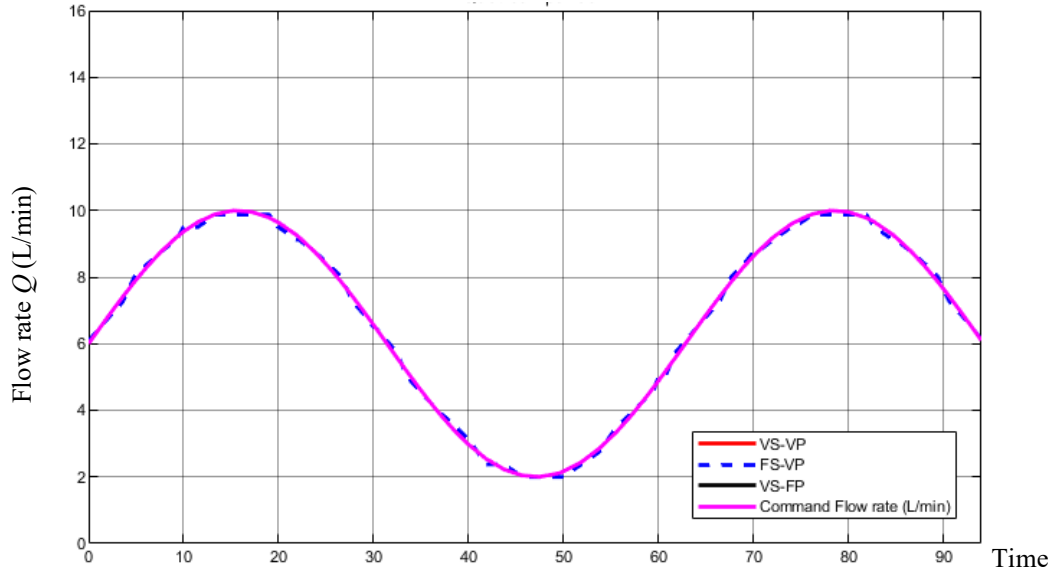


Fig. 4.10. Response flow rate and command flow rate comparison at output constant pressure $\Delta p = 10$ MPa for command sine wave flow rate (improvement by using interpolation efficiency maps)

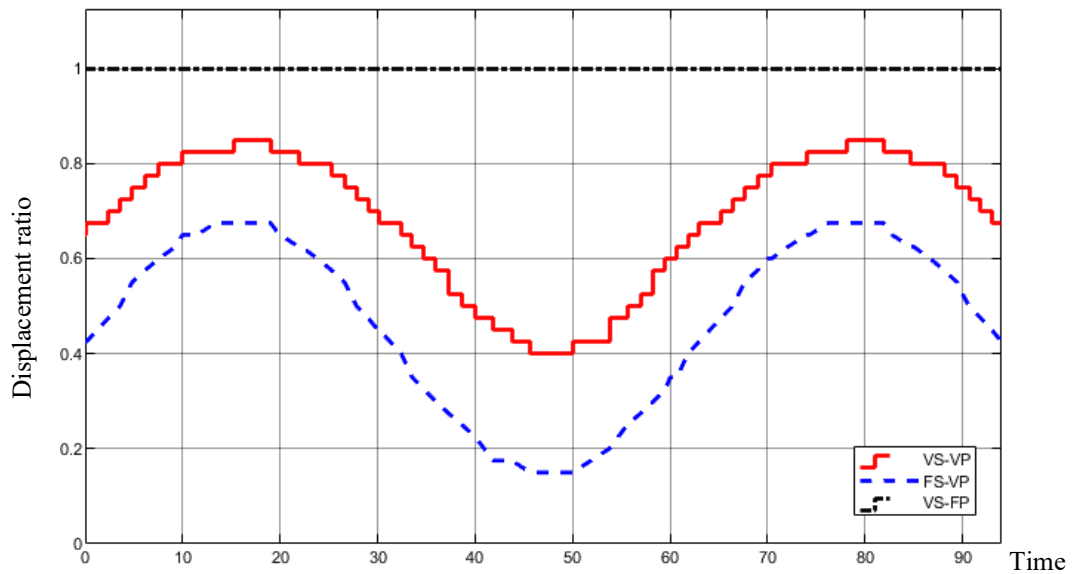


Fig. 4.11. Displacement ratio at output constant pressure $\Delta p = 10$ MPa for command sine wave flow rate (improvement by using interpolation efficiency maps)

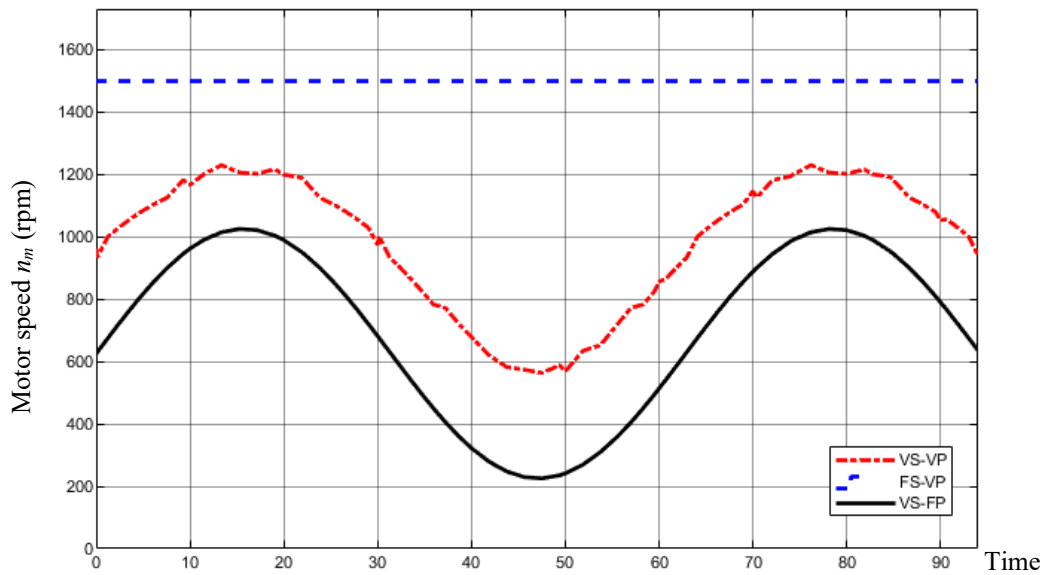


Fig. 4.12. Motor speed command at output constant pressure $\Delta p = 10$ MPa for command sine wave flow rate (improvement by using interpolation efficiency maps)

4.1.3 Improvement of control command by using low pass filter

The improvement of displacement ratio and speed commands in Figure 4.11, 4.12 will be implemented by using a low pass filter at output signal. Figure 4.13 to Figure 4.16 present the improved results with a low pass filter with time constant $t=1$. The smoothness of control commands in Figures 4.15 and 4.16 are improved than these ones in Figures 4.11 and 4.12. These results may be good enough to use for controlling the actual hydraulic pump and electric motor.

Regarding the response flow rate in Figure 4.14, there is a small delay between response flow rate and command flow rate.

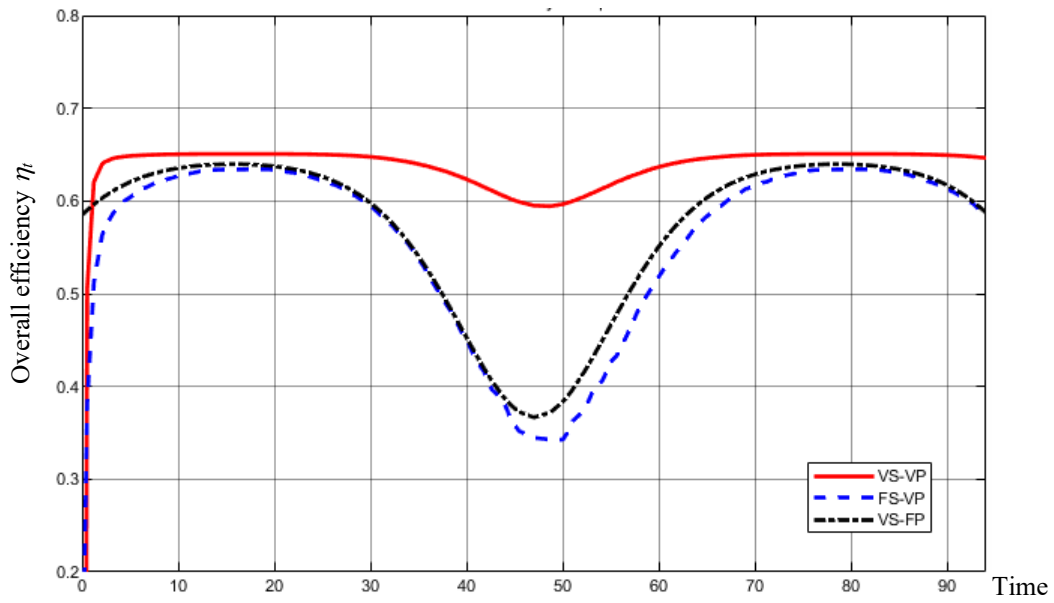


Fig. 4.13. Overall efficiency η_t comparison at output constant pressure $\Delta p = 10$ MPa for command sine wave flow rate (improvement by using interpolation efficiency maps and low pass filter with time constant $t = 1$)

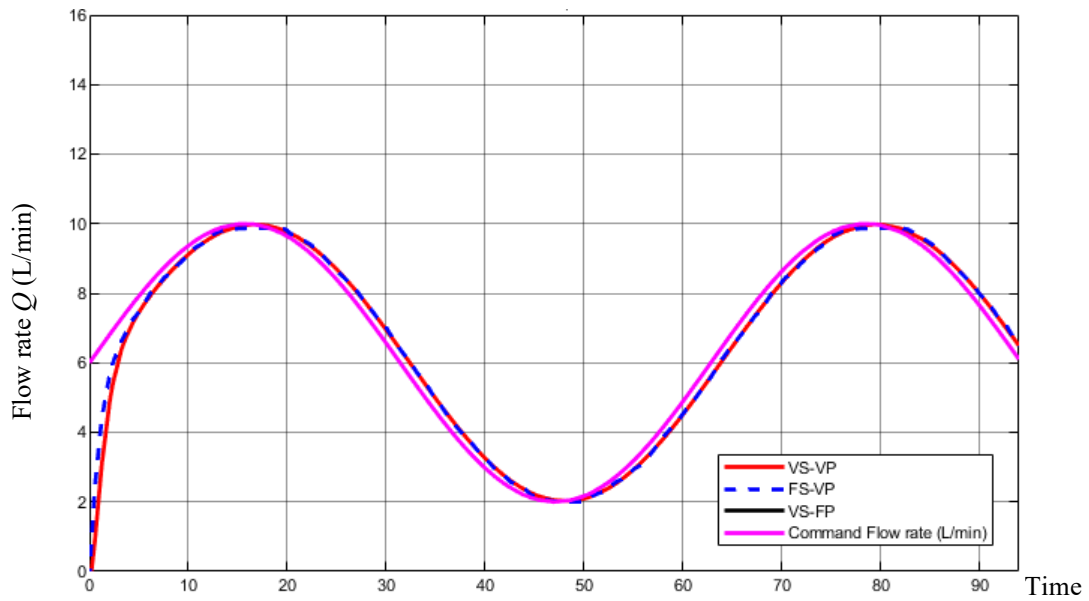


Fig. 4.14. Response flow rate and command flow rate comparison at output constant pressure $\Delta p = 10$ MPa for command sine wave flow rate (improvement by using interpolation efficiency maps and low pass filter with time constant $t = 1$)

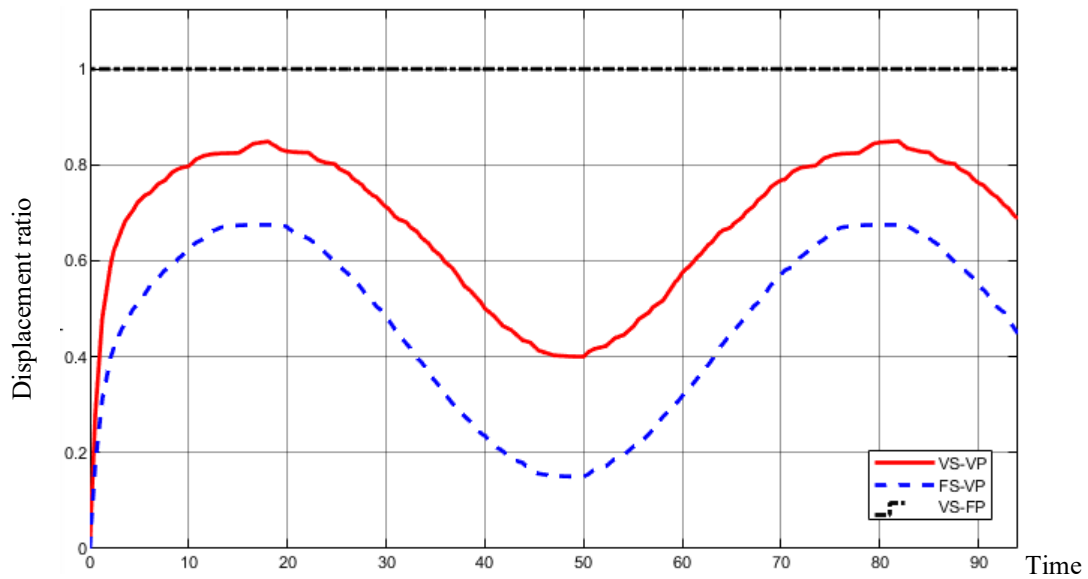


Fig. 4.15. Displacement ratio at output constant pressure $\Delta p = 10$ MPa for command sine wave flow rate (improvement by using interpolation efficiency maps and low pass filter with time constant $t = 1$)

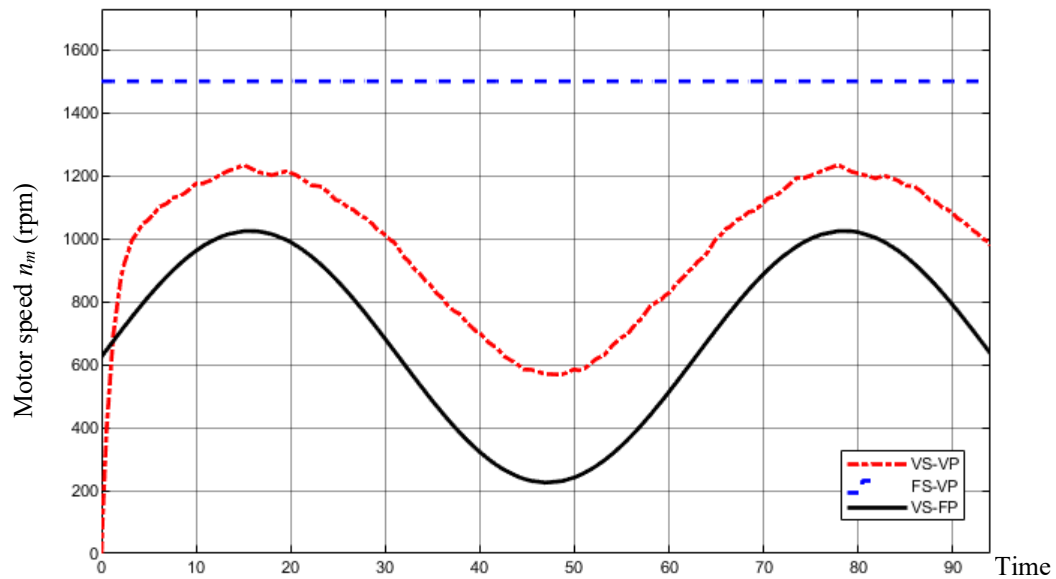


Fig. 4.16. Motor speed command at output constant pressure $\Delta p = 10$ MPa for command sine wave flow rate (improvement by using interpolation efficiency maps and low pass filter with time constant $t = 1$)

To decrease the delay in Figure 4.14, the time constant t is set at 0.5. The simulation results according to $t=0.5$ are presented in Figure 4.17 to Figure 4.20.

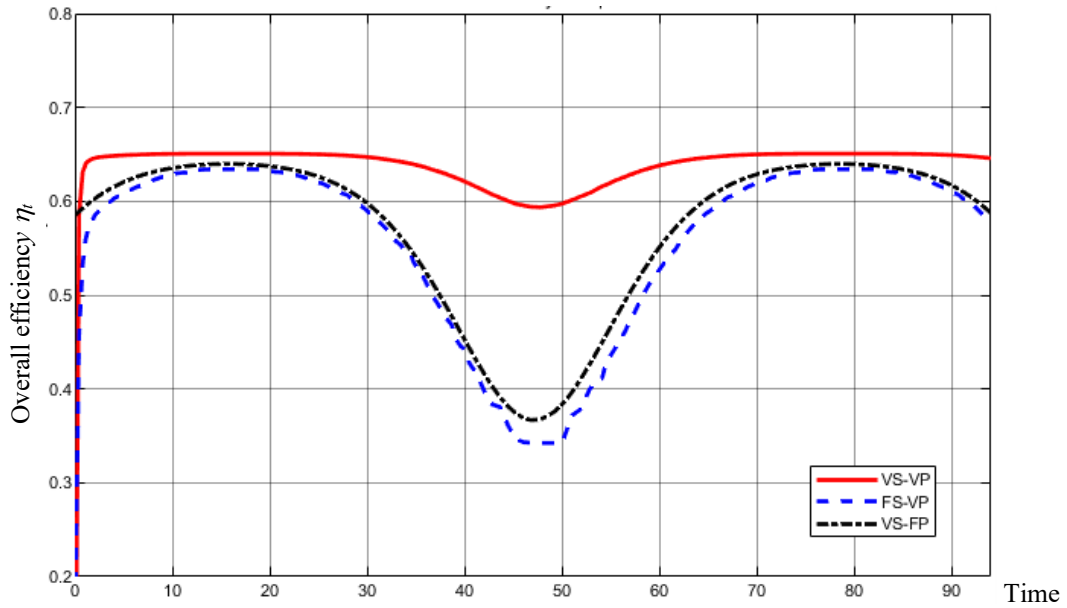


Fig. 4.17. Overall efficiency η_t comparison at output constant pressure $\Delta p = 10$ MPa for command sine wave flow rate (improvement by using interpolation efficiency maps and low pass filter with time constant $t = 0.5$)

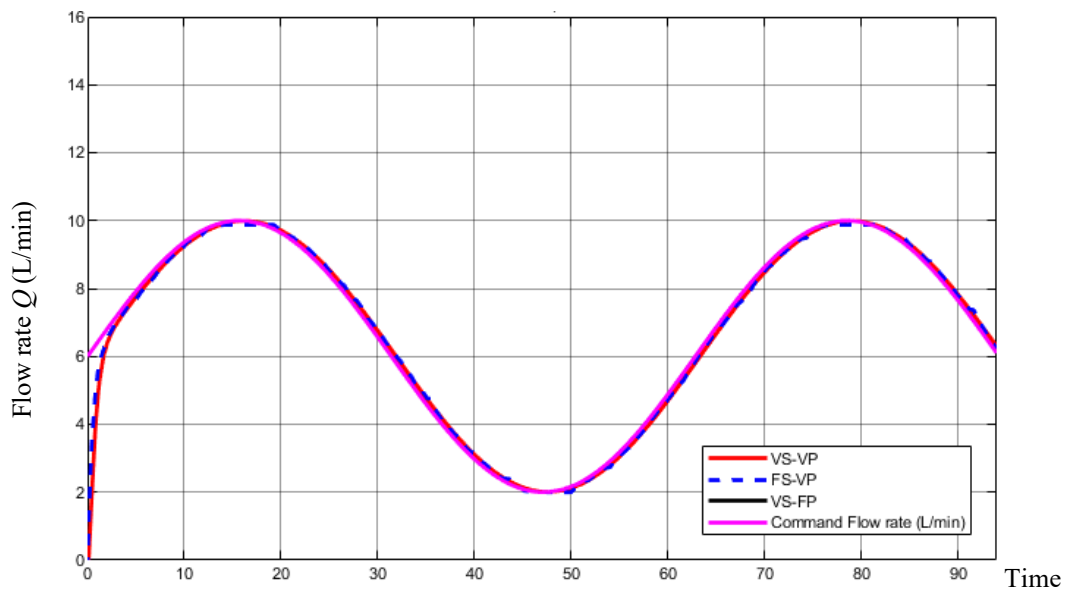


Fig. 4.18. Response flow rate and command flow rate comparison at output constant pressure $\Delta p = 10$ MPa for command sine wave flow rate (improvement by using interpolation efficiency maps and low pass filter with time constant $t = 0.5$)

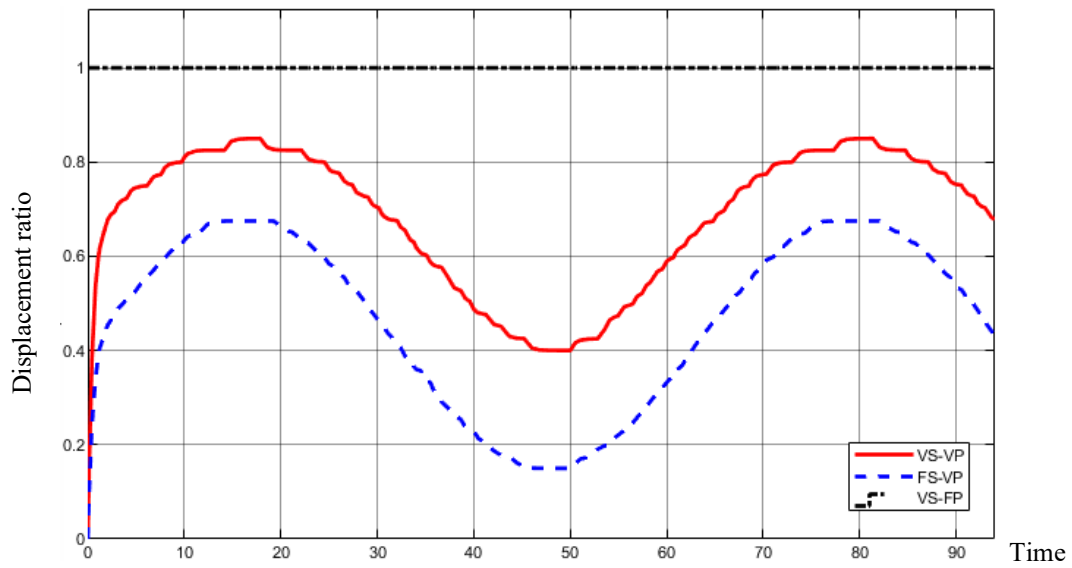


Fig. 4.19. Displacement ratio at output constant pressure $\Delta p = 10 \text{ MPa}$ for command sine wave flow rate (improvement by using interpolation efficiency maps and low pass filter with time constant $t = 0.5$)

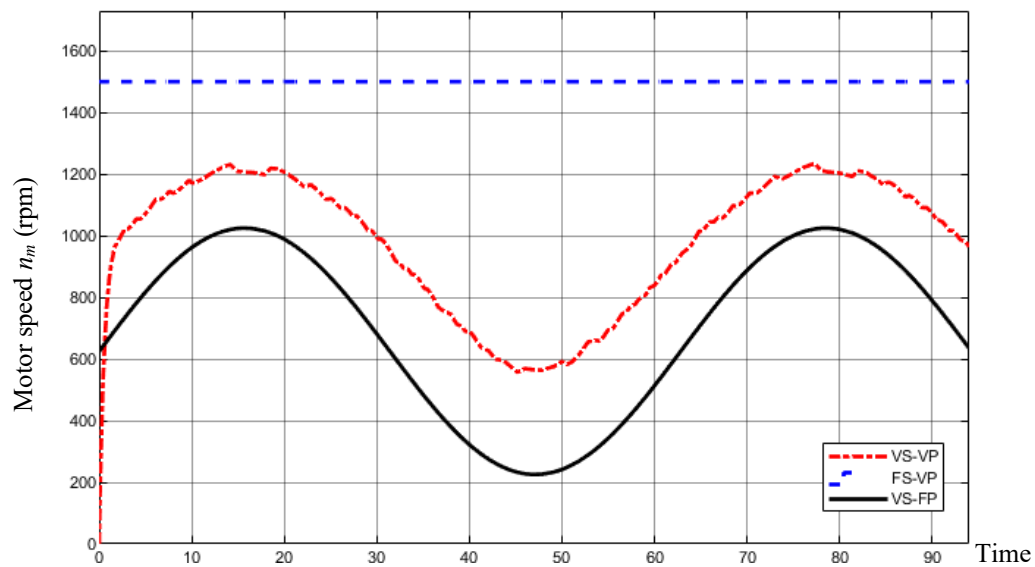


Fig. 4.20. Motor speed command at output constant pressure $\Delta p = 10 \text{ MPa}$ for command sine wave flow rate (improvement by using interpolation efficiency maps and low pass filter with time constant $t = 0.5$)

As shown in Figure 4.18, the delay between response flow rate and command flow rate is decreased. However, the control commands in this case are not smooth as shown in the case with time constant $t = 1$.

Another simulation case is done with time constant $t = 2$ as shown in Figure 4.21 to Figure 4.24. The smoothness of control commands is better than these ones in the cases with time constant $t=1$ and 0.5 . However, the delay of response flow rate in this case is increased.

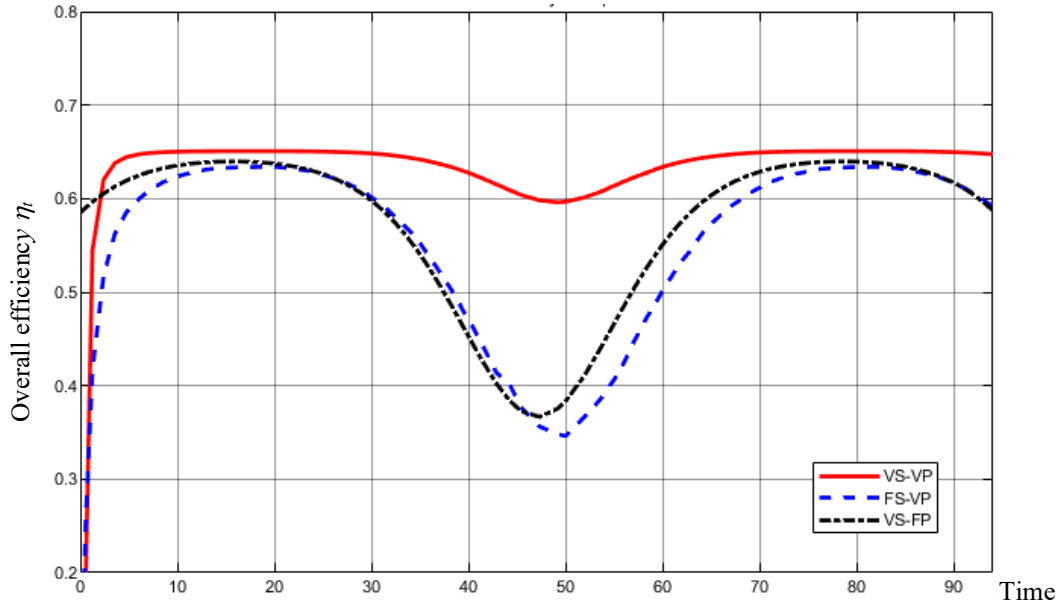


Fig. 4.21. Overall efficiency η_t comparison at output constant pressure $\Delta p = 10$ MPa for command sine wave flow rate (improvement by using interpolation efficiency maps and low pass filter with time constant $t = 2$)

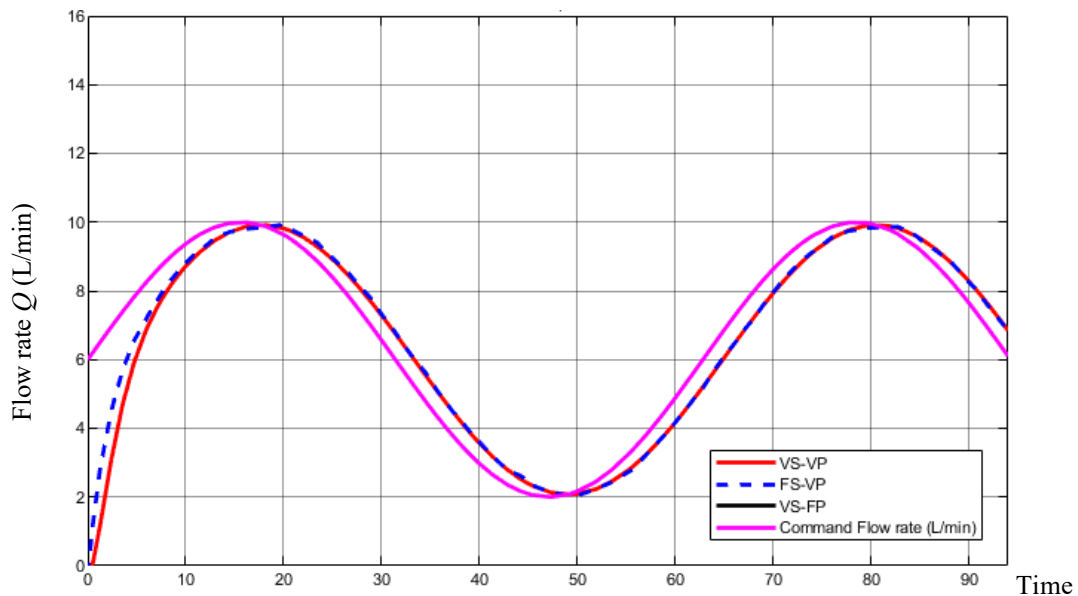


Fig. 4.22. Response flow rate and command flow rate comparison at output constant pressure $\Delta p = 10$ MPa for command sine wave flow rate (improvement by using interpolation efficiency maps and low pass filter with time constant $t = 2$)

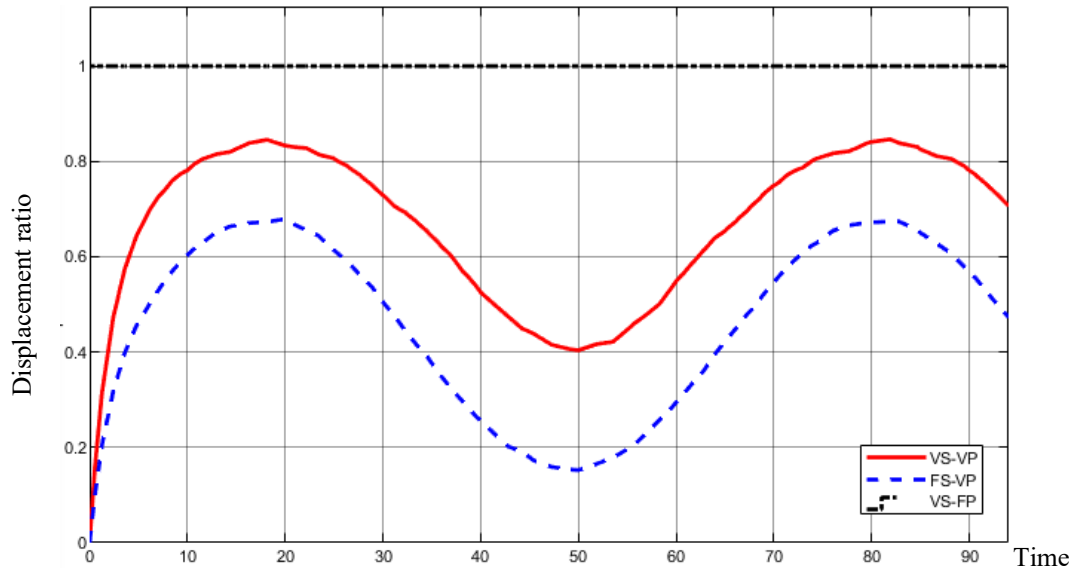


Fig. 4.23. Displacement ratio at output constant pressure $\Delta p = 10$ MPa for command sine wave flow rate (improvement by using interpolation efficiency maps and low pass filter with time constant $t = 2$)

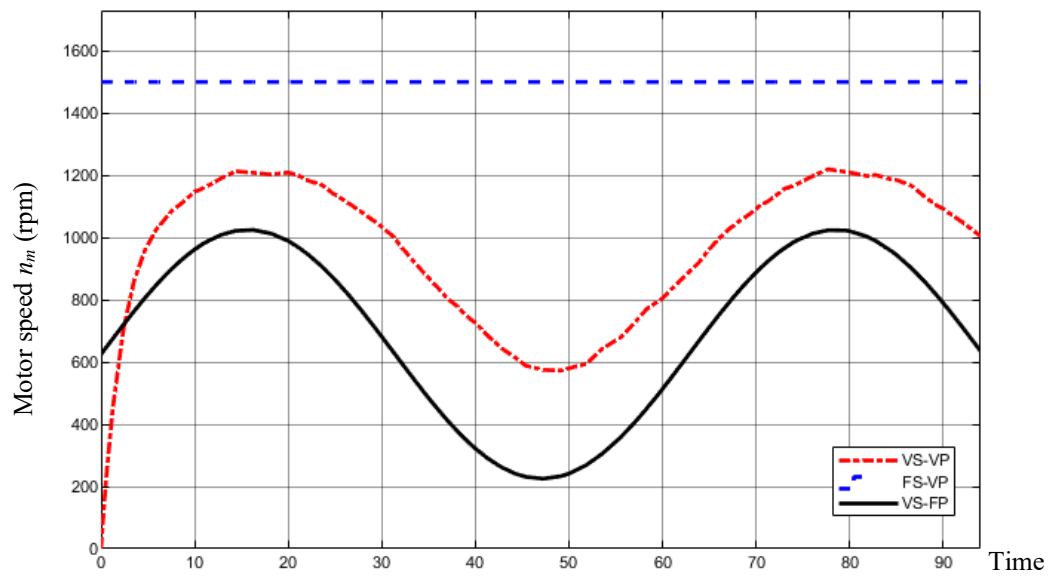


Fig. 4.24. Motor speed command at output constant pressure $\Delta p = 10$ MPa for command sine wave flow rate (improvement by using interpolation efficiency maps and low pass filter with time constant $t = 2$)

From simulation above, for both types of signals, the efficiency of VS-VP system is higher than VS-FP and FS-VP system, especially for low flow rate operation. For large flow rate operation, the efficiency of 3 concepts is identical since pump displacement ratio α and motor speed n_m are at high value to supply large flow rate.

When the number of efficiency maps is increased and the low pass filter is used, the smoothness of control command for hydraulic pump and electric motor is considerably improved to apply in actual machine. However, a delay between response flow rate and command flow rate occurs. If the time constant t is increased, this delay will be increased, and the control command of displacement and speed is smooth or continuous. On the otherhand, this delay will be decreased if the time constant t is decreased, however, this leads to the control commands become discontinuous. It concludes that, there is a trade-off between discontinuity reduction of control command and response delay of flow rate in this study. Therefore, it is necessary to study for the optimum conditions according to the actual machine.

4.2 Controllers with efficiency maps for regulating displacement ratio and motor speed

The diagram of improvement of the transient efficiency for EHDS is presented in Figure 4.25. Based on the efficiency maps created by experiment, Simulink model generates the control command for regulating the speed of electric motor and displacement ratio of hydraulic pump to control the VS-VP system working at high-efficient mode.

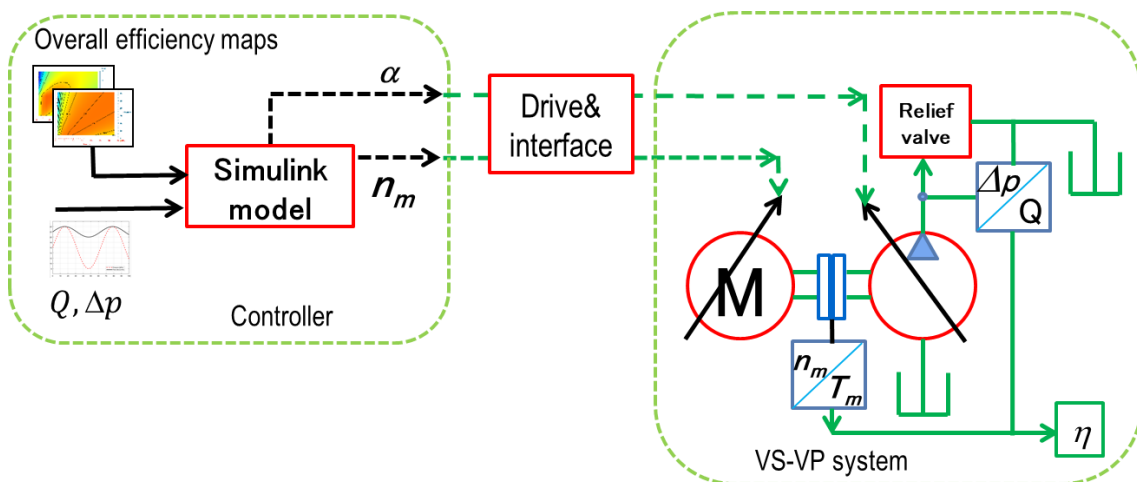


Fig. 4.25. Diagram of improvement of the transient efficiency for EHDS

This method could be applied for the VS-VP system includes electric motor and hydraulic pump which are not limited to the servo motor and swash plate pump used in this study. For example, the VS-VP system can be equipped with servo motor, inverter-driven variable speed induction motor, SR motor; and with pumps that control the swash plate by an external mechanical or by an internal hydraulic servo mechanism. For each VS-VP system combined from electric motor and hydraulic pump as mentioned above, if the efficiency maps are obtained in the experiment as shown in Chapter 3, VS-VP system can be operated with the effectiveness has been confirmed in this study.

The configurations of drive and interface in Figure 4.25 are depended on the type of electric motor and hydraulic pump. The configuration of drive for servo motor in this study is presented in Figure 4.26. The speed command from Simulink model in DSP (Digital Signal Processor) is transferred to junction terminal blocks to I/O interface connection in servo amplifier. Based on the control command from Simulink model, the rotational direction and rotational speed of servo motor will be regulated by amplifier. The details of this configuration is presented in Appendix A.2.

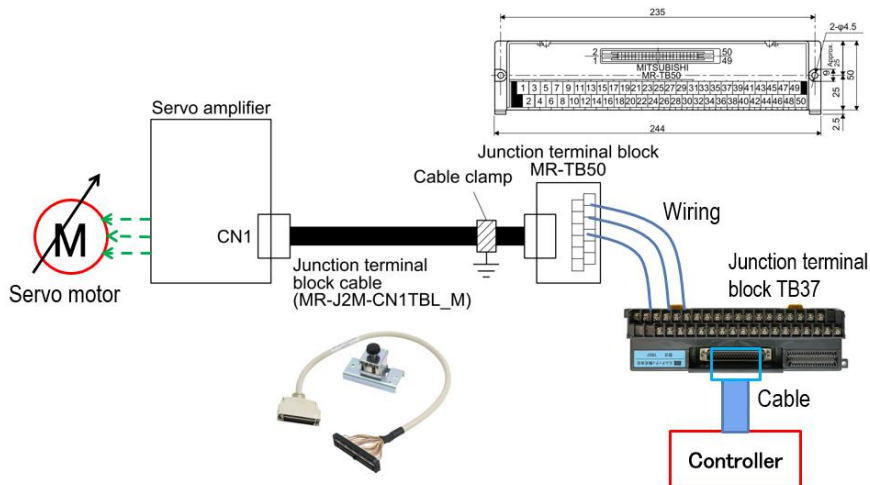


Fig. 4.26. Configuration of drive for servo amplifier^{4.1), 4.2)}

To control displacement ratio of hydraulic pump, there are two methods. The first one that controls the swash plate with the hydraulic servo mechanism inside the pump based on the pump discharge pressure. With the type of hydraulic servo mechanism inside the pump, even if the swash plate position is constant, the pressure reducing valve always consumes a part of the discharge flow rate, so the

pump efficiency map changes. The second one is to use an external motor such as step motor to control displacement screw of hydraulic pump. With this mechanical type (screw type), efficiency map is not affected by displacement controller because controller does not use any part of the pump discharge flow rate. Moreover, the power consumption of step motor is low, so it affects slightly on the overall energy efficiency.

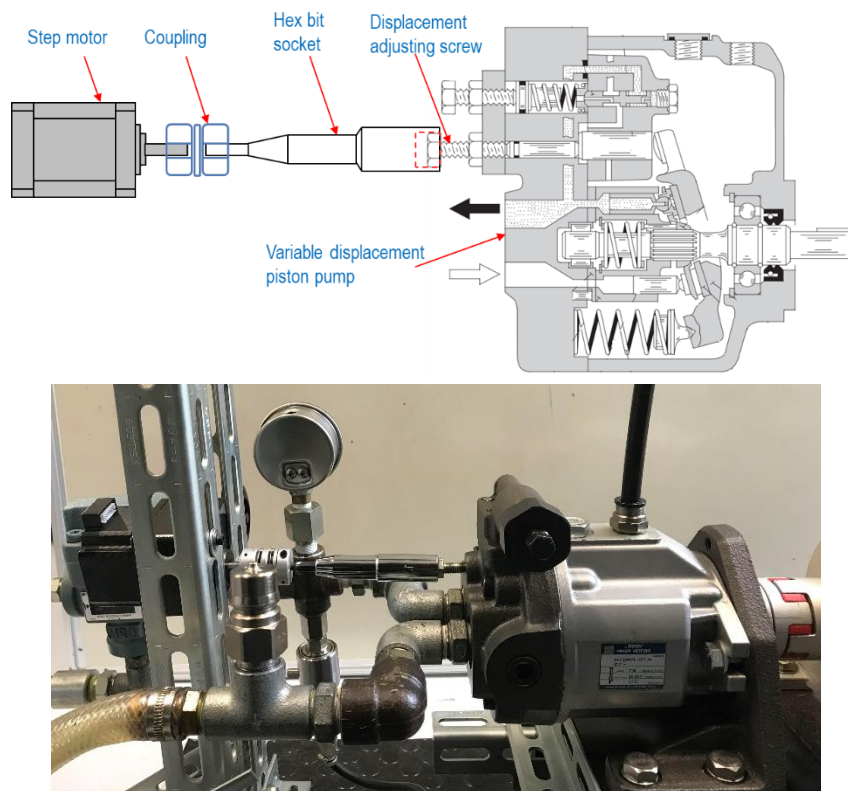


Fig. 4.27. Mechanism for rotating the displacement adjusting screw of hydraulic pump

To control the movement of displacement adjusting screw of hydraulic pump, this study proposed a mechanism that the shaft of step motor is joined to that screw through coupling and hex bit socket as shown in Figure 4.27. The step motor is operated at position control mode. The appearance of step motor is shown in Figure 4.28. The details of step motor are presented in Appendix A.2.

The equipments as shown in Figure 4.26 and Figure 4.27 is a typical apparatus setup for regulating the speed of servo motor and displacement ratio of hydraulic pump. This apparatus setup could be used for various servo motors and variable displacement pumps.

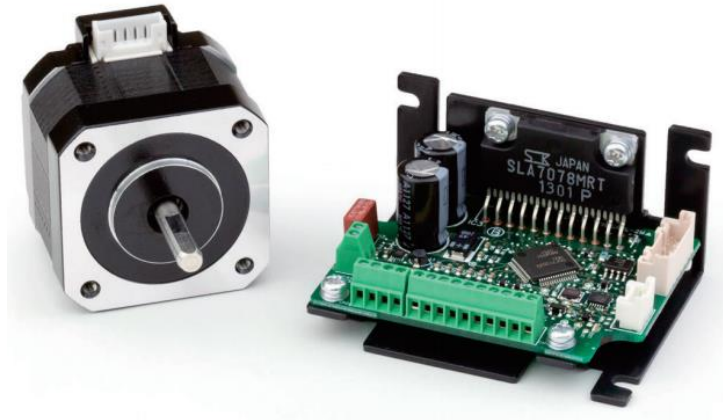


Fig. 4.28. Step motor and driver ^{4.3)}

Based on the experiment efficiency maps in Chapter 3, controller generates and outputs n_m and α to control the speed of servo motor and motion of stepping motor to change the displacement adjusting screw of hydraulic piston pump. By these outputs n_m and α , VS-VP system could supply the required flow rate and keep the overall efficiency of system at the highest values continuously.

4.3 Summary of Chapter 4

- The configuration for improving transient efficiency of EHDS is proposed in this Chapter. Based on command flow rate and overall efficiency maps, Simulink model will determine motor speed and displacement determined to remain high-efficient working condition of EHDS. This configuration could be realized with various servo motors and variable displacement pumps by applying the simulink model built in this study.
- The amplifier is controlled by output signal of Simulink model to regulate motor speed. On the other hand, the swash plate angle control of the variable displacement pump includes the choice of internal hydraulic servo mechanism and external mechanical swash plate control. In this study, a stepping motor is proposed to regulate the movement of displacement adjusting screw (displacement ratio).

4.4 References

4.1) MR-J4-_A_(-RJ), MR-J4-03A6(-RJ), Servo amplifier instruction manual, Mitsubishi Electric company, 2013.

4.2) HG-SR series, Servo motor instruction manual, Mitsubishi Electric company, 2013.

4.3) Step motor instruction manual, Plexmotion company, 2020.

Chapter 5

**Development of EHDS using SRM with
servo function and improvement of
overall efficiency by using overall
efficiency maps**

Chapter 5. Development of EHDS using SRM with servo function and improvement of overall efficiency by using overall efficiency maps

In industrial applications, a permanent magnet synchronous motor (PMSM) is used as a high-performance electric servomotor to drive a hydraulic pump in a closed hydraulic circuit. However, PMSMs are expensive and present a few drawbacks due to permanent magnets, such as insufficient heat and vibration resistance and a significant usage of rare-earth materials. Other type of motor called the switched reluctance motor is robust and requires no permanent magnet and rare-earth materials owing to its driving principle. Compared with permanent magnet and induction motors, switched reluctance motor (SRM) have a simpler and more robust construction owing to its rotor structure without coils or permanent magnets, thereby affording a lower fabrication cost. In this chapter, SRM motor is studied to drive hydraulic pump in valveless EHDS.

5.1 Operational principle of SRM

An SRM is identified by the numbers of stator and rotor poles. A typical SRM has salient poles on both the stator and rotor, and its windings are wound only on the stator, as shown in Fig. 5.1.

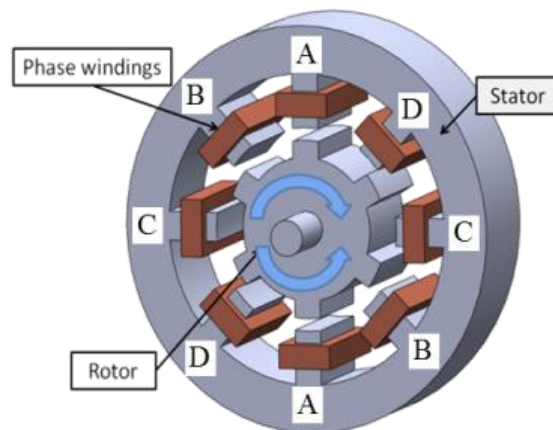


Fig. 5.1. Typical structure of 8/6-type SRM

The sets of opposing poles of the stator are denoted as phases A, B, C, and D. Stator windings that generate a magnetic flux penetrating the air gap between the rotor and stator are wound in series in each phase, and four phases are connected in parallel. In this study, an 8/6-type structure with four phases, a 6-teeth rotor, and an 8-teeth stator was used. In the SRM, when the winding was

excited, a force attracting the salient poles of the rotor and stator was generated, thereby producing a reluctance torque. Fig. 5.2 shows the inductance distribution L due to the rotor angular position θ .

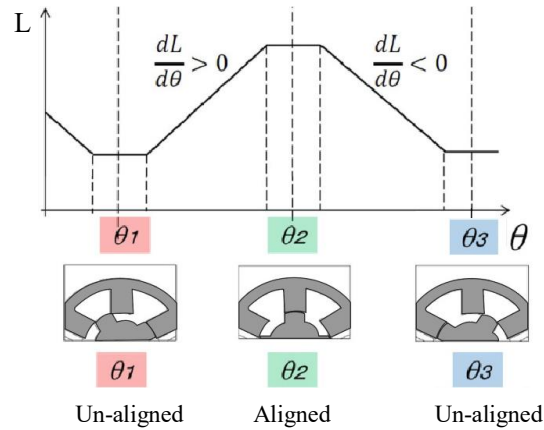
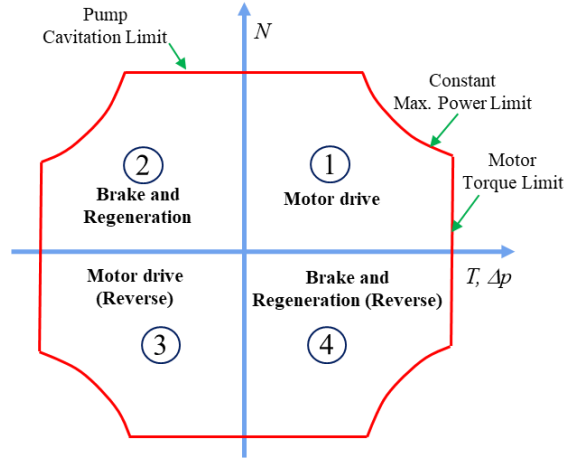


Fig. 5.2. Inductance change in rotational direction of rotor.
 L : Flux linkage; θ : Rotor angular position

As shown in Fig. 5.2, at the unaligned position, the flux linkage is the minimum owing to the large air gap. By contrast, when the rotor and stator poles are aligned, the resulting air gap between the stator and rotor poles is minimized. Here, the flux linkage is at its maximum and is dependent on the excitation current. As a higher level of current is applied, the incremental increase in the flux linkage will decrease owing to the higher magnetic flux density, hence, the saturation level of the core will decrease. Fig. 5.3 shows the operating range of a hydraulic pump driven by an SR servomotor. Quadrant ① is the region where the hydraulic power is supplied to the hydraulic actuator by a positive torque with forward rotation; it energizes the phase current in the region of $dL/d\theta$ to be positive, as shown in Fig. 5.2. Quadrant ② is the region where braking is applied to the hydraulic actuator with a negative torque and a forward rotation. At the time of transition to the region of negative $dL/d\theta$ shown in Fig. 5.2, the magnetic flux remains and is disconnected from the power supply, and a negative torque is generated by power regeneration. When the negative torque is insufficient, the power supply is connected and the phase current is energized to increase the negative torque. Quadrants ③ , ④ are the states in the reverse rotational directions of ① , ② respectively.



T : Motor torque; Δp : Pressure difference of hydraulic pump;
 N : Speed of motor/pump

Fig. 5.3. Four-quadrant operation of hydraulic pump driven by servomotor

5.2 Control principle of SRM

To operate the four-quadrant drive in N-T coordinated plane in Fig. 5.3, the control method for SR servomotor should contain the following controls^{5.1)}:

1) Firing order control (Rotational direction control)

The rotational direction will be decided by the order of phase excitations - in other words, the SRM rotates forward direction by the firing order of A-B-C-D-A, reverse direction by the order of A-D-C-B-A in Fig. 5.1.

2) Torque amplitude control

SRM has a salient structure, which is an essential part of its torque production mechanism. Because of this, SRM characteristics such as flux linkage and torque are functions of rotor position. At the same time, these characteristics are dependent on the phase current.

The torque amplitude of a SRM is given by Eq. (5.1)^{5.2)}.

$$T = \frac{1}{2} i^2 \frac{dL}{d\theta} \quad (5.1)$$

where, T , i , L , and θ are output torque of SRM, electric current of winding, inductance, and rotor teeth angular position of SRM, respectively. The amplitude of output torque is controlled by the current of winding in each phase. The magnitude of the phase current is controlled by PWM (Pulse Width Modulation) switching under constant voltage supply.

3) Torque direction control

The torque direction is determined by the rotor teeth position in firing. The region of positive $dL/d\theta$ - the range where L in Fig. 5.2 increases upward to the right - is called the motor region. In case of the firing in this region, the positive torque is generated, and the SRM accelerates. The region of negative $dL/d\theta$ - the range where L in Fig. 5.2 decreases downward to the right - is called the generator region and the negative torque is also generated in the same manner in the region, and the SRM decelerates. Further, if magnetic flux remains at the time of transition to this region, an electromotive force that generates a magnetic field that hinders a decrease in magnetic flux due to a decrease in inductance is generated in the winding, and power generation - regeneration - that continues to flow a phase current without connection with the power supply is performed.

The angular position of the rotor is detected by a rotary encoder. The controller of the SRM determines an appropriate angle and angle range for generating a positive torque or a negative torque based on the command. As shown in Fig. 5.1, the datum of the angle of the rotor position was set to 0^0 as the rotor and stator poles are in alignment - aligned position. Based on the previous studies^{5.3), 5.4)}, in the motor region, when exciting on the plus side than the excitation range from -30^0 to -15^0 , the current starts to be applied to the generator region and prevents rotation, so it was set to -30^0 to -15^0 . In the generator region, since the braking force was the largest, it was set to 0^0 to 15^0 .

5.3 Proposed SRM controller

Fig. 5.4 and Fig. 5.5 show a schematic diagram of SRM controller. The magnitude of the phase current is determined by the PI control according to the difference in the response speed between the SRM and the command speed. The direction of the torque is decided by the value sign (positive or negative) of the difference between the command speed and the response speed and the positive or negative of the response speed itself. Moreover, it is also determined by the command rotational direction and the response speed direction in the servo-drive control. In Fig.5.5, the control signal for switching devices such as field effect transistors (FET) is sent from the DSP installed with the driving program of the SRM.

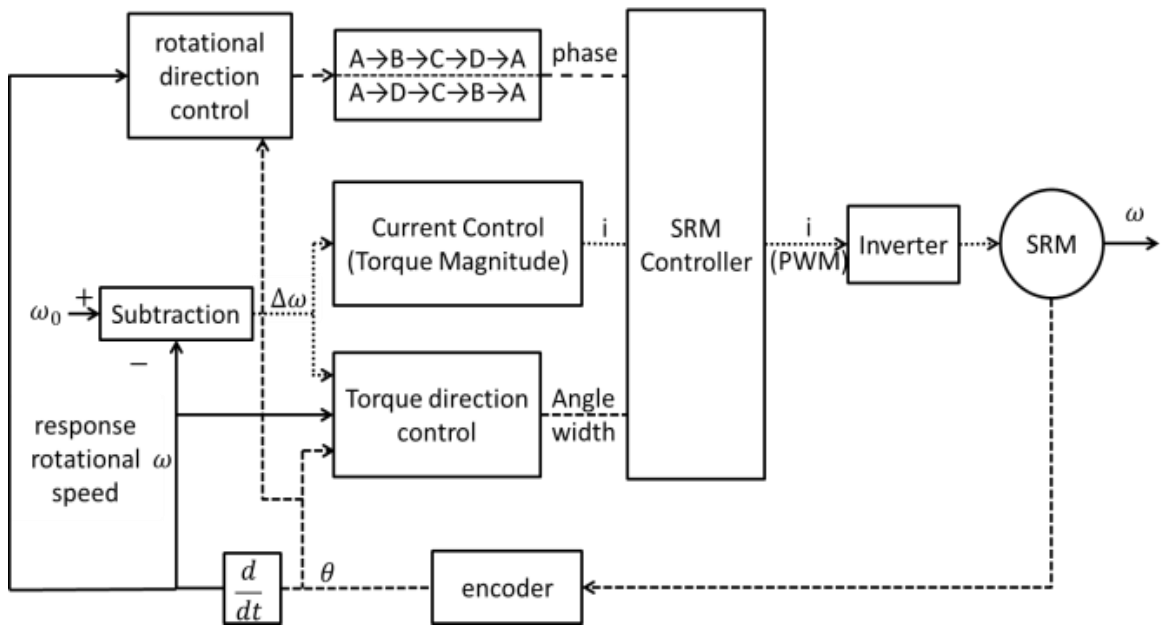


Fig. 5.4. Bidirection rotational speed control system of SRM

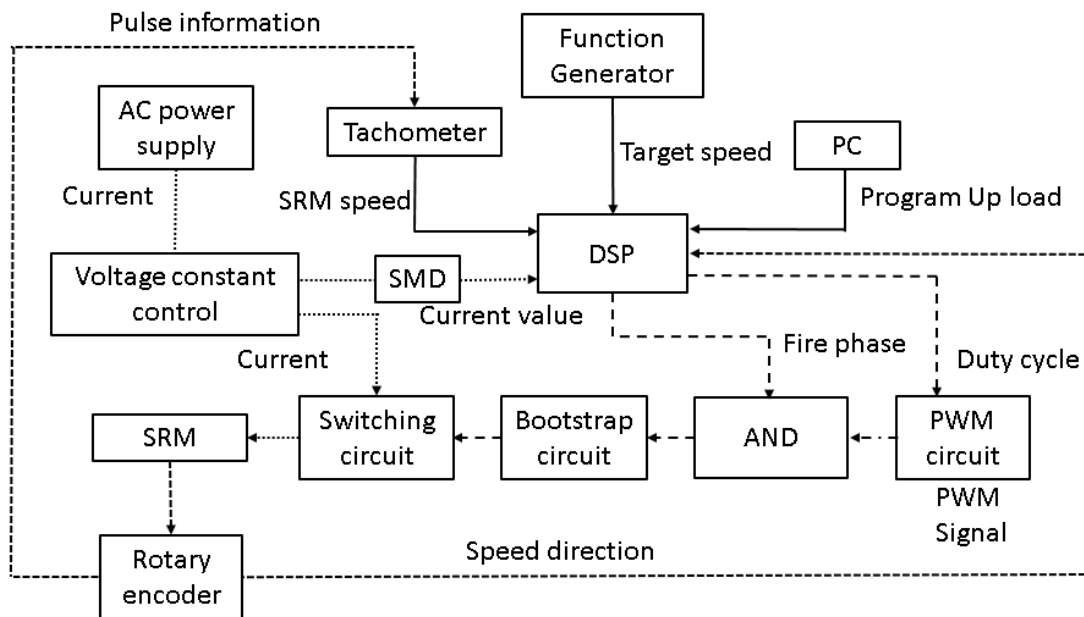


Fig. 5.5. System flow of SRM drive system

In this study, a special control model was added in the startup drive because an incremental rotary encoder was used. To determine the appropriate excitation timing to drive the SRM, it is necessary to accurately determine the origin of the SRM body (origin of the rotor) in the startup drive. It is desirable to calculate the

angle origin of the SRM body as the position of the A-phase allied position (the part where the inductance has the maximum value). When the SRM was started, to calculate using this position as the origin, t_{step} (0.5 [s]) was excited in the order of A phase-B phase-C phase-D phase-A phase, and the A phase was forced to the allied position. This “startup” procedure is then followed by the driving of the SRM, as shown in Fig. 5.6.

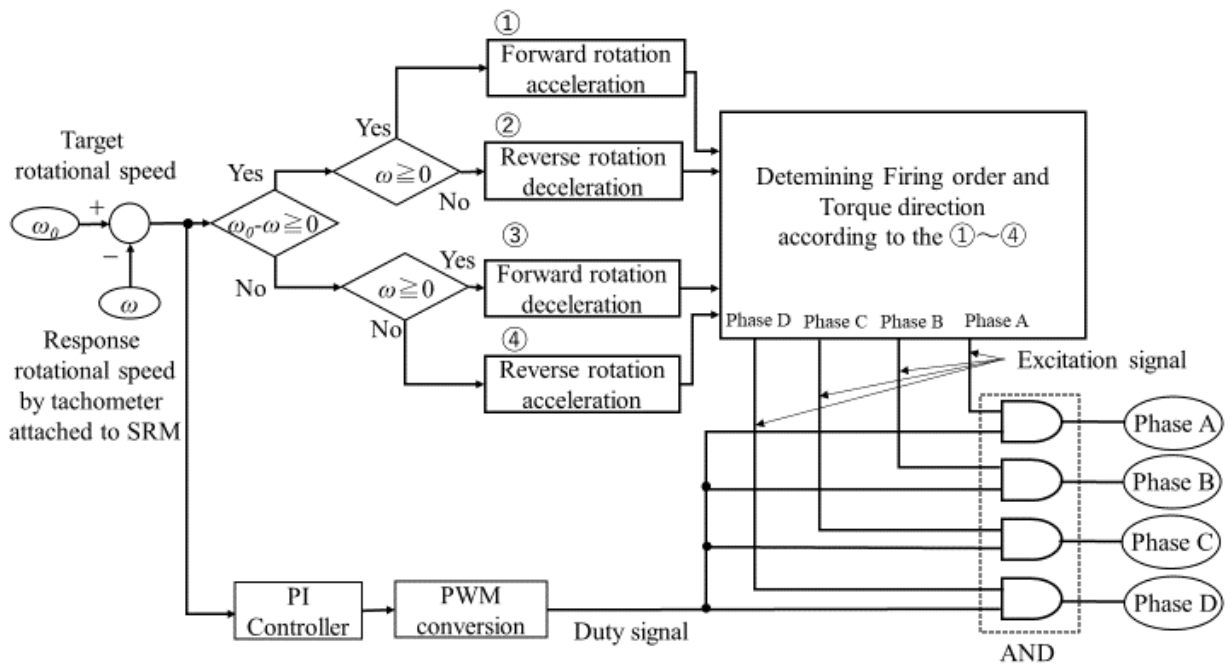


Fig. 5.6. SRM drive system

In the SRM drive system (Figure 5.6) after the “startup” processing, the rotation was stopped, and information regarding the rotor angle origin (rotary encoder reset origin) was acquired. When starting the SRM, whether the rotation was a forward or reverse rotation was determined based on the drive command signal, and the order was A phase-B phase-C phase-D phase-A phase (positive direction). The combination of the rotor angle and excitation phase was set such that the excitation of each phase proceeded in the excitation order in which the rotation continued.

In the reverse rotation, a combination of the rotor angle and excitation phase was set in the order of A phase-D phase-C phase-B phase-A phase (the excitation order in which the reverse rotation continued). The torque of the forward/reverse rotation was determined based on the magnitude of the phase winding current,

regardless of the rotation direction. Therefore, the winding current was PWM controlled to be consistent with the target rotation speed.

Furthermore, in the motoring/regeneration state, the section where the winding current of the phase was conducted indicated a positive gradient ($dL/d\theta > 0$, motoring) or a negative gradient ($dL/d\theta < 0$) of the inductance distribution of the SRM. Therefore, to control the SRM like a servomotor with both forward and reverse rotations, variable torques, and switching between motoring and regenerative modes, regeneration must be performed by motoring or rotating based on the excitation phase order according to the rotating direction, winding current magnitude, and rotor angle. Furthermore, control must be performed continuously by combining the three elements of winding energization timing in the region.

5.4 PI gain design for improving drive system

A test was performed to determine the feedback gain of the PI control to determine the control amount of the phase current. The experimental conditions were derived from Table 5.1 with reference to the specifications of the hydraulic pump/motor to be directly connected to the SRM.

Table. 5.1 Experimental condition

	Motor mode	Generator mode
Command speed	0 to +1000 (rpm)	-1000 to 0 (rpm)
Command waveform	Step response, frequency response	

Typically, cavitation occurs in a hydraulic pump/motor to be used at approximately ± 2000 rpm. Therefore, the experimental conditions were determined with a target of 50% rotation speed.

However, the goal of this research was not to obtain the optimum value of the PI gain, but to construct a valveless hydraulic system using an SR servo motor. Therefore, the differential gain was omitted, and PI control was used. First, the integral gain K_i was determined experimentally. Subsequently, K_i was tuned to 0.1 with proportional gain $K_p = 0$ and a small settling time with a small overshoot and undershoot of the response speed to the target speed of the square wave. Finally, K_p was determined by evaluating the square error area for a series of experimental conditions with different response waveforms.

The square error area is one of the indexes used to evaluate the controllability of the target model. The equation is expressed as shown in Eq. (5.2), and the square error area in the step response is the shaded area shown in Fig. 5.7. In addition, an evaluation criterion to determine whether speed oscillations are allowed near the target speed applies in the square error area.

$$I = \int_0^{\infty} e^2 dt \quad (e : \text{error}) \quad (5.2)$$

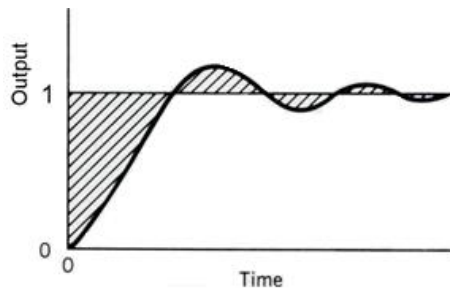


Fig. 5.7. Illustration of square error area

If allowed, the square error area itself is minimized, but velocity oscillations occur near the target speed. On the other hand, when not allowed, the square error area itself becomes larger than when allowed, but no velocity oscillation occurs. In this case, it is not preferable that vibrations occur in the operation of the motor in the electro-hydraulic control. Therefore, a criterion that does not allow speed vibration near the target speed is adopted, and the square error area of the response speed to the command speed is obtained.

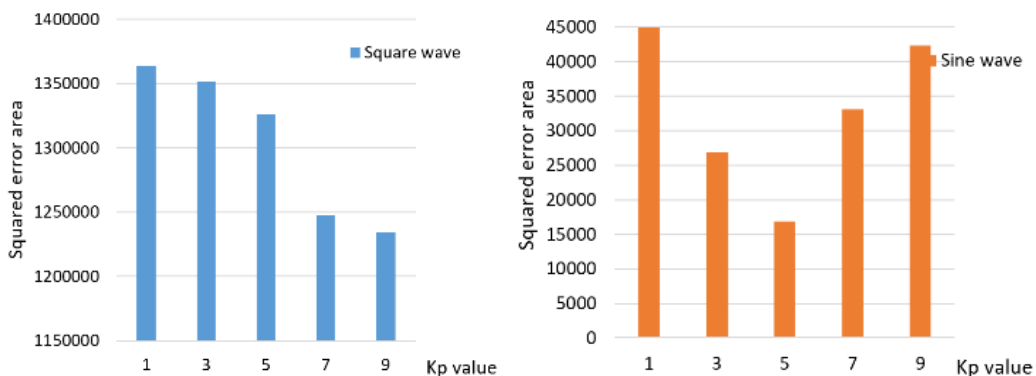


Fig. 5.8. Squared error area with square wave and sine wave

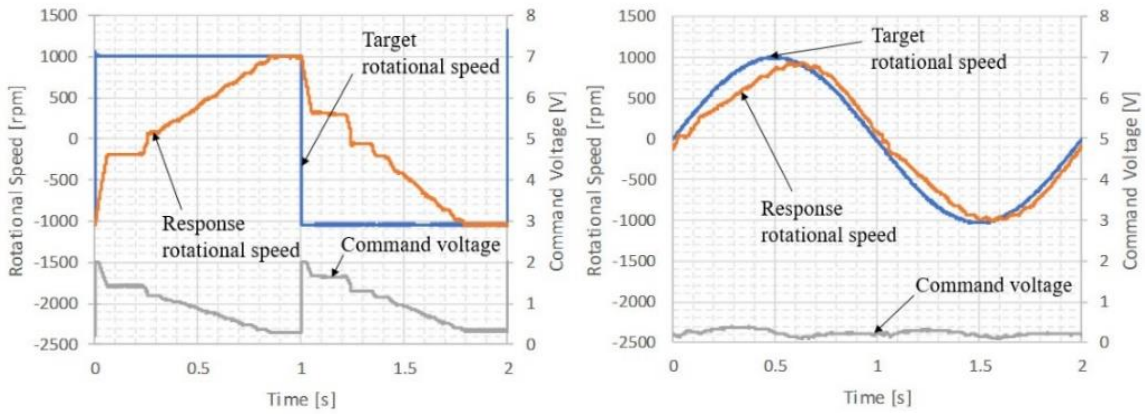


Fig. 5.9. Experimental result for improving drive system response with $K_p = 1$

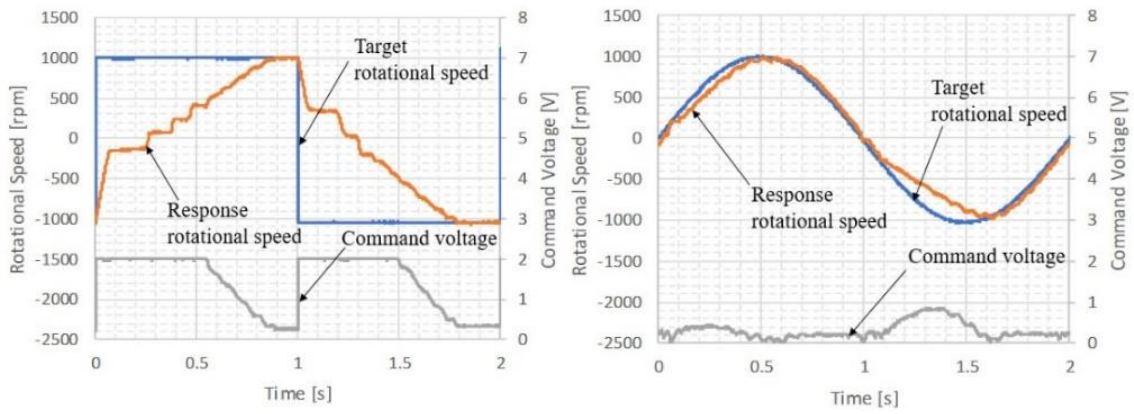


Fig. 5.10. Experimental result for improving drive system response with $K_p = 3$

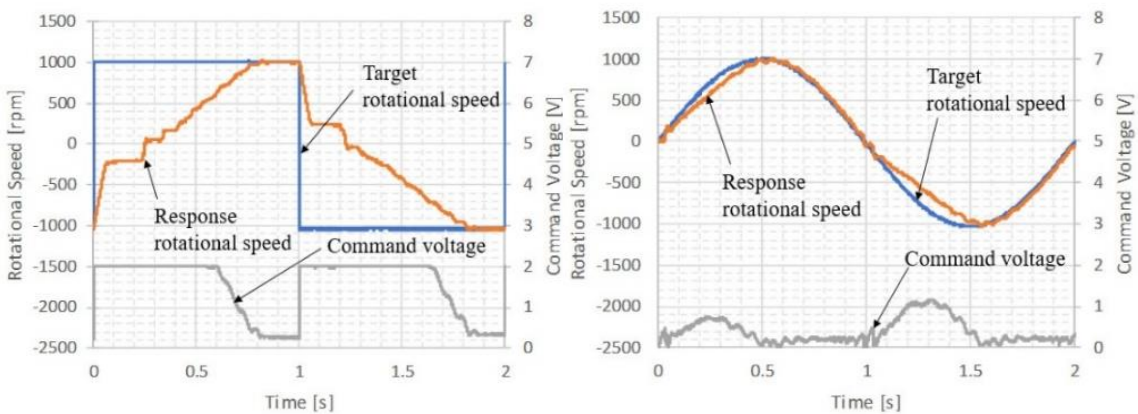


Fig. 5.11. Experimental result for improving drive system response with $K_p = 5$

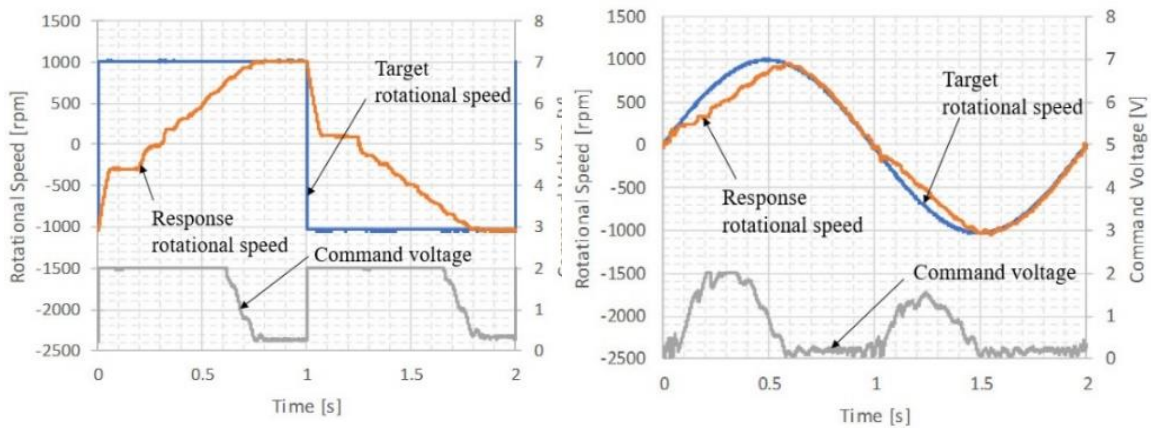


Fig. 5.12. Experimental result for improving drive system response with $K_p = 7$

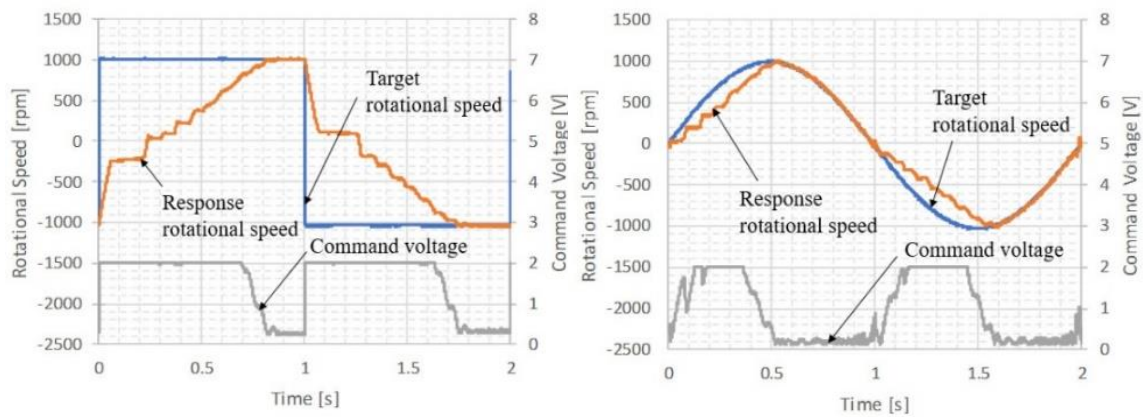


Fig. 5.13. Experimental result for improving drive system response with $K_p = 9$

The values shown in Figure 5.8 to Figure 5.13 were used to determine the optimal value of the proportional gain. The evaluation method was based on the square error area for one cycle when square and sine waves of 0.5 (Hz) were the target rotation speed. The amplitude from -1000 to $+1000$ (rpm) was considered to evaluate in both the forward and reverse directions.

The “command voltage” in Fig. 5.8 to Figure 5.13 is the deviation of the target speed from the response speed converted into a voltage. This value was input to the power amplifier and then amplified, and the input voltage to the SRM fluctuated. Owing to the specifications of the power amplifier, saturation was applied in the DSP such that the maximum value reached 2.0 V and then plateaued at that value.

The results shown in Figure 5.8 to Figure 5.13 indicate that the square error area of the step response decreased as the proportional gain increased. This might

be because when the command voltage remained longer when it was the upper limit of 2 V, the rise was faster. However, even when the proportional gain increased, the rising speed did not differ significantly. This is because the output current was limited to 10 A based on the amplifier specifications, and the torque proportional to the square of the current had saturated, as shown in Eq. (5.1).

As shown in Figure 5.8 to Figure 5.13 for sine waves, $K_p = 5$ yielded the smallest error. The command voltage reached its maximum when the proportional gain was excessively large. Hence, it was assumed that the allowable current value of the power amplifier had been exceeded, the voltage increased and decreased, the rotation speed oscillated, and the tracking was delayed. In addition, when $K_p = 7$ and $K_p = 9$, near the switching between the normal and reverse rotations of the sine wave in the low-frequency range, oscillations at the following rotational speeds, which were not observed at $K_p = 5$ or less, were observed frequently. Hence, subsequent experiments were performed with $K_p = 5$ and $K_i = 0.1$.

In the next experiments, the response curve to the frequency input of the SRM controlled by the feedback gain derived accordingly is shown in Figure 14 to Figure 5.16. The rotation speed was set to ± 500 and ± 1000 rpm, and the frequency required in the frequency response was set to 0.5, 1.0, and 2.0 Hz. However, even at 1 Hz, the tracking was delayed for 1000 rpm. When the frequency was 2.0 Hz, the response curves became almost identical for both 500 and 1000 rpm. These values were considered as the limits of the switching speed of this circuit. Based on this result, the hydraulic pump/motor drive performed subsequently was controlled with a maximum command waveform of 1000 (rpm)/0.5 (Hz).

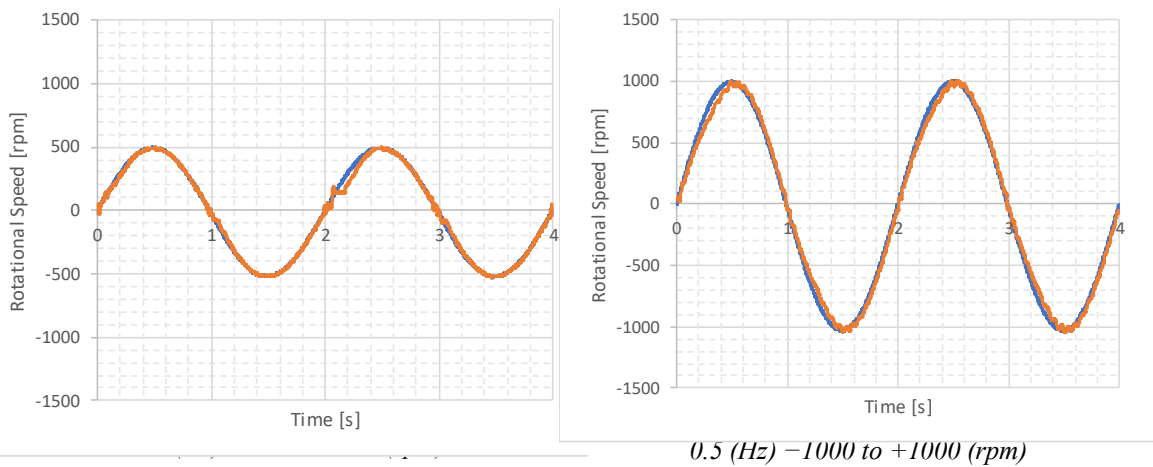


Fig. 5.14. Experimental results for improving drive system response with frequency response 0.5 Hz

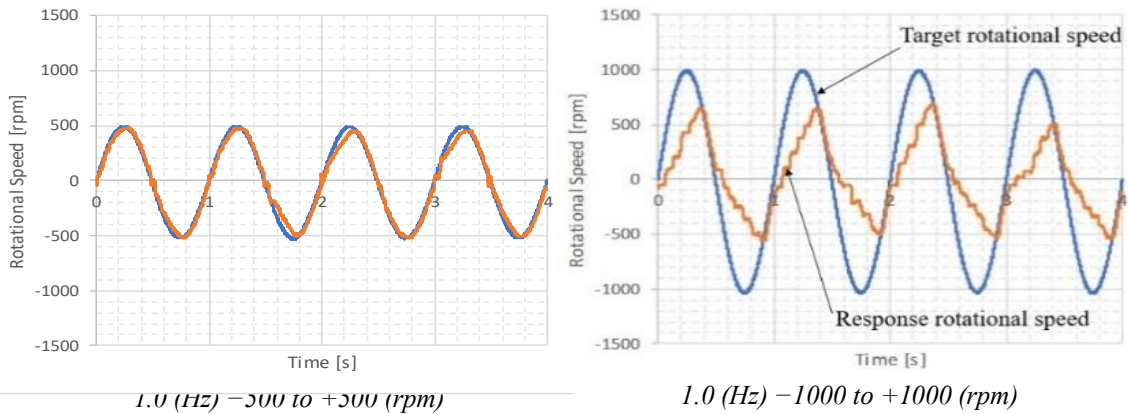


Fig. 5.15. Experimental results for improving drive system response with frequency response 1.0 Hz

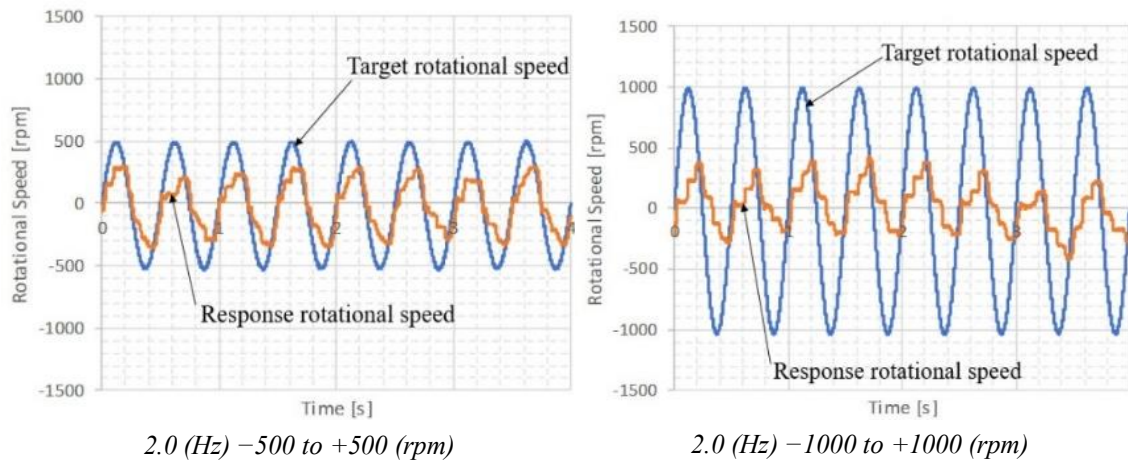


Fig. 5.16. Experimental results for improving drive system response with frequency response 2.0 Hz

5.5 Flow rate control experiment of hydraulic pump driven by SR servomotor in closed loop circuit

Fig. 5.17 shows the applications for the flow rate control of the hydraulic pump driven by the SR servomotor in a closed circuit with an actuator, such as a hydraulic cylinder, hydraulic motor, or rotary cylinder.

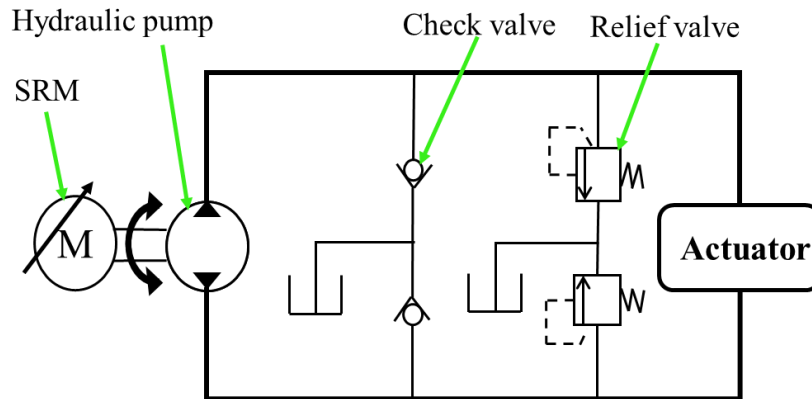


Fig. 5.17. Hydraulic closed circuit with cylinder and motor application for bidirectional flow rate control using hydraulic servo pump driven by SR servomotor

Using the proposed SRM controller, the speed and moving/rotating directions of the actuators can be regulated in both directions based on the direction of the SRM.

To evaluate the proposed driving method for the SR motor, two experimental configurations were implemented for the flow rate control of a fixed displacement bidirectional rotational axial piston pump driven by a four-phase 8/6-type SR servomotor in a closed circuit, as shown in Figure 5.17 and 5.5.2. Table 5.2 shows the specifications of the test SRM and test hydraulic pump/motor.

Table 5.2. Specifications of SRM and hydraulic pump/motor

Switched Reluctance Motor	
Topology	Four-phase 8/6 SRM
Rated Power	490 W
Rated Rotational Speed	8000 rpm
Input Voltage	24 V
Hydraulic Pump/Motor	
Type	Axial piston pump/motor
Displacement	0.8 cm ³ /rev
Max. Rotational Speed	2000 rpm (bidirection)
Max. Pressure	16 MPa
Relief Valve	
Set pressure range	5.17~10.3 MPa

5.5.1 Evaluation of flow rate controllability

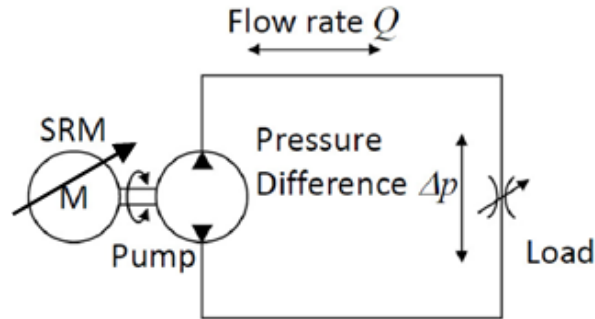


Fig. 5.18. Bidirectional rotational speed control system of SRM with variable orifice load

As shown in Fig. 5.18, a variable orifice was used as a load in the system. The aim of this experiment was to evaluate the controllability of the pump flow rate and hydraulic oil direction by regulating the SR servo motor. Therefore, the variable orifice was adjusted such that the differential pressure Δp , which is the load, was the value at which the hydraulic pump was driven. Because of the target of this study (as mentioned above), the fluctuation of the differential pressure Δp was not considered in this experiment.

The flow rate of pump Q was estimated from the pump rotation speed n_p and displacement D (Eq. 5.3).

$$Q = Dn_p \quad (5.3)$$

Because the maximum rotational speed was 2000 rpm according to the specifications of the test pump, the pump drive was set to rotate bidirectionally with amplitudes of ± 1000 (rpm)/0.5 (Hz) and ± 500 (rpm)/0.5 (Hz) to ensure the self-suction performance of the pump and to prevent cavitation.

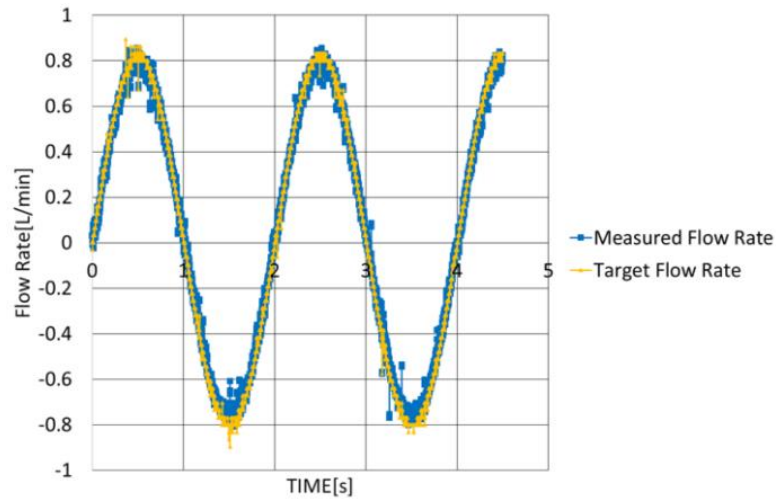


Fig. 5.19. Sinusoidal bidirection flow rate control of hydraulic pump driven by SR servomotor (SRM speed -1000 to $+1000$ rpm, sine wave 0.5 Hz)

As shown in Fig. 5.19, the pump flow rate was consistent with the sinusoidal command corresponding to the forward and reverse rotations of the SRM. Hence, it was confirmed that the flow direction was switched smoothly even in the vicinity where the rotational direction of the SRM was switched and the flow rate was 0.

5.5.2 Evaluation of hydraulic motor speed response

In the subsequent experiment, a fixed displacement bidirectional rotation axial piston motor was installed into the system, as shown in Fig. 5.20. Because the rated rotational speed of the SRM was significantly higher than the maximum rotational speed of the hydraulic pump, a planetary gear reducer (with a gear ratio of five) was used to connect the SR motor and hydraulic pump to increase the applied torque to the hydraulic pump. The aim of the experiment shown in Fig. 5.20 was to evaluate the speed response of the hydraulic motor compared with the command and SRM speed response. Fig. 5.21 shows the experimental results of the speed and flow rate control of the hydraulic pump driven by the SR servomotor. The target flow rate was converted to the command signal of the SR motor, and the measured flow rate was obtained using Eq. (5.3).

As shown in Fig. 5.21, the hydraulic motor speed was consistent with the sinusoidal command corresponding to the forward and reverse rotations of the SRM. However, the SRM speed and hydraulic motor speed deviated slightly at the maximum speed points shown in Fig. 5.21. This may be explained by the volumetric losses in the hydraulic pump and hydraulic motor.

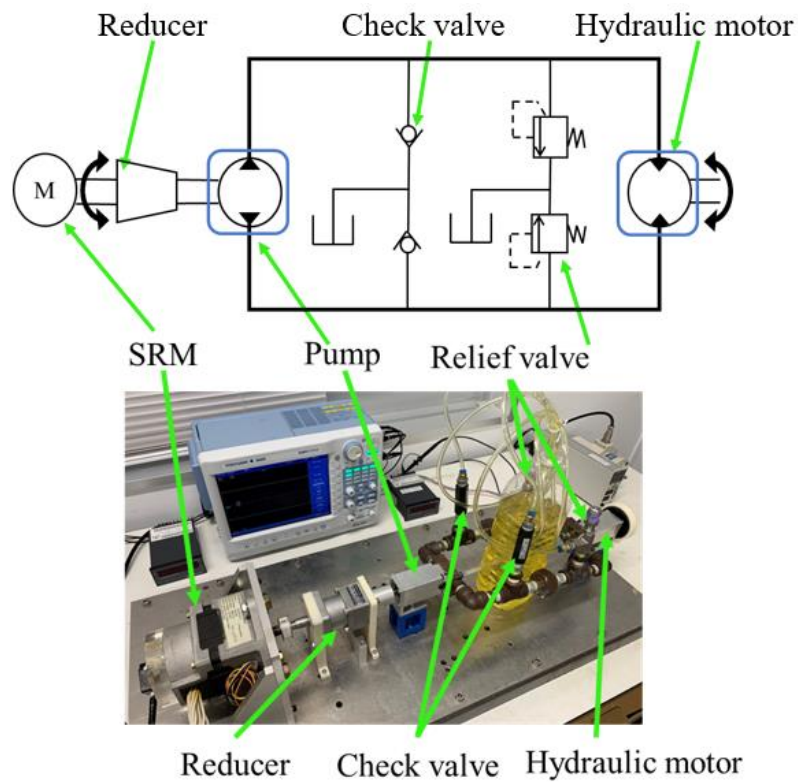


Fig. 5.20. Bidirectional rotational speed control system of SRM with hydraulic motor

In this experimental setup, the load was the only variable orifice in the hydraulic closed circuit. This system can be applied to a load as a hydraulic cylinder, enabling the moving direction, position, and speed of the cylinder to be controlled.

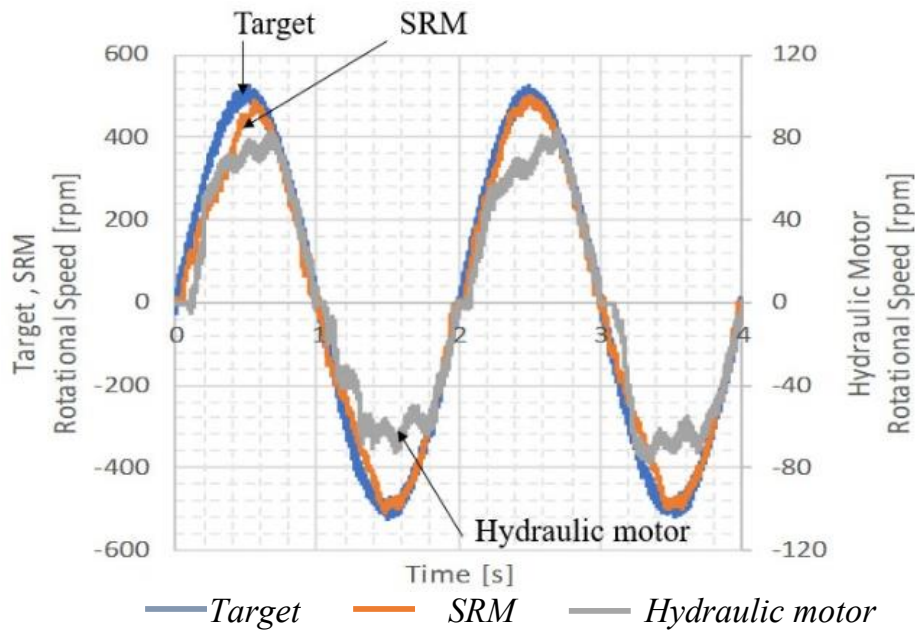


Fig. 5.21. Sinusoidal bidirection speed control of hydraulic pump driven by SR servomotor (SRM speed -500 to $+500$ rpm, sine wave 0.5 Hz)

5.6 Improvement overall efficiency of EHDS with switched reluctance motor and hydraulic pump by using overall efficiency maps

In this study, the controllability of SRM motor in electro-hydraulic drive system was evaluated. By using SRM motor, the cost of drive sytem is reduced and the system can work more efficient in working life entirely. Moreover, to improve the overall energy efficiency of drive system, the proposed control strategy in Chapter 2 could be applied for the drive system with SRM motor. Since efficiency map of SRM motor was not studied in YNU Laboratory so a SRM efficiency map is referenced from literature as shown in figure below.

In Figure 5.22 shows the efficiency map of SRM motor referenced from Jiang, J.W. et al.^{5.5}). It is not efficiency map of SRM motor with servo function but it could be a representative map of SRM motor. Regarding Figure 5.22, although the efficiency map of SRM changes depending on the excitation timing and excitation current waveform of each phase of the drive circuit, but it has the same shape as the permanent magnet synchronous motor (servomotor). Based on the data of this map, the coefficients in motor efficiency equation as shown in Table 3.2 could be determined to simulate the efficiency of SRM motor. Then this map could be combined with the efficiency maps of the hydraulic pump in Chapter 2 and 3 to create overall efficiency maps. By these overall efficiency maps, the electro-hydraulic drive system with SRM motor could be controlled to operate at high-efficient operating points.

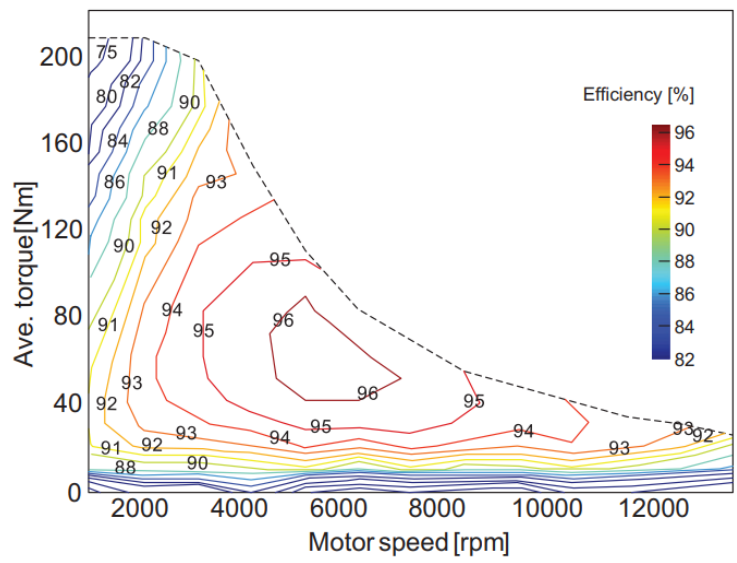


Fig. 5.22. Efficiency map of SRM motor

(From Jiang, J.W. et al., Design optimization of switched reluctance machine using genetic algorithm, in Proceedings of the IEEE International Electric Machines and Drives Conference (IEMDC), Coeur d'Alene, ID, May 2015, pp. 1671–1677)

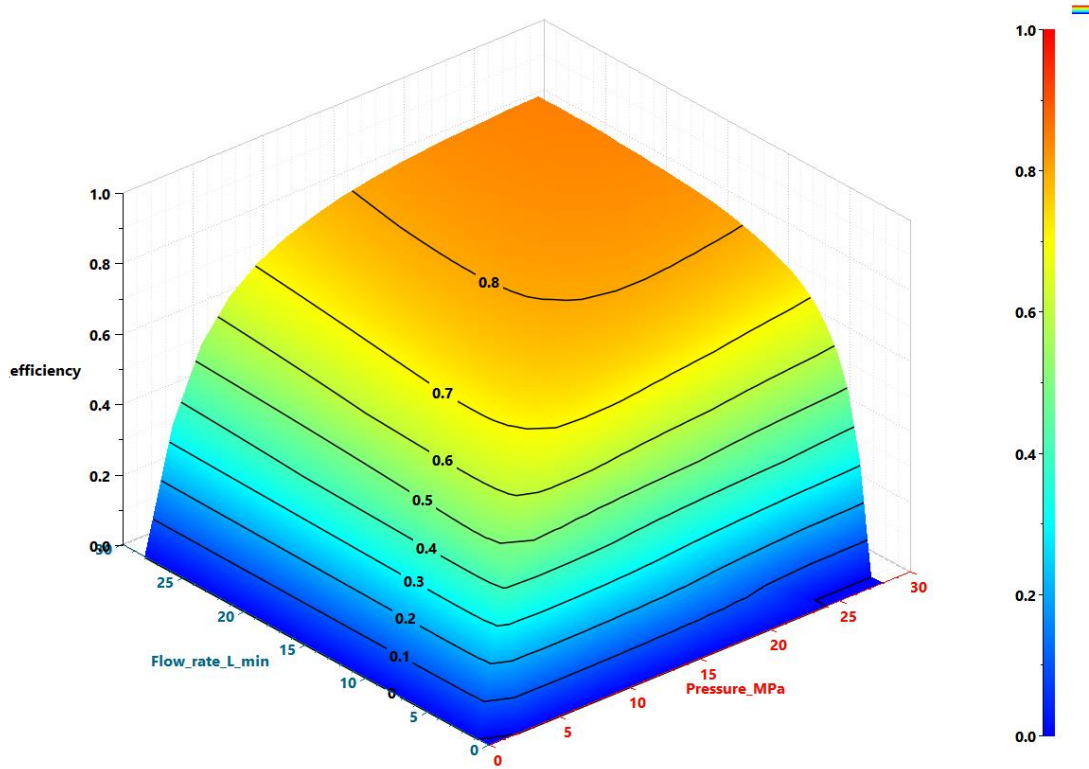


Fig. 5.23. Overall efficiency map of EHDS driven by SRM motor (displacement ratio $\alpha = 1.0$)

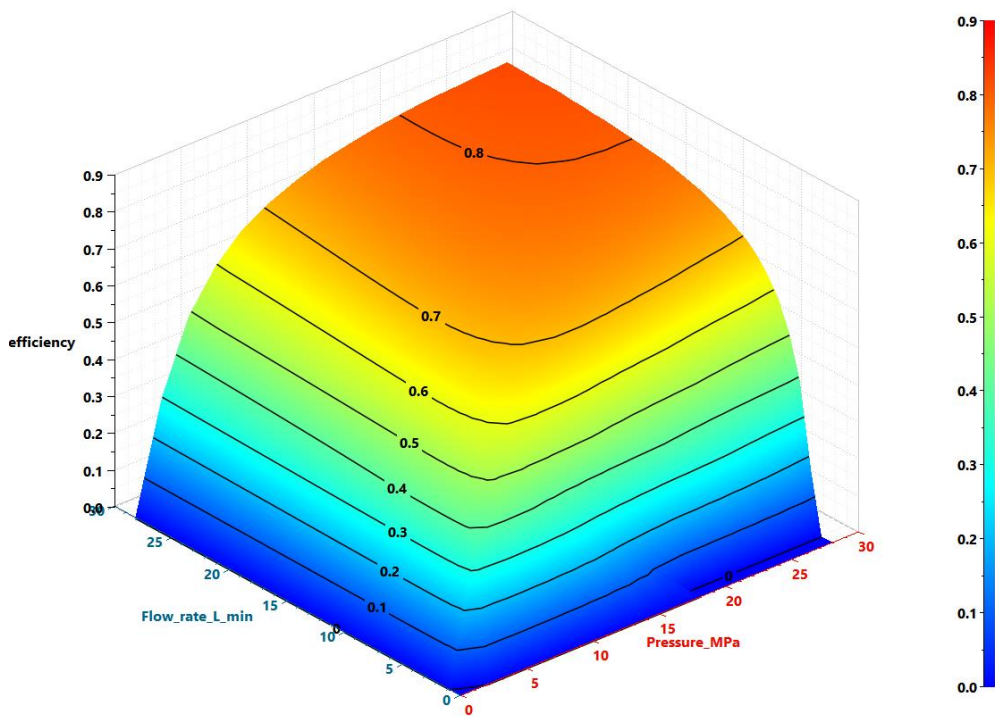


Fig. 5.24. Overall efficiency map of EHDS driven by SRM motor (displacement ratio $\alpha = 0.75$)

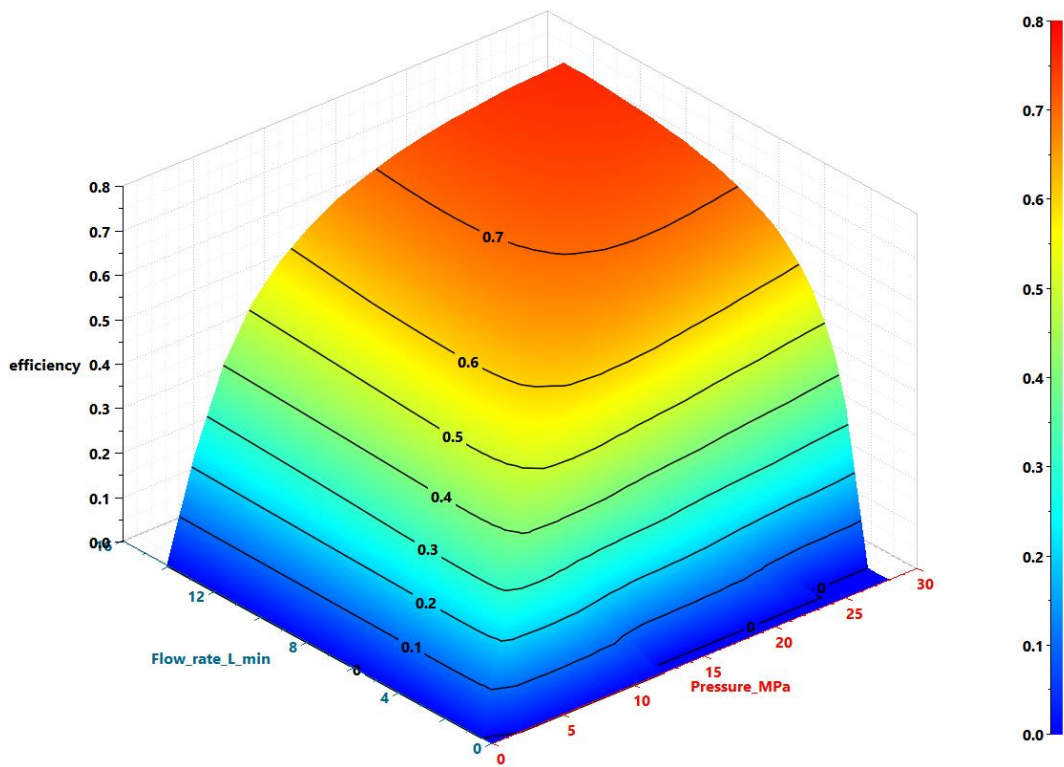


Fig. 5.25. Overall efficiency map of EHDS driven by SRM motor (displacement ratio $\alpha = 0.5$)

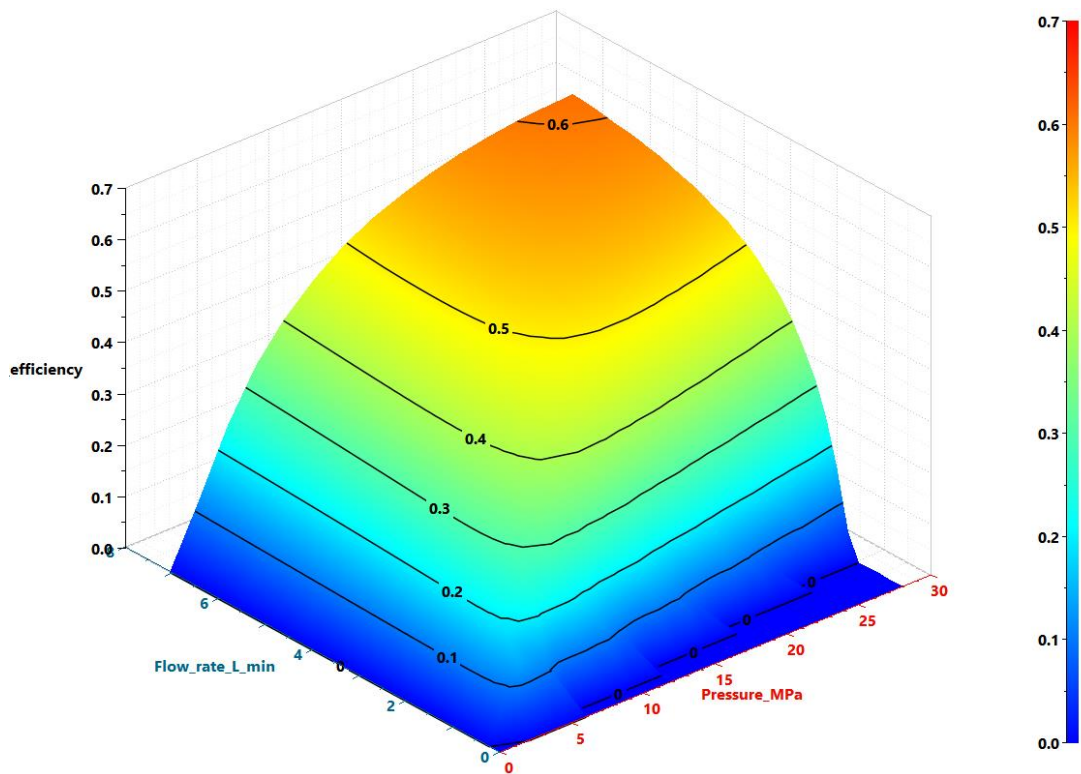


Fig. 5.26. Overall efficiency map of EHDS driven by SRM motor (displacement ratio $\alpha = 0.25$)

5.7 Summary of Chapter 5

- A control system for an SR motor with some servo functions added to the SRM was proposed in this chapter. The experimental results of EHDS with SR servo motor show that the flow rate direction was switched smoothly even in the vicinity where the rotational direction of the SRM was switched and the flow rate was 0.
- Using proposed control strategy in Chapter 2, the overall efficiency of EHDS with SRM could be improved by regulating motor speed and displacement ratio to operate EHDS at high-efficient working points.

5.8 References

5.1) Y. Sato, K. Murakami, Y. Tsuboi, “Sensorless Torque and Thrust Estimation of a Rotational/Linear Two Degrees-of-Freedom Switched Reluctance Motor”, IEEE Trans. Mag., 52-7, Paper No. 8204504, 2016.

5.2) Miller, TJE, “Switched Reluctance Motors and Their Control”, Clarendon Press, 1993.

5.3) T.Husain, W.Uddin, Y.Sozer, “Performance Comparison of Short Pitched and Fully Pitched Switched Reluctance Machines Over Wide Speed Operations”, IEEE Energy Conversion Congress and Exposition (ECCE),

5.4) K. Aiso, K. Akatsu, “High Speed SRM using vector Control for Electric Vehicle”, CES Transactions on Electrical Machines and Systems, Vol.4, Issue:1, 2020.

5.5) Jiang, J.W. et al., Design optimization of switched reluctance machine using genetic algorithm, in Proceedings of the IEEE International Electric Machines and Drives Conference (IEMDC), Coeur d’Alene, ID, May 2015, pp. 1671–1677

Chapter 6

Conclusion

Chapter 6. Conclusion

6.1 Summary

In the industrial applications, electro-hydraulic drive system is preferred to the mechanical and electrical drive systems for its many advantages. To reduce throttling losses, the valveless electro-hydraulic drive system has been proposed and shown its high efficiency. This system uses a variable-speed motor and variable-displacement pump to supply hydraulic power to an actuator. The required flow rate is adapted by controlling both motor speed and pump displacement. The key advantage of this system is that it avoids both an excessive flow rate and power losses in the hydraulic control valves. With this principle, the EHDS motor must have ability to operate at wide speed range, especially at very low speed to supply low flow rate for actuator. In current electric motors, the servo motor could match with this requirement, and it is used to drive hydraulic pump in this research.

In valveless EHDS, the most power losses occur in the stage during which electrical power is converted into hydraulic power (hydraulic pump). Therefore, the overall efficiency of EHDSs depends primarily on the efficiency of the hydraulic power unit combined from electric motor and hydraulic pump. Therefore, to improve the overall efficiency of the hydraulic power unit, it should be considered as a composite system, in other words, the interaction between electric motor and hydraulic pump must be studied.

In this study, a novel control strategy was proposed to improve the overall efficiency of an EHDS by considering the efficiency of various EHDS components and the influence of these components on overall efficiency. Based on the knowledge of overall efficiency, the optimized values of the working parameters (motor speed and pump displacement ratio) can be determined to achieve the highest efficiency for a given working point. Next, the numerical simulation was implemented for a series of operating points. The results show that the efficiency of the proposed control strategy was improved significantly compared with conventional single-variable power units. This study illustrates the concept of high-efficiency power transmission and the usefulness of two-degree-of-freedom control. The simulation results of the proposed control strategy were verified by experiment for not only separated working points and transient commands of flow rate. Compared with one-degree-of-freedom controller, the efficiency of the proposed concept is improved significantly. The experiment with VS-VP system

(two-degree-of-freedom control) is conducted with 486 separated working points and experiment results have matched with simulation results. From these experiment results, experiment efficiency maps have been built and used for generating motor speed n_m and displacement ratio α to control VS-VP system operating at high-efficient areas.

Recently, another electric motor called switched reluctance motor as the potential to become a new EHDS drive motor because of its advantages compared with permanent magnet synchronous motor. SRM motor has a simpler and more robust construction owing to its rotor structure without coils or permanent magnets, thereby affording a lower fabrication cost. Moreover, SRMs can provide similar or higher efficiencies in the medium and high-speed ranges. However, to use SRM motor for driving hydraulic pump in a valveless EHDS, it is necessary to operate SRM motor as a servo motor. In this research, switched reluctance motor is studied to apply in electro-hydraulic drive system. To control SRM motor with bidirectional ability, a control system for an SR motor with servo functions, such as bidirectional rotation, speed control, and torque control, added to the SRM was proposed herein. Subsequently, the closed-circuit flow control performance of a pump driven by an SR servo motor was presented. This method solved problems arising from the permanent magnets of the motor in the flow rate control system of a hydraulic closed-loop circuit. The experimental results confirmed that the flow rate direction was switched smoothly even in the vicinity where the rotational direction of the SRM was switched at the flow rate was 0. The authors will consider the effects of the speed-torque characteristics of the system by conducting further experiments that include inertial loads.

6.2 Future work

In this research, the results show the advantage of the two-degree-of-freedom control strategy in electro-hydraulic drive system. The overall efficiency of system was improved not only at separated working point but also entire working cycle.

The least squares method and interpolation method are used to determine the coefficients from experimental data and efficiency value from efficiency maps, respectively. These methods could be replaced by applying Neural network method to achieve higher accurate, however, this requires a large volume of experimental data.

The change of oil viscosity and compressibility due to changing of pressure has a considerable influence in volumetric losses and mechanical losses. In the

future work, this influence should be considered by using viscosity value which is a function of pressure and displacement ratio.

This study only considered a single design of variable displacement axial piston pump. If there is a distinct difference in the design of a set of pumps, it could consider the influence of these design differences for different applications. Also, comparisons of pumps within a family but different displacements could also be of interest to the pump designer.

Appendix

A.1. Simulink models for determining the highest overall efficiency

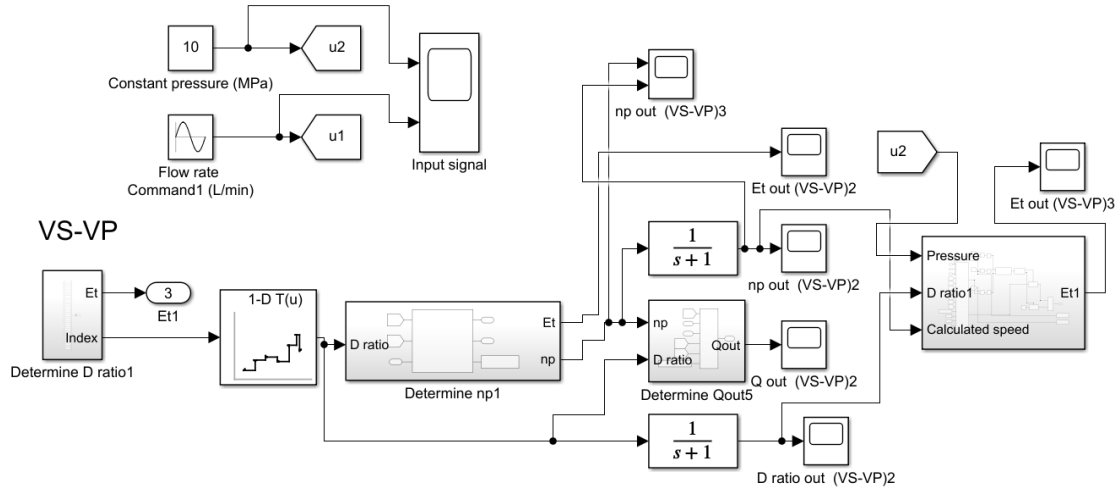


Fig. A.1. Simulink model of variable speed motor – variable hydraulic pump EHDS

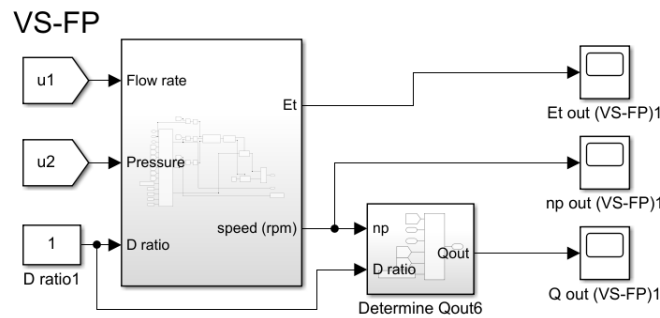


Fig. A.2. Simulink model of variable speed motor – fixed hydraulic pump EHDS

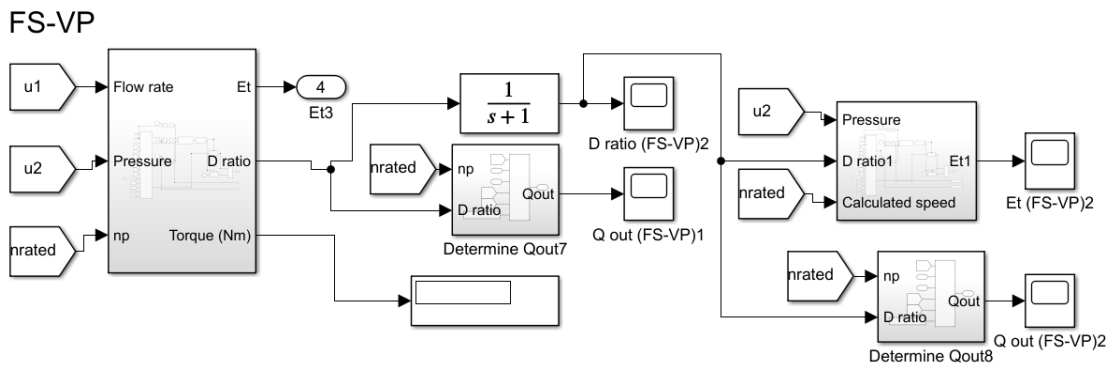


Fig. A.3. Simulink model of fixed speed motor – variable hydraulic pump EHDS

A.2. Control method of servo amplifier and stepping motor for regulating servo motor speed n_m and displacement ratio α (by adjusting screw) used in this study

In this study, to operate VS-VP system at high-efficient areas as shown in overall efficiency maps while still ensuring the required flow rate, the servo motor speed n_m and displacement ratio α will be regulated to the values obtained from Simulink model. The servo motor speed n_m is controlled by servo amplifier, while stepping motor and displacement adjusting screw are combined to control the swash plate angle of hydraulic piston pump as shown in Figure A.4..

The details of connection for drive and interface in servo motor controller and stepping motor controller are presented from Figure A.5 to Figure A.9.

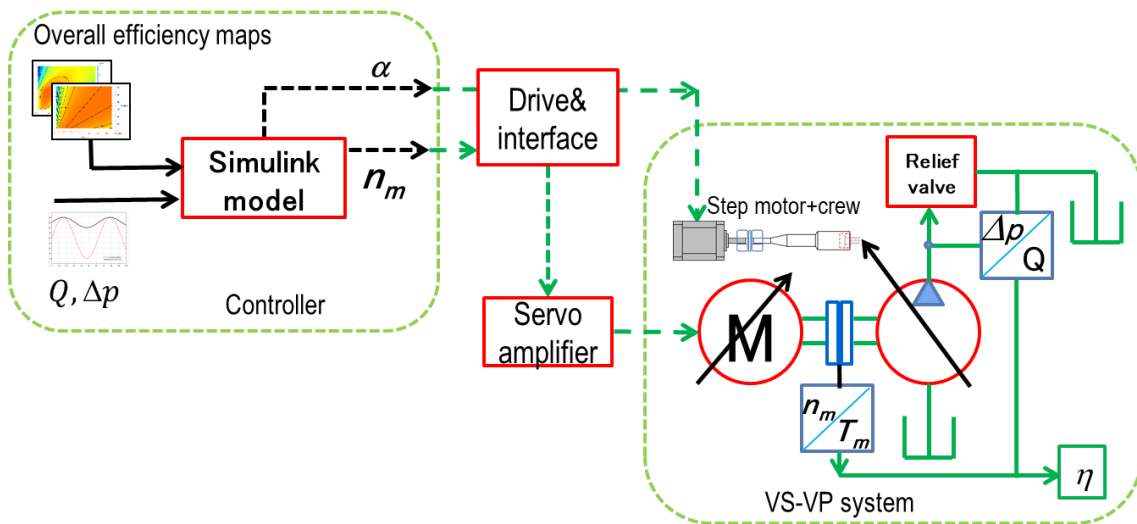


Fig. A.4. Control method of servo amplifier and stepping motor for regulating servo motor speed n_m and displacement ratio α

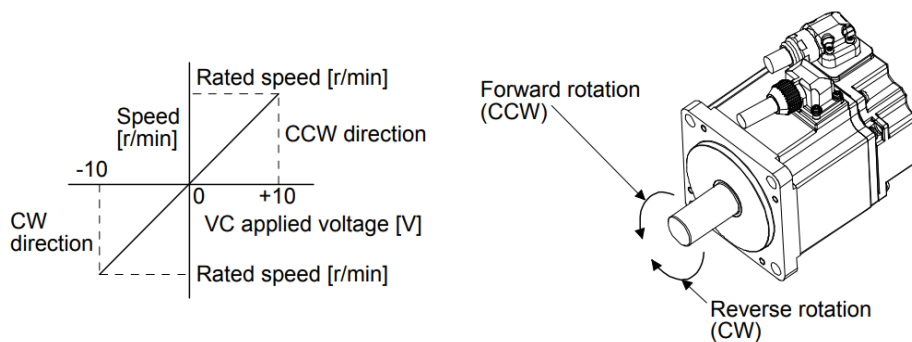


Fig.A.5. Relation between VC (analog speed command) applied voltage and the servo motor speed

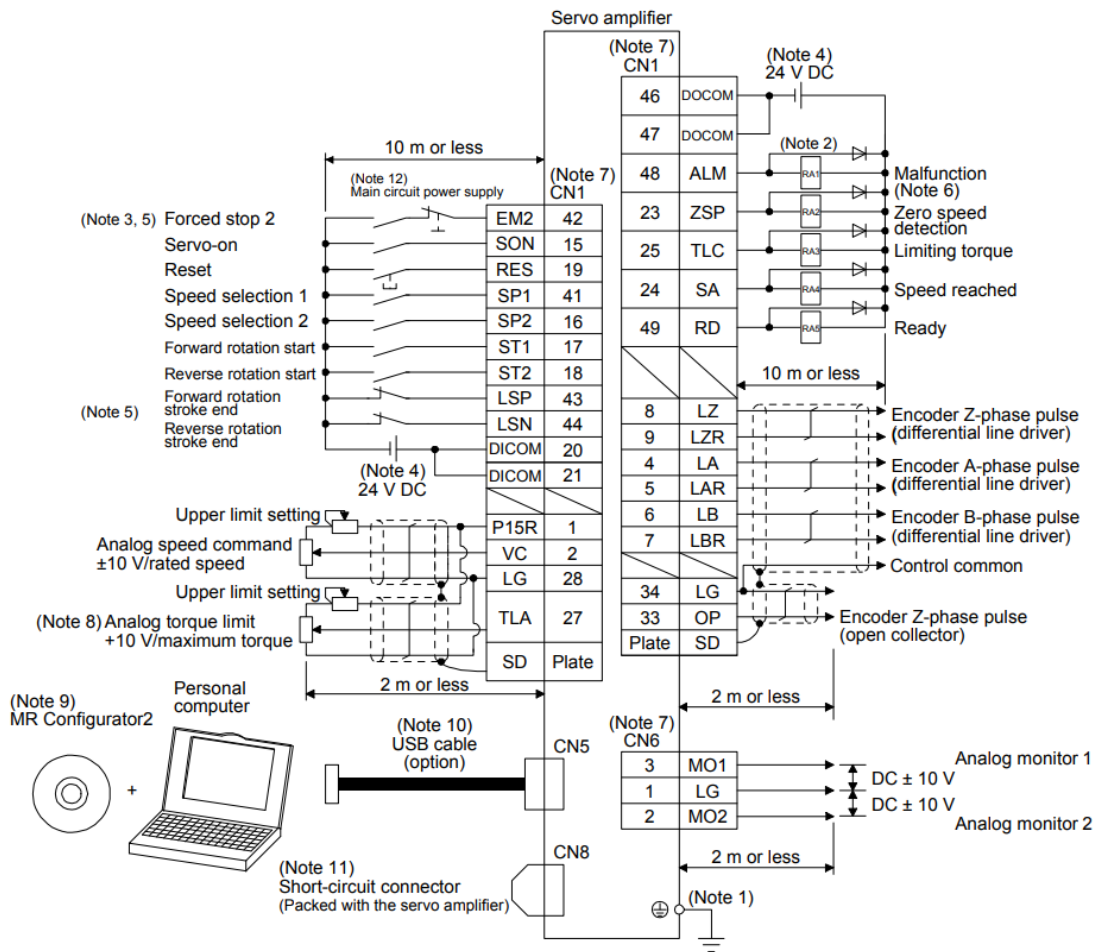


Fig.A.6. Sink I/O interface of servo amplifier

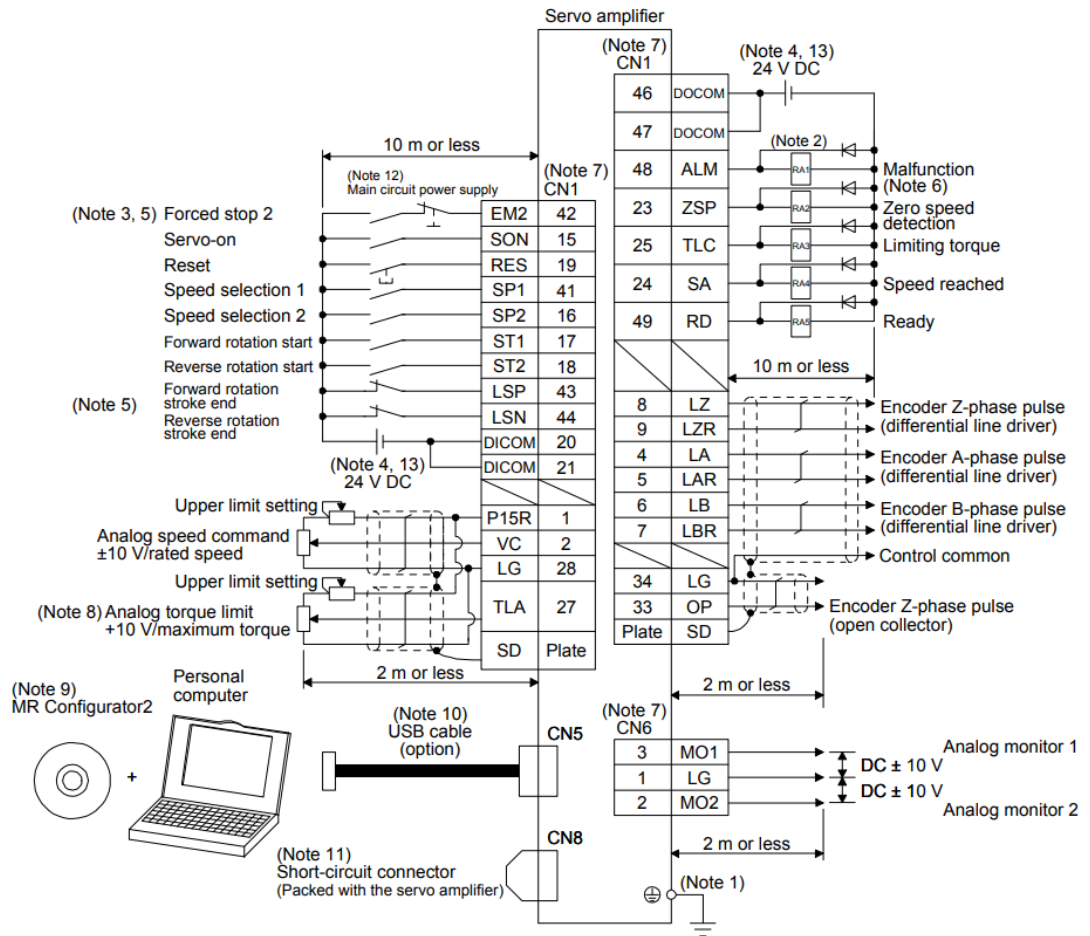


Fig.A.7. Source I/O interface of servo amplifier

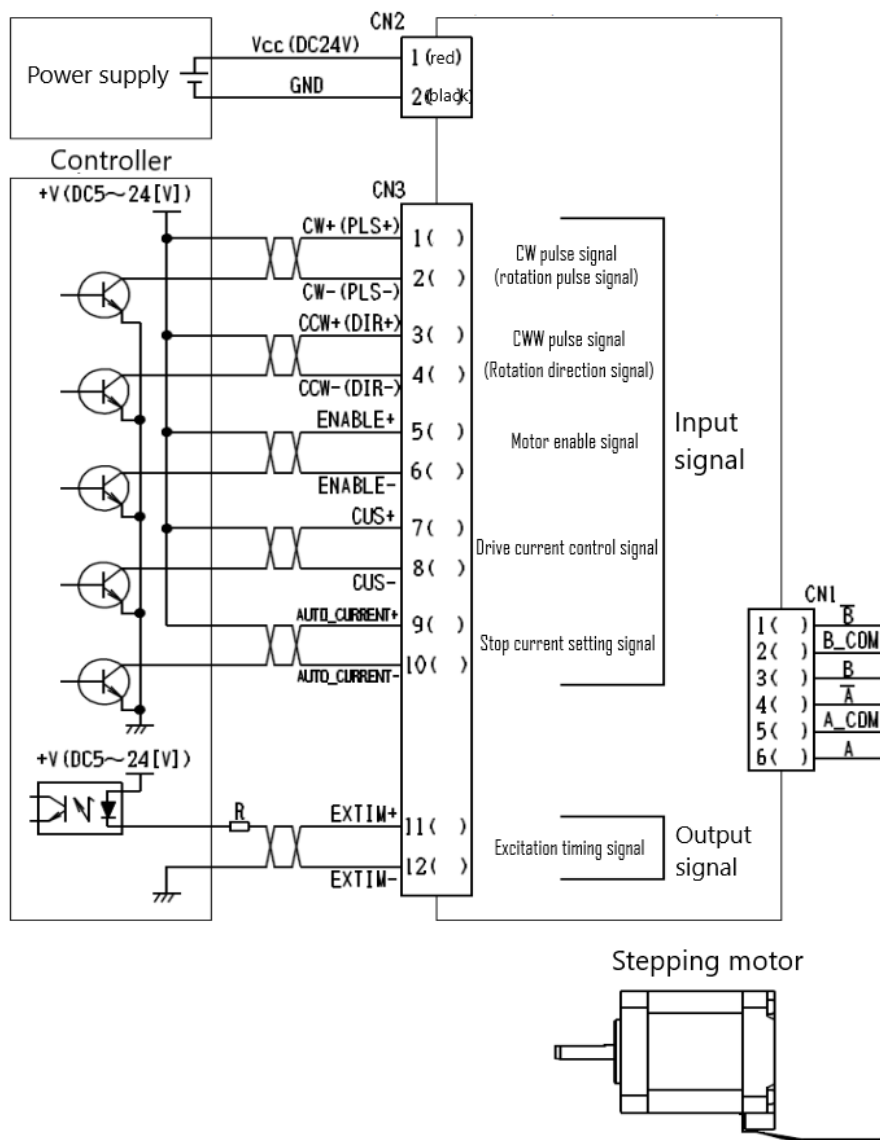


Fig.A.8. Connection of driver, power supply, controller and stepping motor

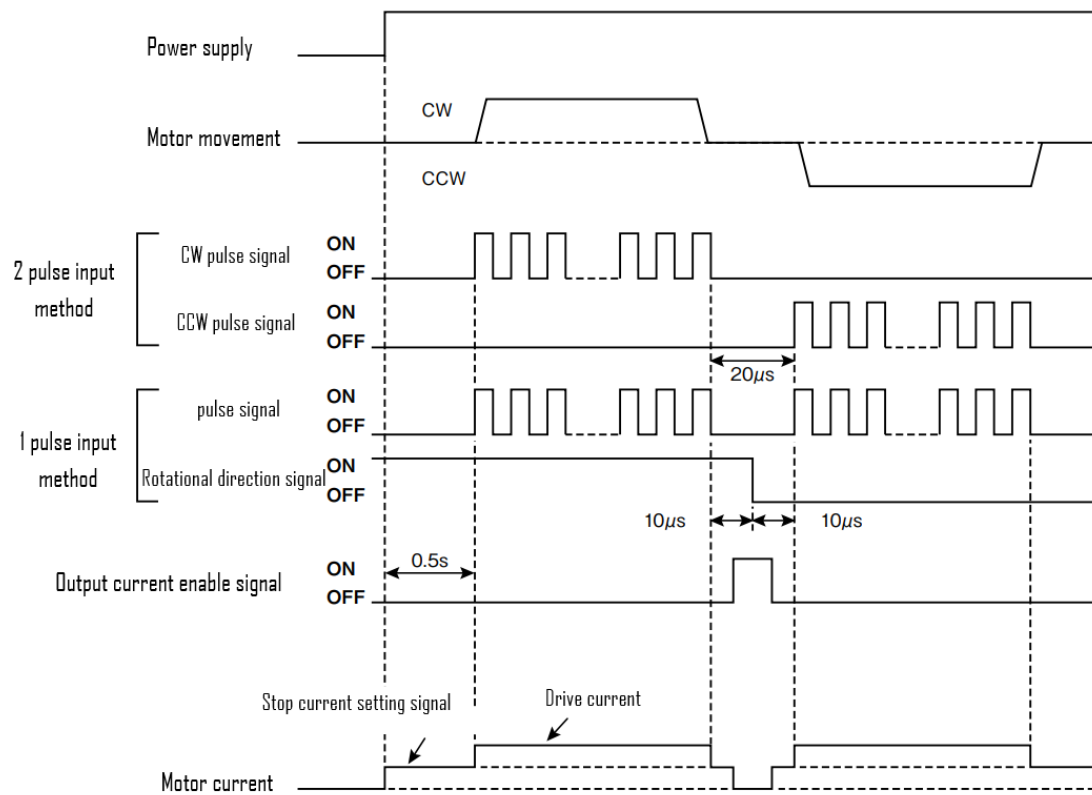


Fig.A.9. Stepping motor movement and timing chart

Related publications

The most relevant publications related to this thesis as following:

- 1) Ha Tham Phan, Seiya Itagaki, and Yasukazu Sato, Development of hydraulic pump drive system using switched reluctance motor with servo function, *Journal of Robotics and Mechatronics*, Vol. 32 No. 5, p. 984-993 (2020)
- 2) Ha Tham PHAN, Yasukazu SATO, Improving the overall efficiency of an electro-hydraulic drive system by using efficiency maps, *JFPS International Journal of Fluid Power System*, 14-1, 10/18, 2021 (Online ISSN : 1881-5286)

Acknowledgements

I would like to express my deep gratitude to my supervisors, Professor Yasukazu Sato for his great guidance and encouragement in advancing this research. The advice I received when my research got stuck was really accurate, and even if I asked persistent questions, I was kindly instructed.

I also express my thank to all the team of Sato Laboratory (Mechatronics/Fluid Power Laboratory, Yokohama National Univeristy), especially Mr. Nakamura Yuki, Mr. Seiya Itagaki, Mr. Arihito Ushigome for their contribution to this work. They made my research life at graduate school enjoyable and always gave me meaningful advice.

Most of all I would like to thank all my lovely my family: my parents, my children for always being there. Last but not least, thank you Diep for being such a wonderful wife.